## ABSTRACT

LIANG, ZHANHAO. Progress towards Total Synthesis of Marine Natural Product Ansalactam A. (Under the direction of Dr. Joshua G. Pierce).

Ansalactam A is an ansa macrolide natural product that contains a densely functionalized spiro-γ-lactam core containing three contiguous stereocenters. This unusual motif distinguishes it from other members of this family and represents a significant synthetic challenge. Herein, we report the development of a stereoselective formal [3+2] cycloaddition reaction to construct this key spiro-γ-lactam motif for the first time, thereby enabling access to the northern domain of ansalactam A. Additionally, we repot explorations toward the assembly of the southern chain fragments.

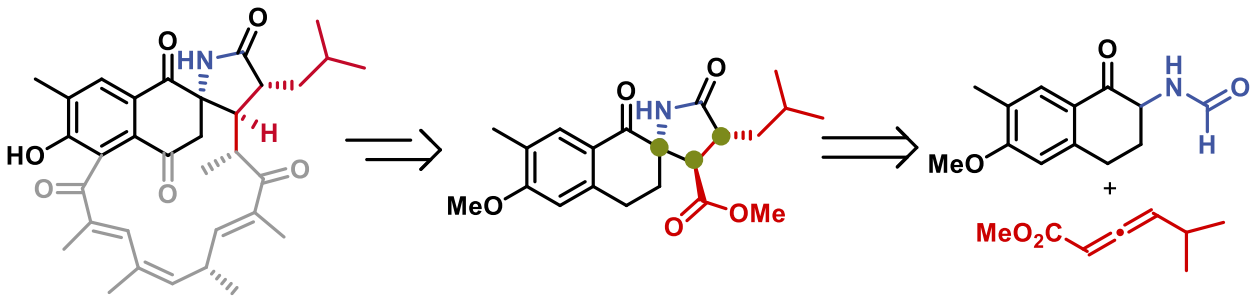


ansalactam A

# Progress towards Total Synthesis of Marine Natural Product Ansalactam A

by
Zhanhao Liang

A dissertation submitted to the Graduate Faculty of
North Carolina State University
In partial fulfillment of the
requirements for the degree of
Doctor of Philosophy

Chemistry

Raleigh, North Carolina

2022

APPROVED BY:

| | |
|---|---|
| _____ | _____ |
| Dr. Joshua Pierce<br>Committee Chair | Dr. Gavin Williams |
| _____ | _____ |
| Dr. Vincent Lindsay | Dr. Wei-Chen Chang |

## BIOGRAPHY

Zhanhao Liang was born in 1995, in Urumqi, Xinjiang, China. His interests in organic chemistry grew from his senior year in Urumqi No. 1 Senior High School. Afterward, he pursued his interest in organic chemistry and unhesitatingly became an undergraduate student in the department of chemistry in Xiamen University. He started his research career in Prof. Yandong Zhang's group with a systematic training in organic synthesis and participation in a project exploring the total synthesis of marine natural product aplydactone. In 2017, he obtained his bachelor's degree and then began his PhD studies at North Carolina State University. Under the supervision of Dr. Joshua Pierce, he mastered synthetic chemistry and the ability to perform of independent research.

## ACKNOWLEDGEMENTS

**Dr. Joshua Pierce**

I am grateful for your guidance and inspiration in every piece of my project and life during my 5 years in your group. Under your mentorship, I realized how fascinating total synthesis is and how exciting it is to develop my own chemistry. The experiences and impact here have become an unforgettable memory for me. I have become more professional, confident and successful by being your student and a member of the Pierce lab.

**Dr. Vincent Lindsay, Dr. Wei-Chen Chang and Dr. Gavin Williams**

I appreciate you for being my committee members and for your helpful advice for my prelim and the final defense. Also, the courses you taught have become very useful tools during my PhD life. Your knowledge and kindness have helped me significantly over the past 5 years.

**Dr. Elisabeth Brown**

Thanks for being my GSR committee and supporting me over the years.

**All the group members in Pierce lab**

Thanks to all of you for supporting me over the past few years. It's really an amazing journey working with you all.

**Dr. Jennifer Sun, Dr. Roger Sommer, Dr. Danielle Lehman and Dr. Peter Thompson**

I am grateful for the training and assistance for NMR spectroscopy, X-ray facility and HR-MS. I also really appreciate the NC state Molecular, Education, Technology and Research Innovation Center (METRIC) for providing graduate students with such an efficient and professional platform.

**Xiaoxia Liu, my mother**

I am grateful for your love and care over my whole life. Without your constant love and support, I would be nothing.

**Jianxin Liang, my father**

I appreciate for your love and support over my whole life. I will prove myself again and again.

**Zi Zhuang, my girlfriend**

Meeting you and fall in love with you is the most fortunate and incredible thing in my life. You are always my motivation to push forward. Thanks for being with me together in this journey.

## Table of Contents

## LIST OF TABLES

## LIST OF FIGURES

## LIST OF SCHEMES

# Chapter 1: General Introduction and Retrosynthesis

## 1.1. Introduction to Polyketide Natural Products and Ansamycin Polyketides

Polyketide natural products are a structurally diverse family of compounds possessing a variety of biological activities, such as antibiotic activity (erythromycin A),[1] immunosuppressant activity (rapamycin),[2] and antitumor/antibiotic activity (doxorubicin)[3] (**Figure 1**).

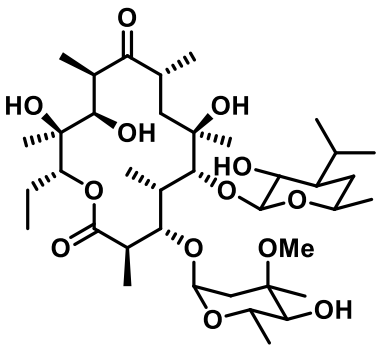


erythromycin A

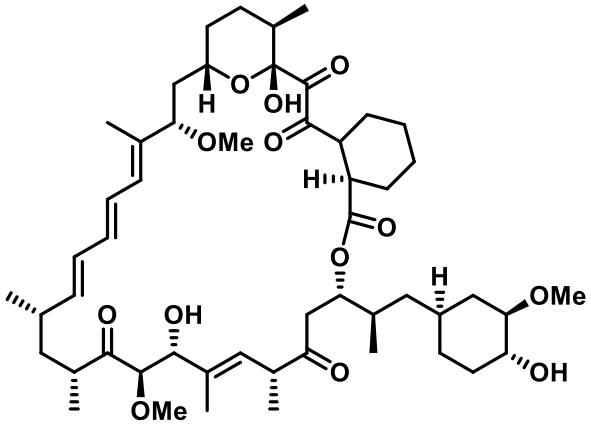


rapamycin

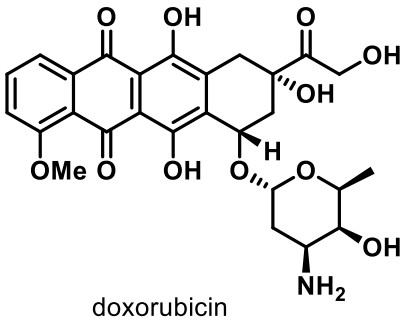


doxorubicin

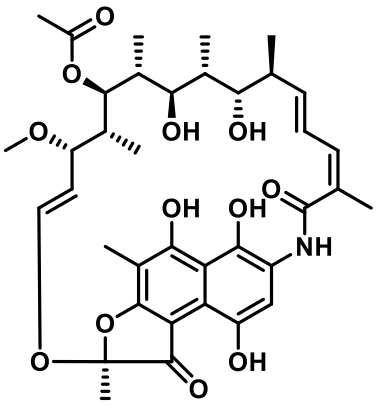


rifamycin SV

**Figure 1.** Structures of erythromycin A, rapamycin, doxorubicin and rifamycin SV.

In particular, the ansamycin class of polyketides has become a significant family of bioactive natural products with the discovery of the antibacterial properties of rifamycin B in 1959.[4] Rifamycins have been used to treat tuberculosis, leprosy and AIDS-associated mycobacterial infections.[5] These kinds of macrolactams are named because of their ‘‘basket-like’’ structure consisting of an aromatic moiety connected at nonadjacent positions by a long polyketide chain, like an ansa.[6] The structure of the aromatic moiety differentiates the two subclasses of these natural products (**Figure 2**).[7]

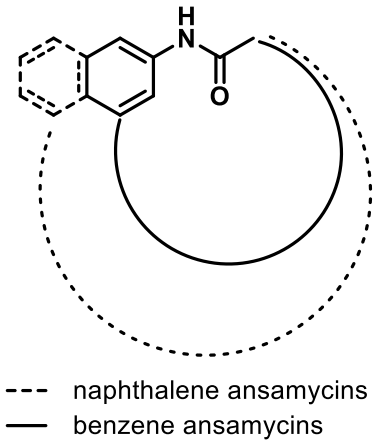


**Figure 2.** “Basket-like” structure of ansamycins.

Naphthalene ansamycins (rifamycin) have potent antimicrobial activities,[8] however, benzene ansamycins (geldanamycin) have showed their potential as antineoplastic agents.[9] Additionally, another type of differentiation can be made within the ansa chain (C15- and C17-) of the benzene ansamycins (**Figure 3**). The geldanamycin type ansamycins **IIa** consist of a 19-membered lactam that contains an isolated

trisubstituted olefin. Alternatively, the 21-membered macrolactam of mycotrienin type ansamycins **IIb** consists of an all (*E*)-triene system.

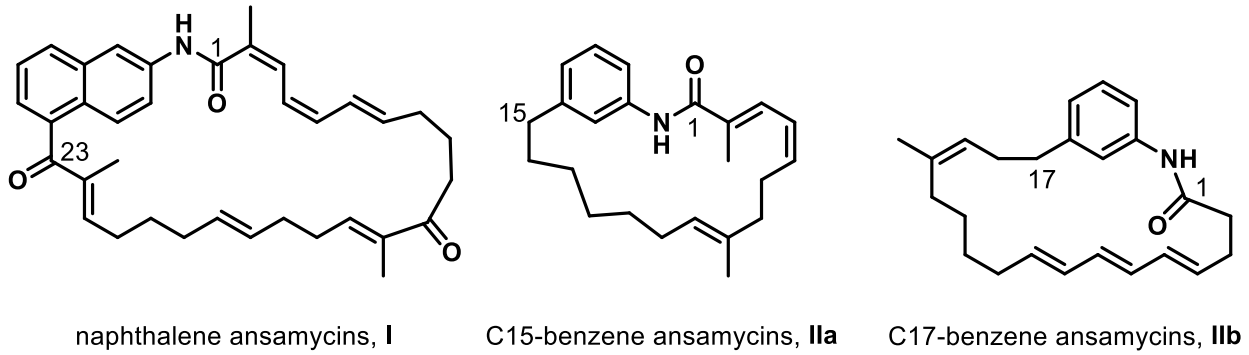


naphthalene ansamycins, **I** C15-benzene ansamycins, **IIa** C17-benzene ansamycins, **IIb**

**Figure 3.** Structures of naphthalene ansamycins **I** and C15- and C17-benzene ansamycins **II**.

### 1.2. Introduction to Marine Natural Product Ansalactam A

Ansalactams A-D represent a sub-class of ansamycin polyketides that were isolated by Moore and Fenical from a *Streptomyces* sp. strain CNH-189 isolated from marine sediments.[10,11] These natural products are members of the broader ansamycin family that includes biologically potent molecules such as rifamycin SV and geldanamycin.[12,13] In addition to their biological activity, the ansamycins have complex biosynthetic origins and are collectively formed from a common aromatic acid 3-amino-5-hydroxybenzoate precursor.[10] The ansamycins are structurally differentiated by variations in a shared spiro-γ-lactamdihydronaphthoquinone core, further bridged by a polyketide chain forming a 16-membered macrocyclic ring (**Figure 4**).

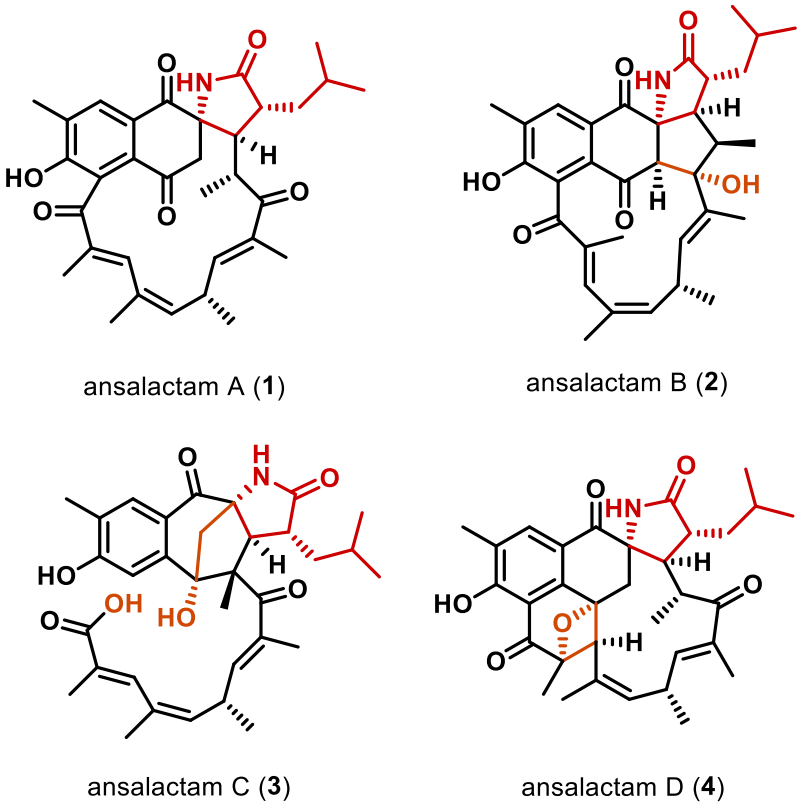


**Figure 4.** Structures of the ansalactam natural products (**1**-**4**).

As part of our broader program targeting bioactive marine natural products,[14] we became interested in developing a synthetic route to the spiro-γ-lactam system unique to the ansalactams. This iso-butyryl substituted lactam has been hypothesized by Trauner's group to arise biosynthetically through either a 5-*exo* or 5-*endo* radical cyclization.

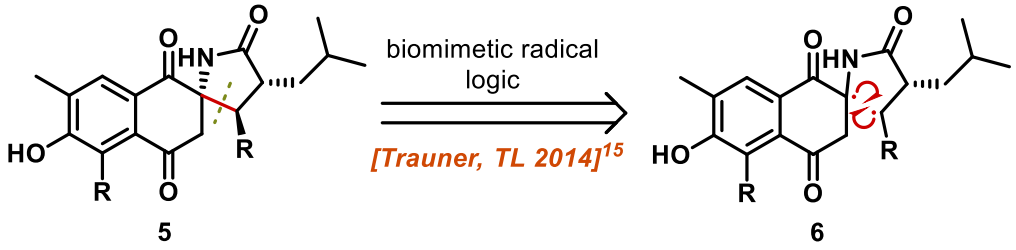


**Figure 5.** Biomimetic logic presented by Trauner.

However, preliminary synthetic studies were not successful in realizing this biomimetic logic to date (Figure 5).[15]

### 1.3. Retrosynthetic strategy towards the northern spiro-lactam core

We envisioned a [3+2] cycloaddition approach to prepare the spiro-γ-lactam core, leveraging the well-studied steric tolerance and stereocontrol of these reactions (**Figure 6).**[16,17] While this approach was attractive, it was not clear at the outset of our work what the identity of the 1,3-dipole (represented by **8**) or dipolarophile (represented by **9**) would be, as the proposed disconnections required inverting the native reactivity of an oxy-azomethine ylide precursor such as **8**. Attempted formation of **8** from a formamide precursor such as **10** may result in formation of an undesired α-isocyanoacetate derivative, precluding formation of the targeted spirocycle due to competitive [4+1] cycloaddition reactions common to these motifs.[18]

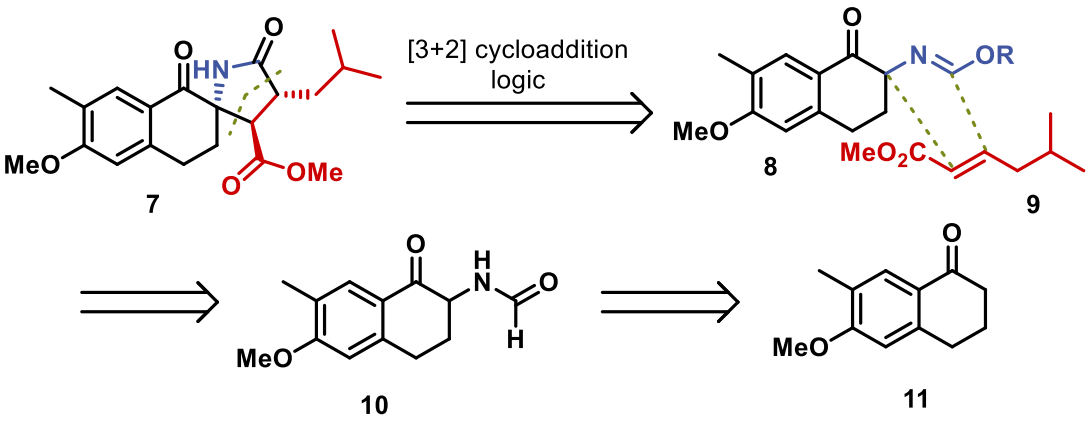


**Figure 6.** Retrosynthetic approach to spiro-lactam core enabled by key [3+2] dipolar cycloaddition.

### 1.4. Retrosynthetic strategy towards the southern polyketide chain

We envisioned a late-stage olefin metathesis to accomplish ring closure of the macrocyclic polyketide. The connections between the northern cyclic core and bottom chain fragments would be enabled by different kinds of cross-coupling reactions. The preparation of the chiral fragment was through a well-developed route from enantio-pure alcohol **30** (**Figure 7**).

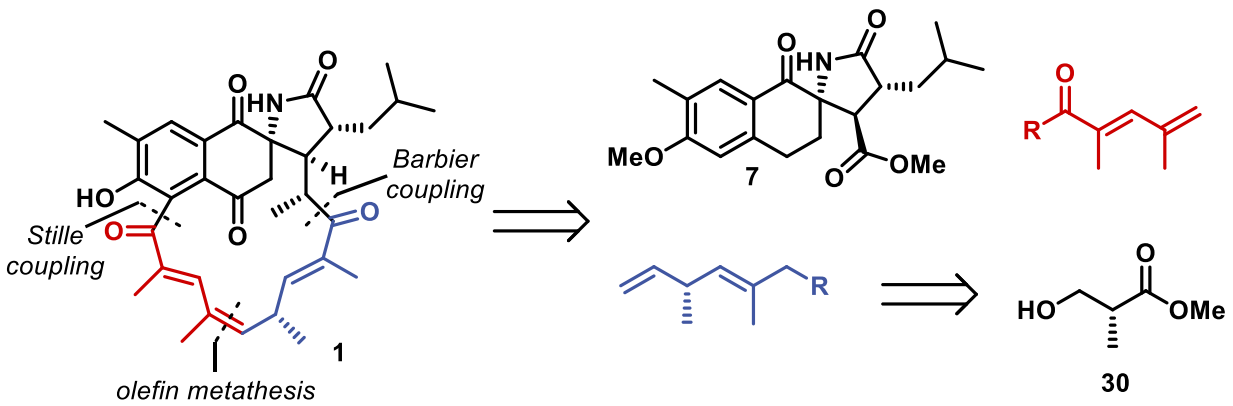


**Figure 7.** Retrosynthetic approach to polyketide chain enabled by olefin metathesis and cross-coupling reactions.

# Chapter 2: Exploration of the Proposed [3+2] Cycloaddition

## 2.1. Preparation of functionalized α-tetralone 11

To start to explore the reactivity of the key [3+2] cycloaddition, we sought to prepare formamide **10**. To find a more efficient synthetic route, a well-developed pathway through two key reactions, Heck coupling reaction and Friedel-Crafts acylation, was applied.[19] The functionalized *α*-tetralone **11** was prepared as described (**Scheme 1**). Beginning with methyl ester **12**, reduction and Appel chlorination afforded benzylic chloride **13** in 99% yield. Subsequent Heck coupling, followed by hydrogenation and saponification, allowed for the preparation of carboxylic acid **15** in excellent yield over 3 steps. Friedel-Crafts acylation proceeded smoothly to generate desired ketone **11**.

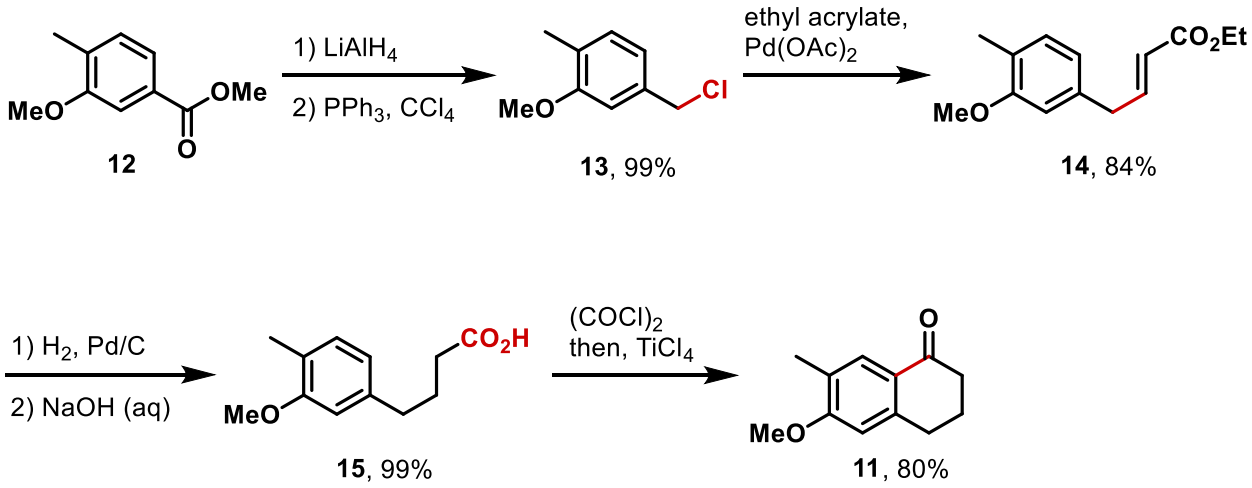


**Scheme 1.** Synthesis of tetralone **11**.

## 2.2. Preparation of formamide 10

Sequential bromination, azide installation, and hydrogenation afforded the desired 2-aminotetralone **16** in 60% yield. Lastly, *N*-formylation of **16** provided the targeted formamide **10** in 75% yield. The presently described sequenced proved highly scalable and has allowed for gram-scale preparation of **10** (**Scheme 2**).

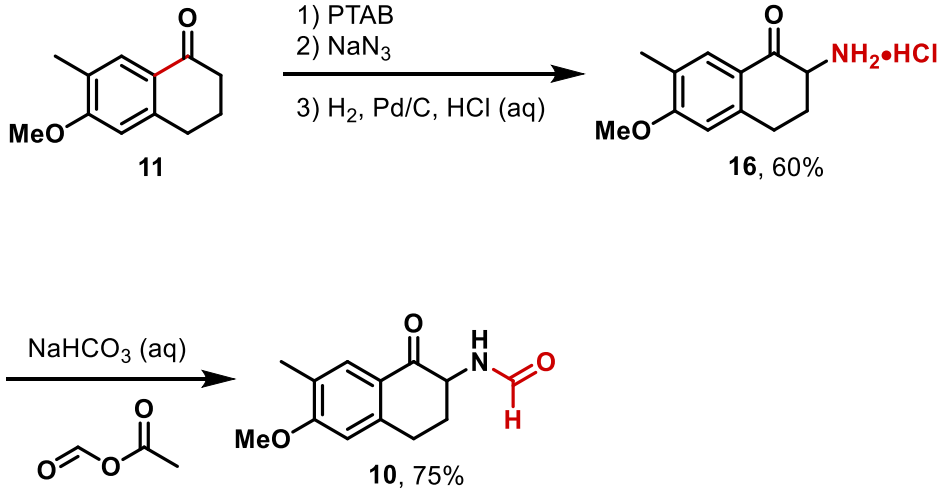


**Scheme 2.** Synthesis of formamide **10**.

## 2.3. Introduction of Azomethine Ylide-type 1,3-dipolar Cycloaddition

In Rolf Huisgen's seminal work, he defined 1,3-dipolar cycloaddition as "1,3-Dipole, A-B-C (**Scheme 3**), must be defined, such that atom A possesses an electron sextet, that is, an incomplete valence shell combined with a positive charge, and that atom C, the negatively charged center, has an unshared electron pair. Combination of a 1,3-dipole with a multiple bond system D-E, termed the dipolarophile, is referred to as a

“1,3-dipolar cycloaddition”. 1,3-dipolar cycloaddition has become a fundamental organic reaction, and its high utility spreads in every aspect of chemistry, from natural product synthesis, material science, and chemical biology. Implementing a 1,3-dipolar cycloaddition in a catalytic asymmetric synthesis is a large research field, which stems from pioneering research mostly done in the 1990s.[20-25]

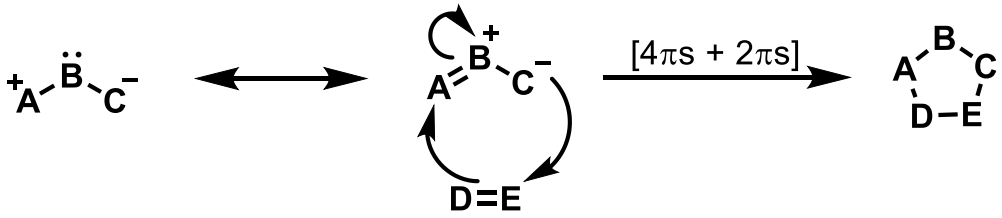


**Scheme 3.** 1,3-dipolar cycloaddition.

The interest in asymmetric synthesis is continuously increasing due to the continuous demand for enantiomerically enriched molecules. One of the biggest challenges in this field is to create the maximum number of stereocenters in one reaction with the minimum number of reagents and do so in a highly stereoselective manner. Therefore, asymmetric catalysis is a powerful tool, especially for pericyclic reactions, where several carbon stereocenters can be established simultaneously.

For instance (**Scheme 4**), 1,3-dipolar cycloaddition of azomethine ylides (from imines a) and alkenes b, which allows the stereoselective synthesis of pyrrolidine derivatives c. Among such molecules, which can be obtained through longer and more complicated routes, are very important pharmaceuticals, natural alkaloids and building blocks in organic synthesis. In the 1,3-dipolar cycloaddition, the structure of the

azomethine ylide promotes characteristic frontier molecular orbital (FMO) controlled reactivity with alkenes, which can lead to the formation of four stereocenters with high levels of stereoselectivity.[26-28]

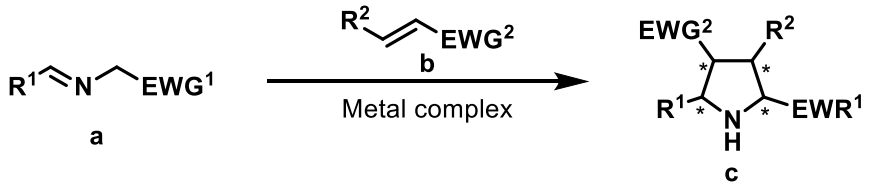


**Scheme 4.** Azomethine ylide-type 1,3-dipolar cycloaddition.

In the field of asymmetric 1,3-dipolar cycloadditions, Lewis acid-catalyzed generation of azomethine ylides (*N*-metalated azomethine ylides) derived from *α*-imino esters and a base has been extensively utilized (**Scheme 5**). This type of Lewis acid catalysis, whose foundation was laid by the work of Grigg from 1980 to the 1990s, relies on the Lewis acid-activation of the *α*-imino esters **38**, which then undergo deprotonation by a base to give *N*-metalated azomethine ylides **39**. The generated azomethine ylides are nucleophilic and react with electron-deficient dipolarophiles to give chiral pyrrolidines **40**. As for the crucial cycloaddition mechanism, not only a concerted 1,3-dipolar cycloaddition, but also a stepwise Michael addition/Mannich-type cyclization is conceivable.[29-34]

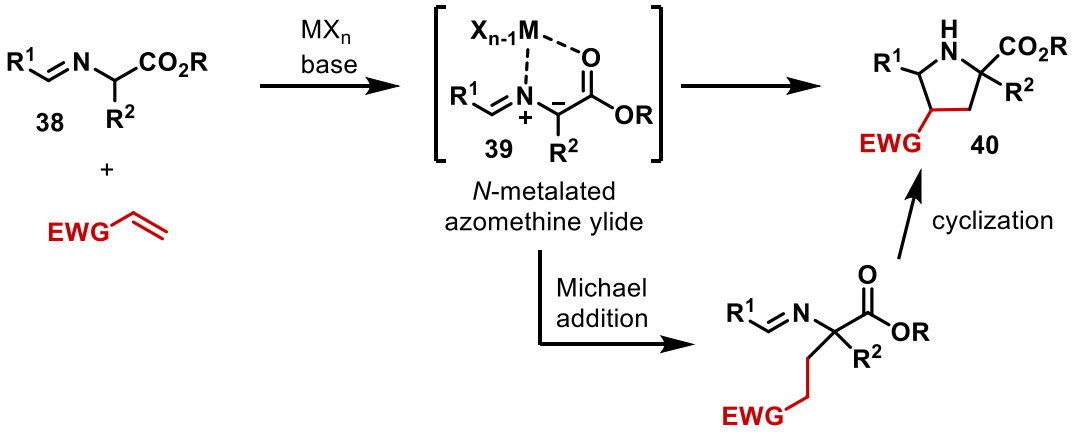


**Scheme 5.** 1,3-dipolar cycloaddition of *N*-metalated azomethine ylides.

What's more, Jørgensen and co-workers developed a variety of Lewis acidic metals in combination with chiral ligands for the highly enantioselective 1,3-dipolar cycloaddition of azomethine ylides with acrylate (**Scheme 6**). The reactions are catalyzed by zinc (II) bisoxazolines and proceed in high yield, thus giving single diastereomer products with up to 94% *ee*. Furthermore, this reaction provides an easy entry to optically active highly substituted pyrrolidines.[35]

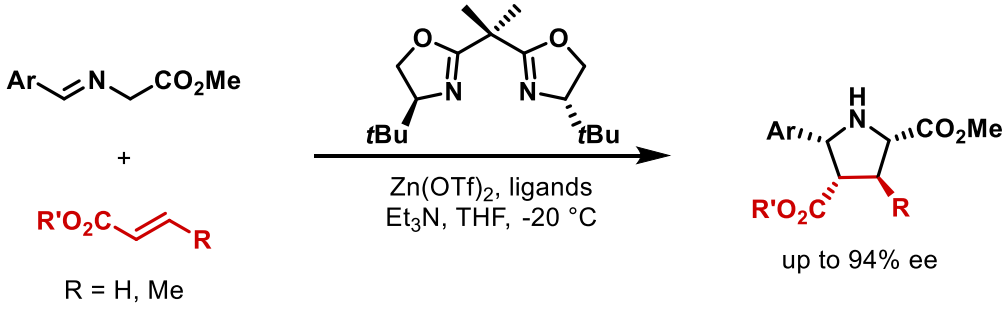


**Scheme 6.** Chiral zinc-catalyzed 1,3-dipolar cycloaddition of azomethine ylides.

In the work by Grigg and co-workers, they mentioned that not only Lewis acid but also Brønsted acid is able to accelerate 1,3-dipolar cycloaddition of azomethine ylides.

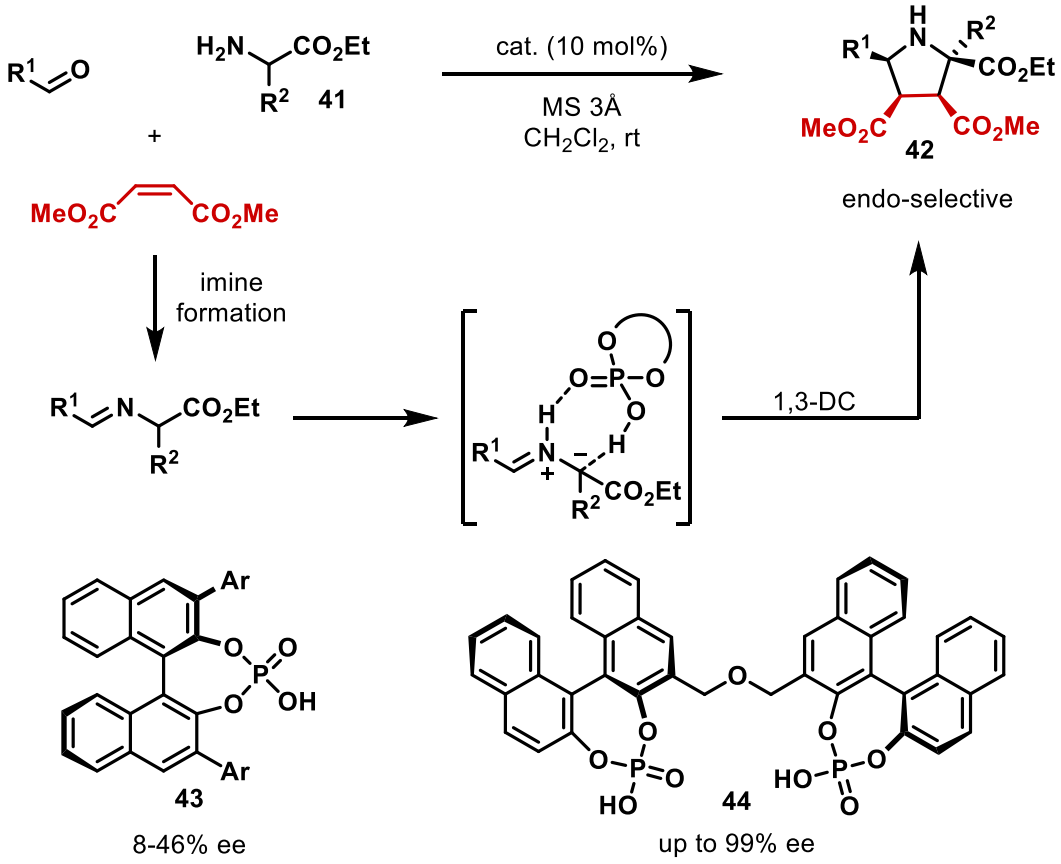


**Scheme 7.** Chiral bisphorsphoric acid-catalyzed 1,3-dipolar cycloaddition.

In 2008, Gong and co-workers reported the first catalytic asymmetric 1,3-dipolar cycloaddition of azomethine ylides catalyzed by chiral Brønsted acids (**Scheme 7**). Gong and co-workers investigated the three-component reaction of aldehydes, 2-aminomalonate **41**, and dimethyl maleate, wherein the separate synthesis of *α*-imino esters is not required. As the screening of chiral monophosphoric acids **43** revealed their

poor performance in terms of the enantioselectivity, they designed chiral bisphosphoric acid **44** based on a linked BINOL to attain high endo- and enantioselectivity. Not only 2-aminomalonate, but a variety of *α*-arylglycine esters were also utilized to give pyrrolidines **42**. While the higher temperature (70 °C) and prolonged reaction time (2−3 days) were required, the reaction could even be implemented with *α*-alkyl amino acid esters with high stereoselectivities.[36-41]

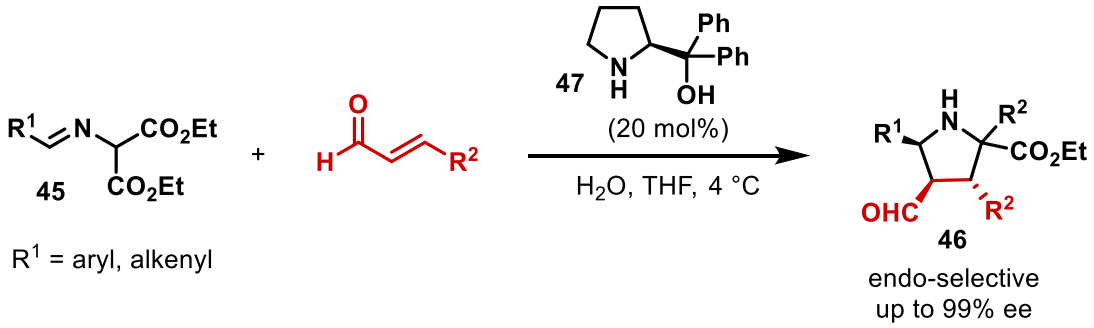


**Scheme 8.** Iminium-catalyzed 1,3-dipolar cycloaddition of *α*-imino malonates with enals.

The application of iminium catalysis in 1,3-DC of azomethine ylides was developed by Vicario's group in 2007 (**Scheme 8**).[42-44] The *α*-imino malonates **45** were selected as a substrate of azomethine ylide in consideration of their higher acidity and screening of chiral secondary amine catalysts using crotonaldehyde as dipolarophile was performed. It was discovered that diphenylprolinol **47** was the best catalyst to give significant quantities of pyrrolidines **46** with high endo- and enantioselectivities. Although their original paper showed the formation of azomethine ylide via 1,2 proton transfer and its concerted 1,3-dipolar cycloaddition with the iminium species, the later computational study supported the stepwise Michael addition/Mannich cyclization sequence.

## 2.4. Model study towards the typical [3+2] cycloaddition of amino salt 16

Model studies were performed to establish the feasibility of the [3+2] cycloaddition reaction which was accomplished using a Brønsted acid catalyzed reaction with azomethine ylides (**Table 1**).

**Table 1.** 1,3-dipolar cycloaddition of amino salt **48**.

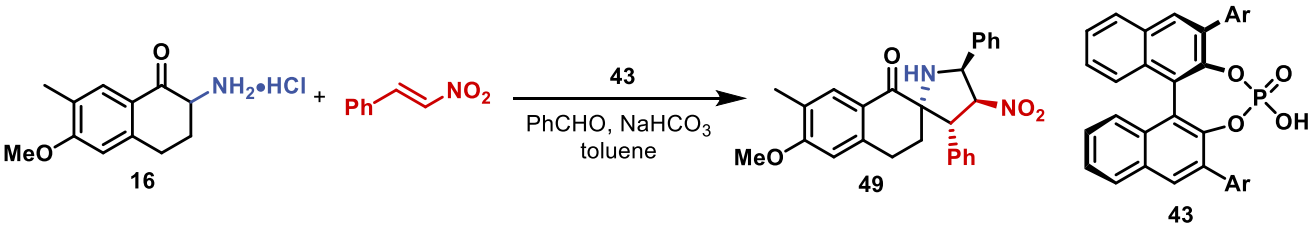


| entry | conditions[a] | temprature | yield (%) |
|---|---|---|---|
| 1 | catalyst (0.1 equiv)<br>12 h | rt | 10% |
| 2 | catalyst (0.1 equiv)<br>48 h | rt | 20% |
| 3 | catalyst (0.1 equiv)<br>16 h | reflux | 22% |
| 4 | catalyst (0 equiv)<br>12 h | rt | none |
| 5 | catalyst (0 equiv)<br>12 h | reflux | trace |

The reaction of the amino salt **16**, prepared in quantitative yield from the *α*-tetralone, with the *trans*-nitro alkene and benzaldehyde in the presence of catalytic quantities of chiral monophosphoric acid **43**. The reaction condition was initially the same as a developed method which can be observed in entry 2. Out of all entries, the reaction time and catalyst affected the yield most significantly; interestingly, the reaction temperature seemed not a factor to the reaction. Moreover, because of the unstable imine

intermediate, we had to set up a one pot reaction combining both the imine formation and the 1,3-dipolar cycloaddition.[45]

Although the yield of this 1,3-dipolar cycloaddition was not optimal, we were still delighted to observe that under the almost same reaction conditions as those previously developed the *β*-position of the *α*-tetralone could be functionalized to a spiro-heterocycle moiety in one-pot reaction.

From the outset, we envisioned a bond disconnection which is through a 1,3-dipolar cycloaddition to build up the most challenging spiro-lactam in the natural product. Based on the model study in the **Table 1**, we decided to start with a Lewis acid-catalyzed generation of the azomethine ylides 1,3-dipolar cycloaddition on the amino salt **16** (**Table 2**). The imine intermediate could not be trapped either, due to the high unstability. Therefore, a one-pot reaction between the amino salt **16**, benzaldehyde and monosubstituted alkene was required. In entry 5, a Ag(I) salt as Lewis acid was tried to catalyze the reaction. However, there was no desired product observed. Subsequently, the catalyst was switched to $Zn(OTf)_2$ which performed better than Ag(I). After screening different bases, the reaction with $NaHCO_3$ and catalytic quantities of $Et_3N$ successfully afforded the desired spiro-product **37** in 35% yield.[35]

**Table 2.** Model study towards Lewis acid-catalyzed 1,3-dipolar cycloaddition of amino salt **16**.

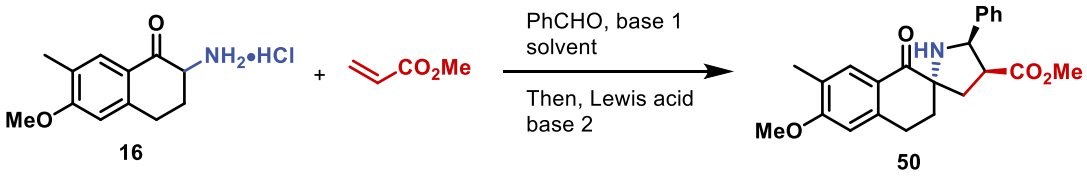


| entry | base 1 + base 2 | conditions | yield (%) |
|---|---|---|---|
| 1 | $NaHCO_3$ (1 equiv) + $NaHCO_3$ (0.1 qeuiv) | $Zn(OTf)_2$, THF | trace |
| 2 | $NaHCO_3$ (1 equiv) + $Et_3N$ (0.1 qeuiv) | $Zn(OTf)_2$, THF | 8% |
| 3 | $Et_3N$ (1 equiv) + $Et_3N$ (0.1 qeuiv) | $Zn(OTf)_2$, THF | 34% |
| 4 | $NaHCO_3$ (1 equiv) + $Et_3N$ (0.1 qeuiv) | $Zn(OTf)_2$, THF | 35% |
| 5 | $NaHCO_3$ (1 equiv) + $Et_3N$ (0.1 qeuiv) | AgOTf, THF | none |
| 6 | $NaHCO_3$ (1 equiv) + $Et_3N$ (0.1 qeuiv) | $Zn(OTf)_2$, DCM | 16% |
| 7 | $NaHCO_3$ (1 equiv) + $Et_3N$ (0 qeuiv) | **43**, toluene | 15% |

Furthermore, to determine the structure of compound **50**, the secondary amine **50** was protected with TsCl to generate the stable white solid **51** in 61% yield. Crystallization of **51** was achieved in $CH_2Cl_2$/hexane, and its structure was determined by X-ray diffraction (**Scheme 9**).

Based on the data, although the product is racemic, the 1,3-dipolar cycloaddition was highly diastereoselective with the spiro-pyrrolidine substituents *cis* and both are *trans* to the tosyl group.

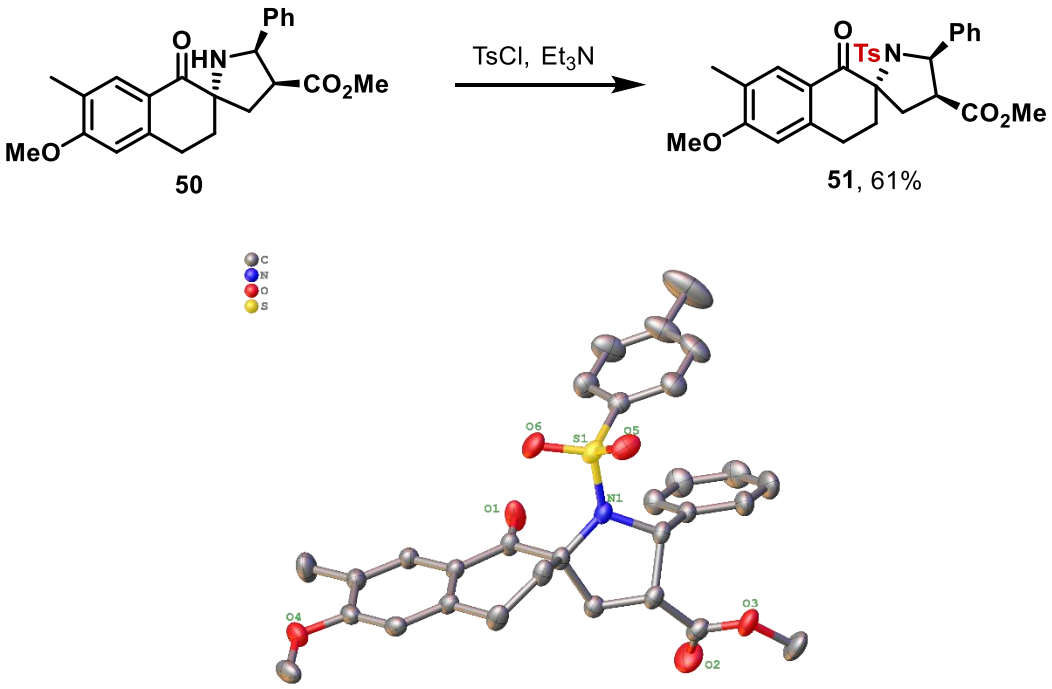


**Scheme 9.** Protecting and structure determination of compound **51**.

### 2.5. Initial strategy towards a novel [3+2] cycloaddition of formamide 10

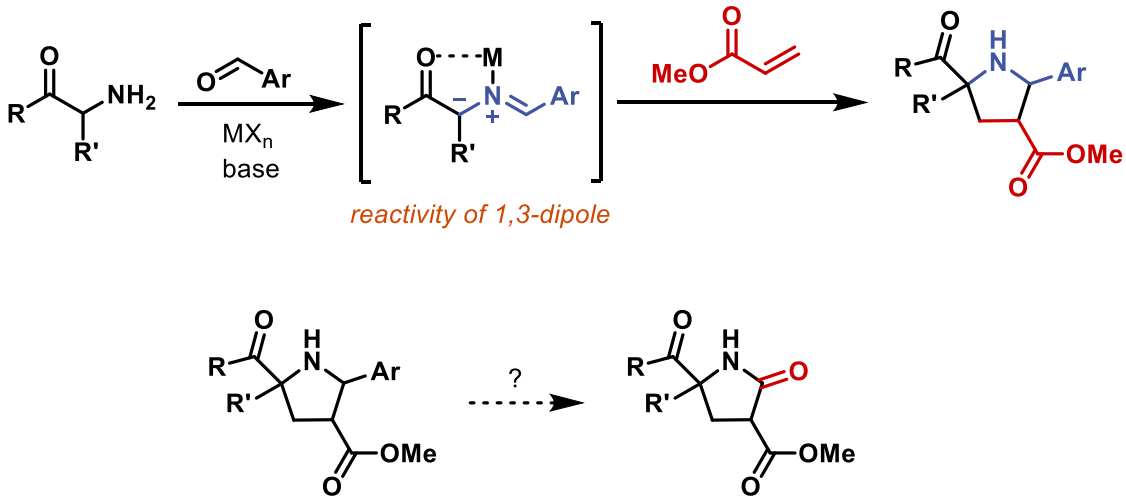


**Scheme 10.** Aryl imine-type 1,3-dipolar cycloaddition.

In most cases of azomethine ylide-type 1,3-dipolar cycloadditions, the aryl imines act as the 1,3-dipole to generate azomethine ylides with Lewis acid and thus there's always an α-aryl group located on the pyrrolidine product (**Scheme 10**). However, due to the structurally demanding core in ansalactam A, the aryl group must be transformed to a carbonyl group. Therefore, we envisioned activation of the formamide group with electrophiles, triggering formation of an oxy-azomethine-type 1,3-dipole. Subsequent reaction with an α, β-unsaturated carbonyl compound, in a concerted or stepwise fashion, would then forge the desired spiro-γ-lactam through a formal [3+2] process (**Scheme 11**).

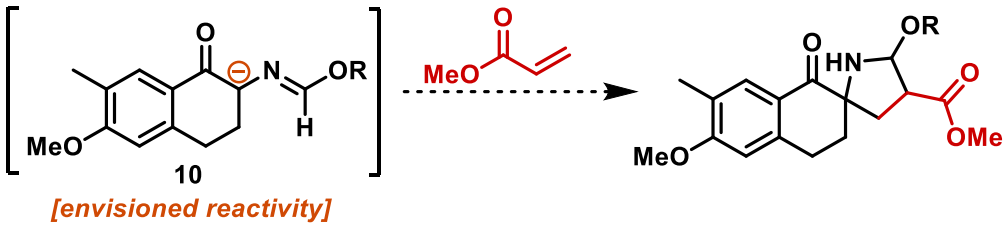


**Scheme 11.** Proposed [3+2] process.

At the beginning, we tried to generate either alkyl (methyl or ethyl) ether **10** or silyl (TMS or TBS) ether **10** as the 1,3-dipole. Unfortunately, none of the substrate **10** could be afforded in the following [3+2] process. Having explored a strong EDG on the imino carbon, we then proposed to stabilize the imino ether intermediate through using a EWG as the R group. Finally, we found that the activation of the formamide group with triflic anhydride, triggering formation of either an oxy-azomethine-type 1,3-dipole or isocyanide. To explore this approach, we first employed methyl acrylate as the reaction partner in the presence of $Et_3N$ (not rigorously dried), resulting in the formation of a five-membered spirocyclic product **17** in 65% yield that possessed an inversed regioselectivity, but

desired stereochemical outcome yet had lost the oxygen atom from the formamide group (**Scheme 12**).

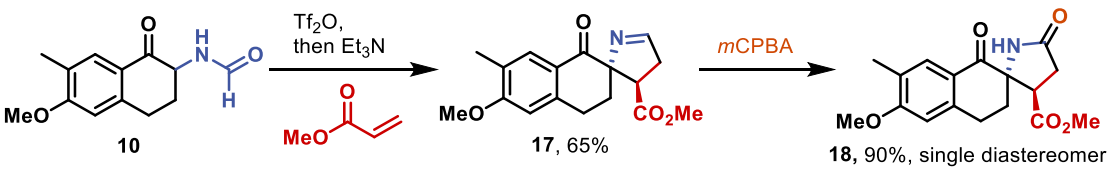


**Scheme 12.** Initial exploration of the proposed [3+2] cycloaddition with methyl acrylate.

This result suggested that the reaction was proceeding through an isocyanide intermediate to afford an inversed regioselectivity, but questions regarding mechanistic aspects of this process remained. Given the stoichiometric quantities of acid present, it is likely that the added amine base was functioning not only as a proton shuttle and a source of trace water (addition of small quantities of water alone was not as effective). The oxidation of imine **17** to the corresponding lactam **18** using *m*CBPA provided the target spiro-γ-lactam in 90% yield and as a single isolated diastereomer, the absolute stereochemistry of which was assigned though X-ray analysis (**Figure 8**).

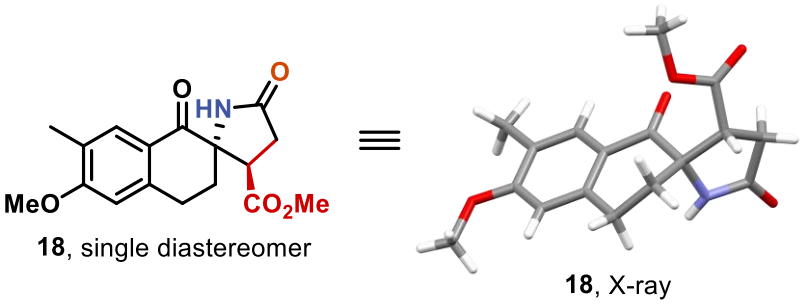


**Figure 8.** X-ray structure of spiro-γ-lactam **18**.

Unfortunately, all attempts to alkylate or otherwise functionalize this compound to install the isobutyl group failed. We then sought to incorporate this sterically demanding group into the dipolarophile component of the key [3+2] reaction. To probe this approach, formamide **10** was activated with triflic anhydride and reacted with enoate **9** (**Scheme 13**), ultimately providing **20** in a modest 28% yield over the two steps after oxidation of **19** with *m*CPBA. Only one regioisomer was isolated from this reaction, albeit the low yield makes the overall selectivity uncertain.

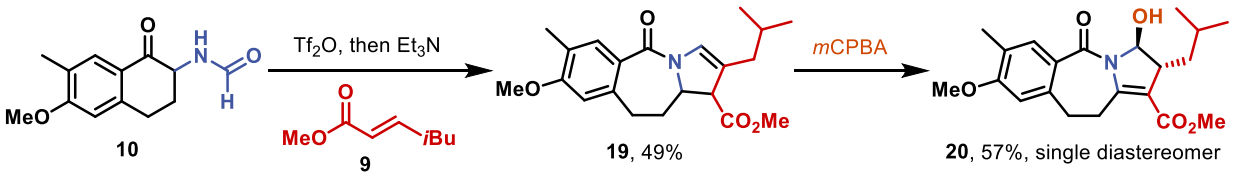


**Scheme 13.** Initial exploration of the proposed [3+2] cycloaddition with enoate **9**.

Characterization of the product revealed that a skeletal rearrangement had occurred, and this was further corroborated by X-ray analysis (**Figure 9**).

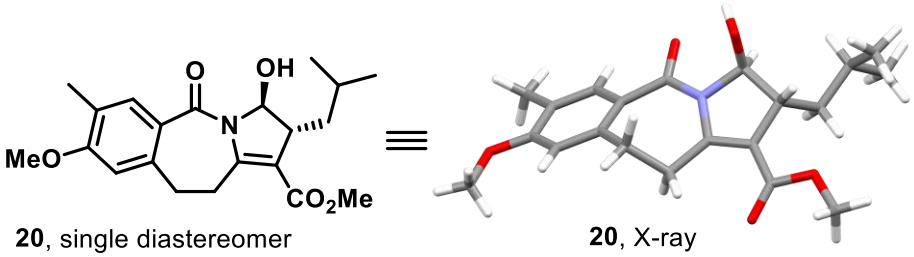


**Figure 9.** X-ray structure of **20**.

At this stage, it was not clear what drives this ring expansion, but we hypothesized that the existence of isobutyl side chain drives a tautomerization from spiro-imine to spiro-enamine, allowing a pathway for the nucleophilic attack of *N* atom to dominate (**Scheme 14**). While this transformation was not relevant to the synthesis of this family of natural products, the structural complexity generated in this process may be of interest in other contexts.

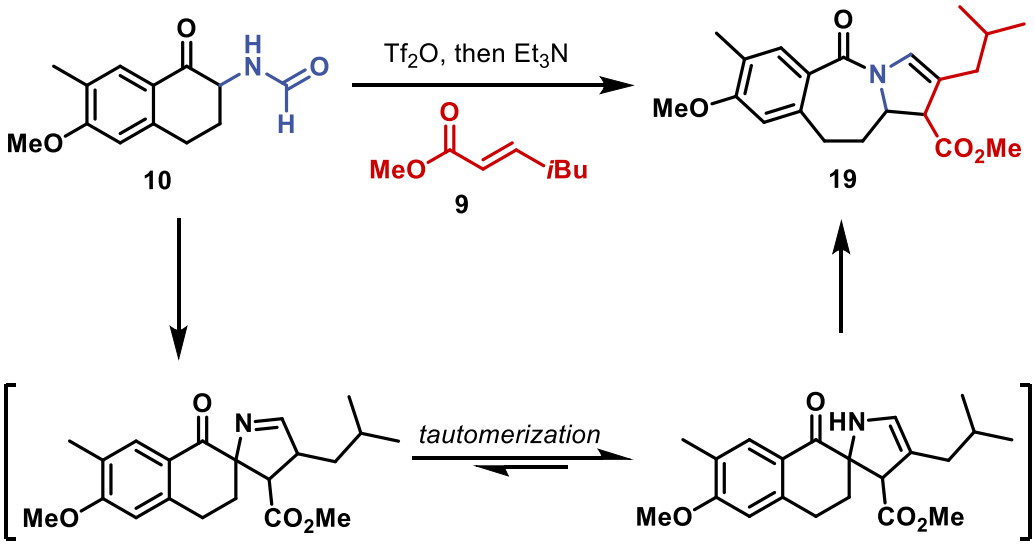


**Scheme 14.** Proposed reaction pathway to provide the rearrange

### 2.6. Studies towards the mechanism of the novel [3+2] cycloaddition

It was clear that a novel [3+2] cycloaddition could be utilized to forge the desired spiro lactam, but further optimization was required to incorporate the isobutyl side chain contained in the natural product. Mechanistically, we originally envisioned this transformation proceeding via azomethine ylide-type reactivity (**Figure 10a**), but observation of deoxygenated imine product **17** and inversed regioselectivity suggest the formation of such an intermediate was unlikely in the presence of strongly electrophilic

activating agents ($Tf_2O$). Instead, we propose formation of a protonated isocyanide intermediate (**22**) under the strongly acidic reaction conditions (**Figure 10b**). Activation of **10** in the absence of an electrophilic reaction partner yielded oxazole **21** (confirmed by X-ray analysis), further suggesting the intermediacy of such an isocyanide species. Furthermore, this isolated compound is a competent reactant in the desired [3+2] reaction under the same conditions, supporting its formation during the course of the reaction. Control experiments have confirmed the requirement of a strong acid, with no reaction observed under neutral or basic reaction conditions. We propose that protonated isocyanide **21** is critical for driving the observed reactivity and inversed regiochemical

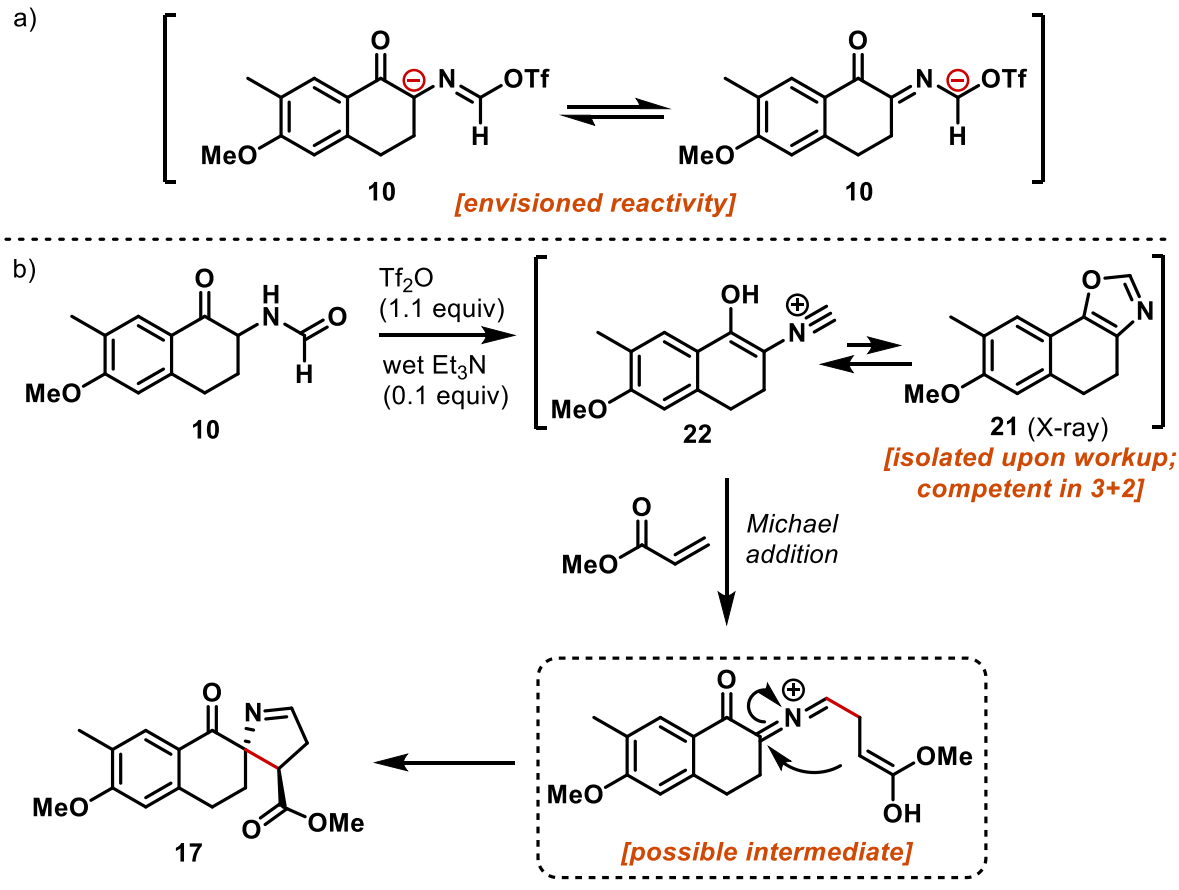


**Figure 10.** (a) Initially envisioned reactivity. (b) Proposed reaction pathway to provide **17**.

outcome as the compound can react between an extended enolate and a possible iminium ion, enabling closure of the ester enol in a stepwise fashion; however, we cannot rule out the possibility of the protonated oxazole itself as an intermediate in the reaction. Additional mechanistic studies are underway to further probe this reaction and identify pathways to render it asymmetric.

### 2.7. Realizing the desired [3+2] cycloaddition with allenes as dipolarophiles

**Table 3.** Optimization of the reaction with allene **23**.

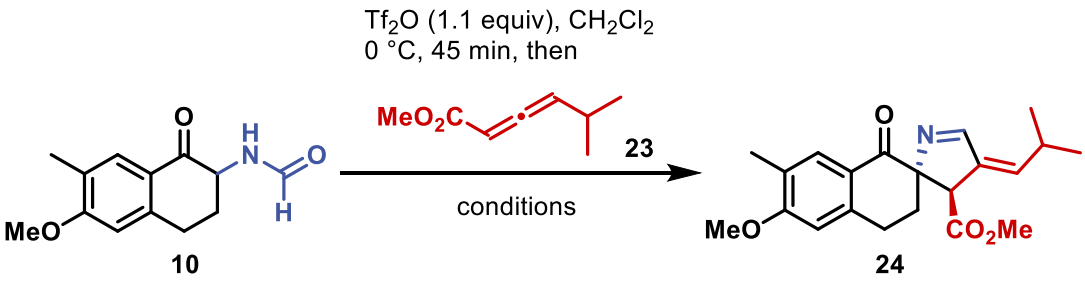


| entry | conditions[a] | concentration | **24** (%)[b,c] |
|---|---|---|---|
| 1 | $Et_3N$ (0.1 equiv), **23** (2 equiv) $CH_2Cl_2$, rt, 16 h | 0.1M | 15% |
| 2 | $Et_3N$ (0.1 equiv), **23** (2 equiv) toluene, rt, 16 h | 0.1M | trace |
| 3 | $Et_3N$ (0.1 equiv), **23** (2 equiv) $CH_2Cl_2$, rt, 16 h | 1 M | 26% |
| 4 | $Et_3N$ (0.1 equiv), **23** (2 equiv) $CH_2Cl_2$, rt, 16 h | 4 M | 40% |
| 5 | $Et_3N$ (0.1 equiv), **23** (2 equiv) $CH_2Cl_2$, rt, 48 h | 4 M | 62% |
| 6 | $Et_3N$ (1 equiv), **23** (2 equiv) $CH_2Cl_2$, rt, 16 h | 0.1 M | trace |

*[a]wet $Et_3N$ used in all cases [b]E/Z isomers isolated after column chromatography [c]isolated yield of E/Z isomers.*

Given our lack of success utilizing substituted electrophilic alkenes as dipolarophiles, we sought to explore allenes as alternate reactants. It was hypothesized that the planar nature of these compounds would limit the impact that sterics may have played in our preliminary studies of the [3+2] cycloaddition and the extra double bond would avoid the undesired tautomerization. Our first effort in this regard employed allene **23** under conditions identical to those utilized previously for the alkene reactants (entry 1, **Table 3**). This reaction proceeded in low conversion after 16 hours, but provided the desired extended imine product **24** in 15% isolated yield as a mixture of *E* and *Z* alkene isomers. We isolated only one diastereomer from these reactions, likely due to the proposed intramolecular sprio center-forming reaction. Further optimization identified $CH_2Cl_2$ as a more suitable solvent at increased concentrations and reaction times, ultimately providing a 62% yield (entries 2−5, **Table 3**). As described above, neutralizing the reaction mixture by employing stoichiometric quantities of triethylamine inhibited the reaction, highlighting the importance of Bronsted acid in this transformation (entry 6, **Table 3**).

# Chapter 3: Synthesis of the Spirocyclic γ-Lactam Core 7

## 3.1. Conversion of 24 to the northern fragment of ansalactam A (7)

With compound **24** in hand, we explored various sequences to reduce the exocyclic alkene and oxidize the imine to reveal the targeted spiro-γ-lactam **7** (**Figure 11**). Hydrogenation of **24** in EtOH using Pd/C chemoselectively reduced the extended imine, forming isobutyl-substituted imine **25**. Oxidation of this compound under Pinnick oxidation conditions resulted in the formation of lactam **7** in 63% yield over the two steps as a single isolated diastereomer.[46] Previously employed *m*CPBA conditions only provided undesired epoxide. Compound **7** represents the entire carbon skeleton of the northern domain of ansalactam A (**1**), lacking only the hemiquinone carbonyl of the natural product.

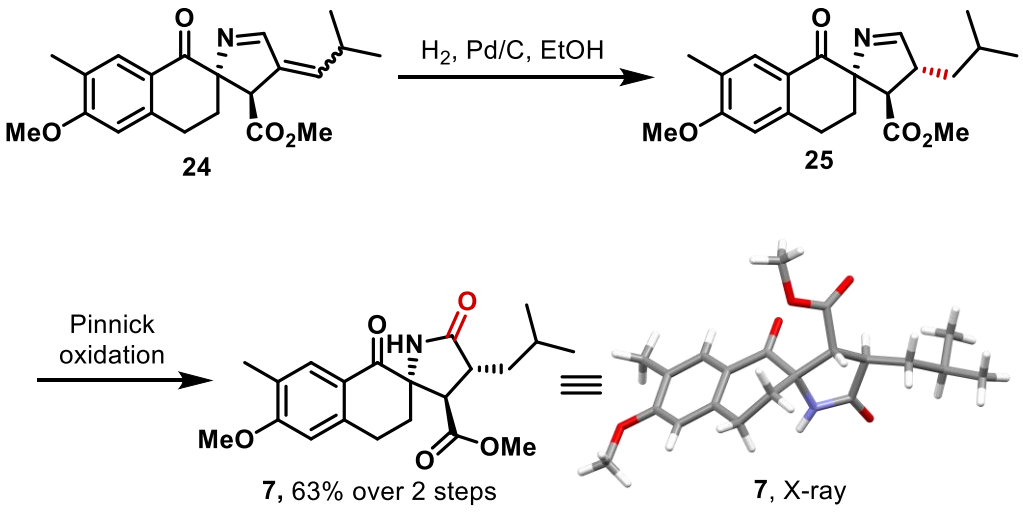


**Figure 11.** Conversion of **24** to northern fragment of ansalactam A (**7**).

In conclusion, we have developed the first stereoselective approach to the core of the ansalactam natural products. Additionally, the methods presented herein are relevant for the synthesis of other natural product scaffolds and bioactive molecules.

# Chapter 4: Exploration to assembly of the chain fragments

## 4.1. Initial strategy and attempts toward assembly of the diene fragment

To finish the installation of the polyketide chain, we sought to assemble the diene fragment first. With **7** in hand, we envisioned a Friedel-Crafts acylation with acid chloride **52**, assuming formation of the desired product **53.** However, after we explored a variety of Lewis acids and reaction conditions, the desired product **53** was never observed. Instead, only trace quantities of the *N*-acylated side product and starting material **7** were detected (**Table 4**).

**Table 4.** Attempts toward Friedel-Crafts acylation.

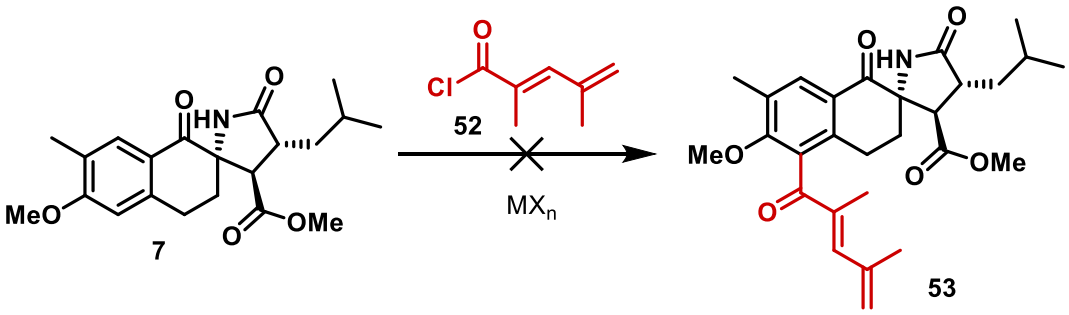


| entry | conditions | results |
|---|---|---|
| 1 | $TiCl_4$, toluene, rt, 16 h | only SM |
| 2 | $AlCl_3$, DCE, rt, 4 h | only SM |
| 3 | $InCl_3$, DCE, rt, 16 h | only SM |
| 4 | $InCl_3$, DCE, 60 °C, 16 h | SM and *N*-acylated product |

Then, the activation of phenyl bromide **26** with a lithium reagent was proposed, triggering nucleophilic attack to the corresponding aldehyde.[7] Although the activation proceeded well, the addition product **55** was never detected under these conditions (**Scheme 15**).

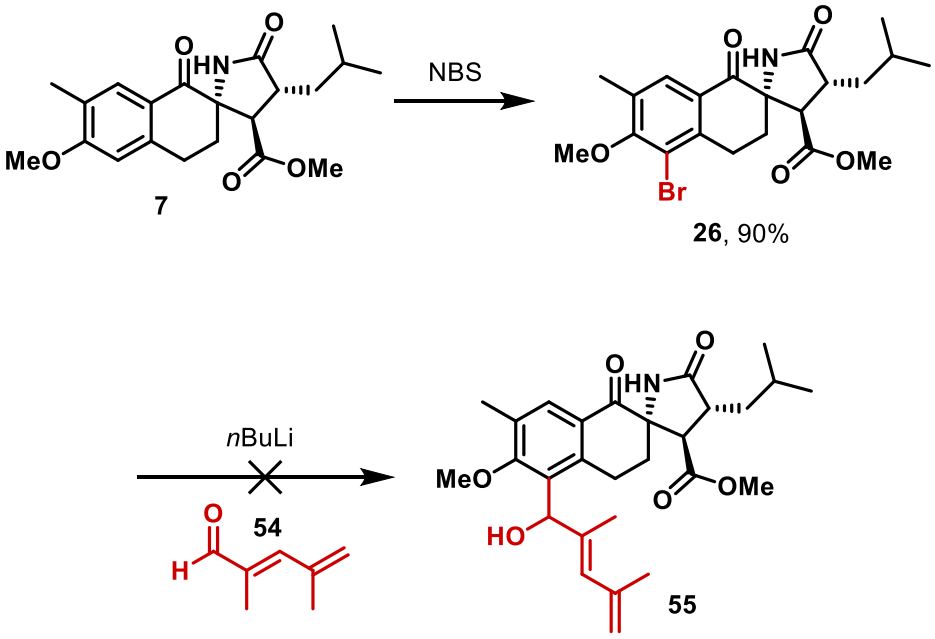


**Scheme 15.** Attempts towards nucleophilic attack to aldehyde **54**.

Additionally, different coupling reactions were tried to afford the desired product **55**, such as NHK reaction (entry 1 and 2, **Table 5**) and Barbier coupling reaction (entry 3, **Table 5**). Unfortunately, neither attempts were able to generate the desired coupling product **55**, instead, only starting material **26** was observed in the crude mixture.

Based on the failed attempts mentioned above, it was concluded that the phenyl site of **7** should be electron-rich enough, but due to the hindered environment, provides no desired reactivity with electrophiles. Therefore, considering removal of the allyl

carbonyl group in the coupling partner **54** might be a better option to strengthen the reactivity of **26**.

**Table 5.** Attempts towards coupling reactions.

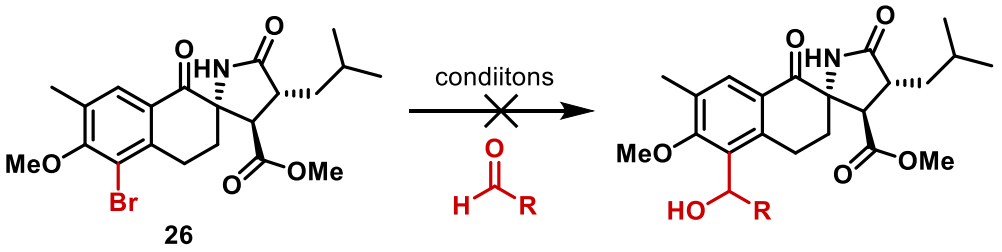


**26**

| entry | conditions | results |
|---|---|---|
| 1 | $NiBr_2$ glyme, Zn<br>THF, 60 °C, 16 h | only SM |
| 2 | $NiI_2$, $CrCl_2$,<br>THF, 60 °C, 16 h | only SM |
| 3 | In, THF,<br>50 °C, 16 h | only SM |

To provide support for our hypothesis, a Pd(0) catalyzed Stille coupling reaction between aryl bromide **26** and diene **27** successfully generated the desired coupling product **28** in 50% yield (**Scheme 16**).[48]

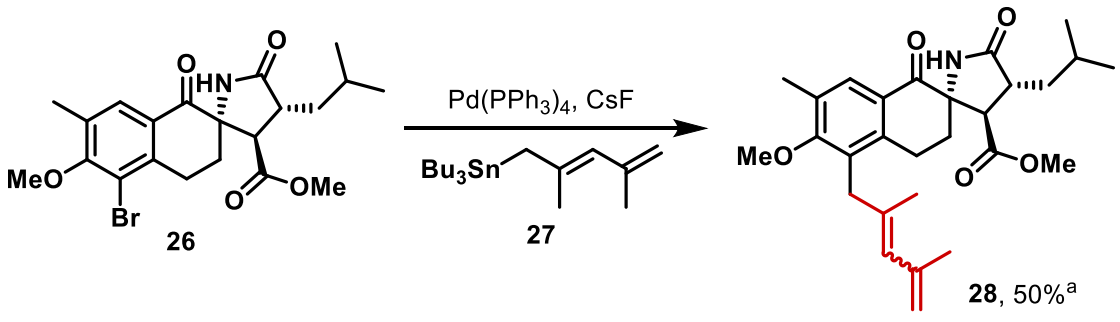


**26** **27**

[a]*isolated yield of E/Z isomers*

**Scheme 16.** Installation of fragment **27**.

### 4.2. Model study towards Barbier coupling reaction and synthesis of fragment 35

With **28** in hand, the stage was set to explore the assembly of the other fragment. We envisioned a Barbier coupling reaction between aldehyde **56** and allyl bromide **58** catalyzed by indium.[57] This reaction has the capability of coupling both partners to afford the desired allylic alcohol **57** in 70% yield (**Scheme 17**).

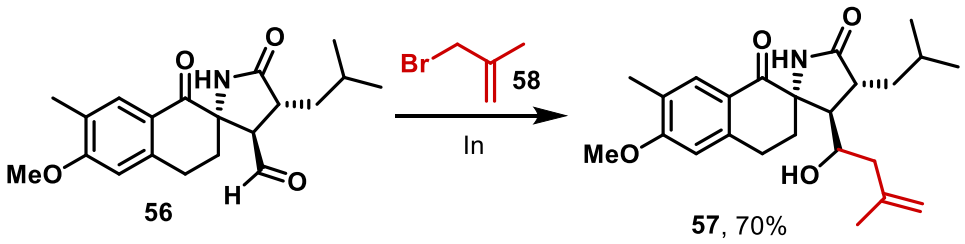


**Scheme 17.** Model study of Barbier coupling reaction.

Based on the success of model study, the preparation of desired allyl bromide

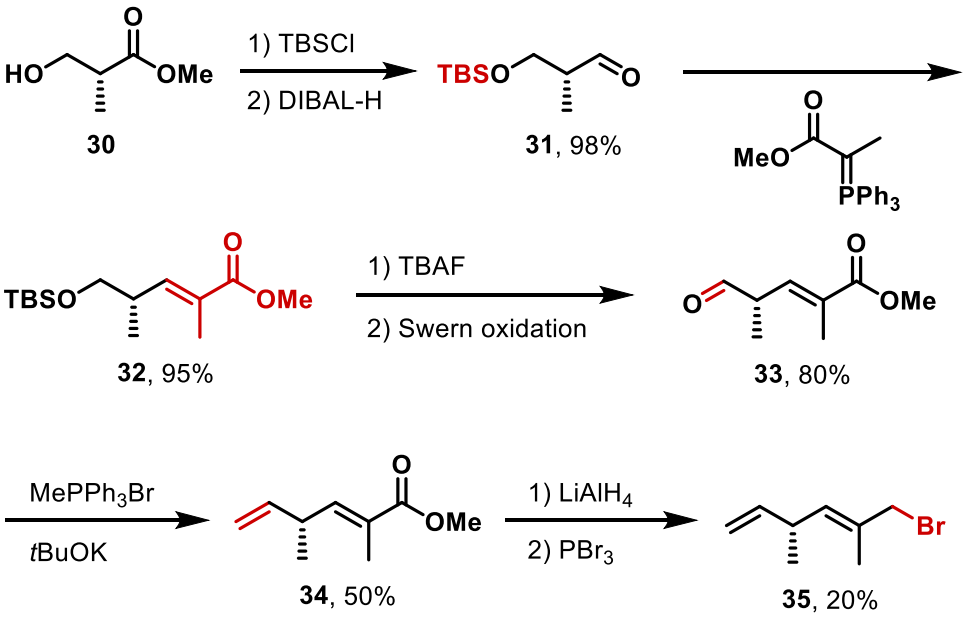


**Scheme 18.** Preparation of bromide **35**.

**35** was achieved through a well-developed route (**Scheme 18**). Beginning with the enantio pure alcohol **30**, TBS protection and reduction provided **31** in 98% yield. Following Wittig olefination, ester **32** was obtained in 95% yield.[49] Subsequent deprotection and oxidation generated desired aldehyde **33** in 94% yield. Lastly, Wittig olefination in 50% yield, LAH reduction and allylic bromination gave the desired fragment **35** in 20% yield over the corresponding steps.

# Chapter 5: Future Plan

With the successful preparation of **57** and allyl bromide **35**, we next planned on installing the fragment **35** through a Barbier coupling reaction. Once complete, we envisioned a subsequent olefin metathesis, thereby closing the southern ring through selective formation of a *Z* alkene.[50-52] The following double allylic oxidations and dehydration would afford the desired product **56**. Finally, the *α*-keto methylation and the late-stage benzylic oxidation would generate the final protected ansalactam A (**Scheme 19**).[53-56]

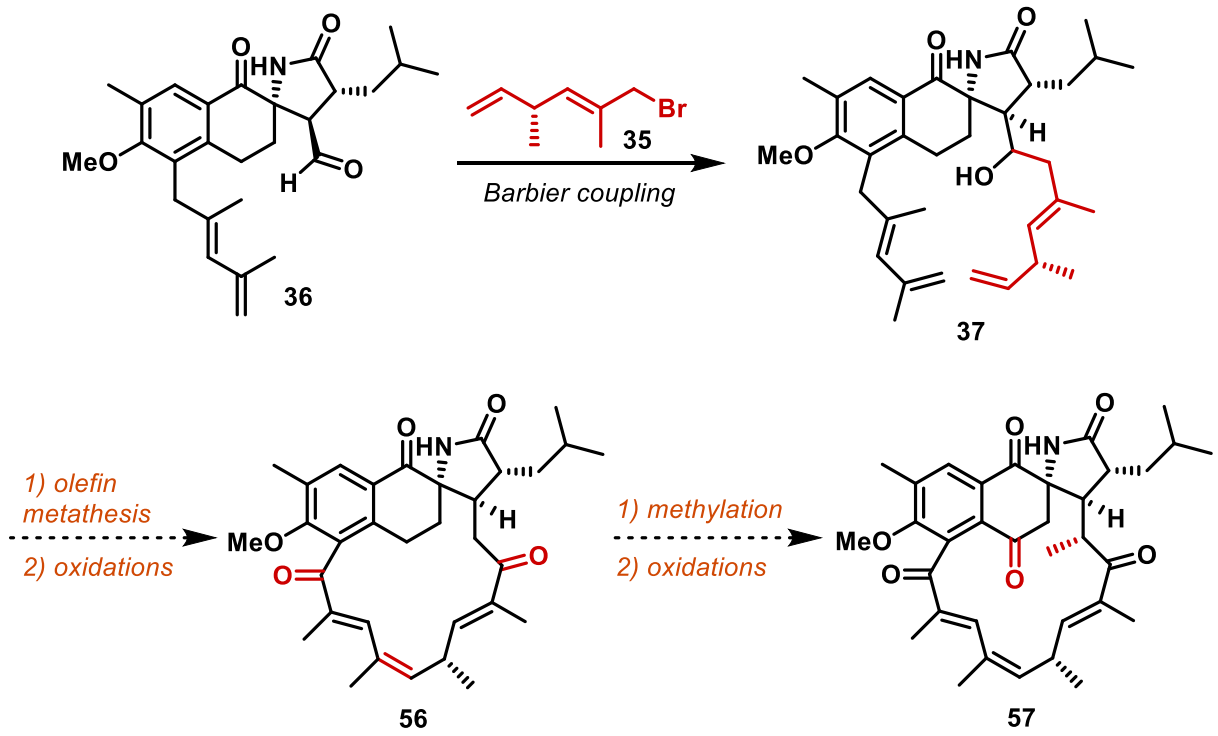


**Scheme 19.** Envisioned route towards protected ansalactam A (**57**).

# Chapter 6: Experimental Data

**General experimental procedures:** All reactions were carried out under an inert argon atmosphere with anhydrous solvents under anhydrous conditions unless otherwise stated. All reactions, except those conducted in the presence of water were carried out in flame-dried apparatus. Heated reactions were performed using an oil bath. Yields refer to chromatographically yield, unless otherwise stated. Reactions were monitored by thin layer chromatography (TLC) analysis (pre-coated silica gel 60 F254 plates, 250 mm layer thickness) and visualization was accomplished with a 254 nm UV light and by staining with $KMnO_4$ solution (1.5 g of $KMnO_4$, 10 g of $K_2CO_3$, and 1.25 mL of a 10% NaOH solution in 200 mL of water) with heating. Reactions were also monitored by LC-MS (2.6 mm C18 50 x 2.10 mm column). Flash chromatography on $SiO_2$ was used to purify the crude reaction mixtures and performed on a Biotage Isolera® utilizing Biotage® cartridges and linear gradients. Diastereomeric ratio was determined by crude $^1H$ NMR spectroscopy.

**Materials:** Tetrahydrofuran (THF) and dichloromethane ($CH_2Cl_2$) were obtained by passing the previously degassed solvents through activated alumina columns under nitrogen atmosphere. Deuterated solvents (containing 0.03 to 0.05 vol % tetramethylsilane, TMS) were purchased from Cambridge Isotope Laboratories. All other reagents were purchased from commercial chemical companies and used without further purification, unless otherwise stated.

**Instrumentation:** Infrared spectra were determined on the Agilent Cary® 630 FTIR spectrometer and data are represented as frequency of absorption ($cm^{-1}$). Melting points were determined on the Thomas Hoover capillary melting point apparatus and data are represented as temperature (°C). $^{1}H$ and $^{13}C$ NMR spectra were obtained on a 500, 600 or 700 MHz instrument in $CDCl_3$ unless otherwise noted. 1D NOE spectra were used to aid structure assignments when necessary. Chemical shifts (δ) were reported in parts per million (ppm) with the residual solvent peak used as an internal standard ($CDCl_3$ $^{1}H$ NMR = 7.26 ppm, $^{13}C$ NMR = 77.16 ppm) and multiplicities are reported as observed. The following abbreviations were used to explain NMR peak multiplicities: s = singlet, d = doublet, t = triplet, q = quartet, p = pentet, dd = doublet of doublets, m = multiples, br = broad. Low resolution mass spectra were obtained using electrospray ionization (ESI). High-resolution mass spectra were obtained on a high-resolution mass spectrometer – the Thermo Fisher Scientific Exactive Plus MS, a benchtop full-scan Orbitrap™ mass spectrometer – using Heated Electrospray Ionization (HESI). The NC State METRIC small molecule X-ray facility collected and analyzed all X-ray diffraction data.

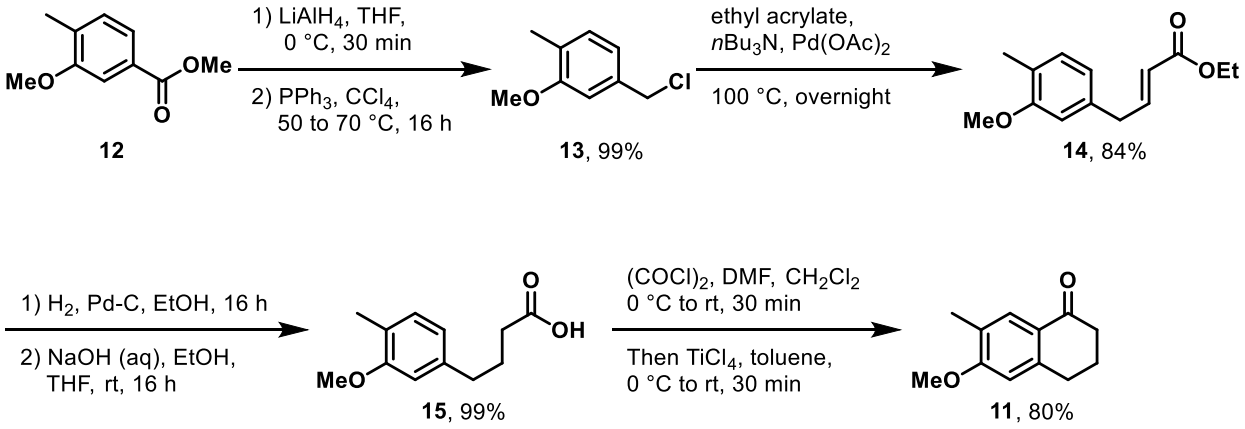


Compound **11**[1,2] was prepared using a reported synthetic method.

***R*f** = 0.35 (1:3, ethyl acetate:hexanes).

**$^1$H NMR** (500 MHz, CDCl3) δ = 7.73 (s, 1 H), 6.54 (s, 1 H), 3.79 (s, 3 H), 2.82 (t, *J* = 7.5 Hz, 2 H), 2.49 (t, *J* = 7.5 Hz, 2 H), 2.11 (s, 3 H), 2.04-1.99 (p, *J* = 6.5 Hz, 2 H).

(1) Kumar, P. Synthesis of substituted 1-tetralones. *Org. Prep. Proced. Int.* **1997**, *29*, 477−480.

(2) Kurata, H., Kusumi, K., Otsuki, K., Suzuki, R., Kurono, M., Komiya, T., Hagiya, H., Mizuno, H., Shioya, H., Ono, T., Takada, Y., Maeda, T., Matsunaga, N., Kondo, T., Tominaga, S., Nunoya, K., Kiyoshi, H., Komeno, M., Nakade, S., Habashita, H. *J. Med. Chem.* **2017**, *60*, 9508-9530.

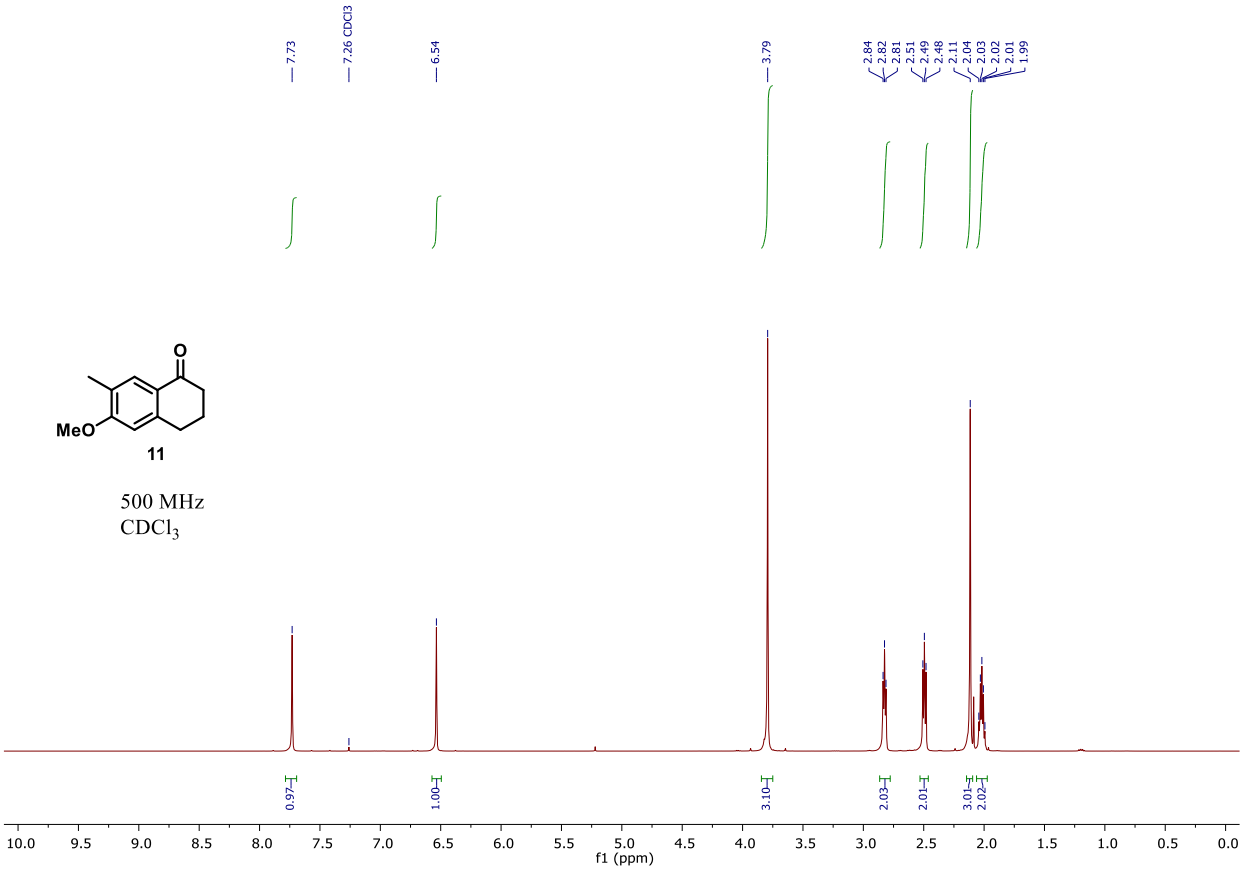


**Figure 12.** $^{1}$H NMR of compound **11**.

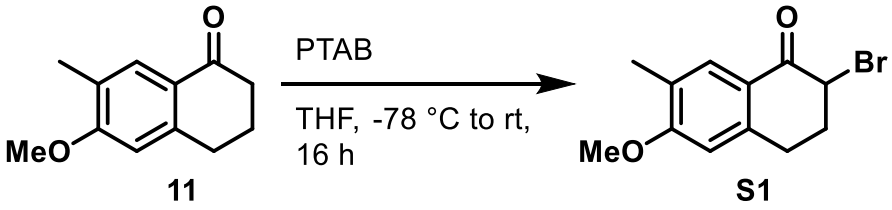


**Compound S1**: To a solution of *α*-tetralone **11** (9.16g, 48.2 mmol) in anhydrous THF (200 mL) was added a solution of phenyltrimethylammonium tribromide (19.0 g, 50.6 mmol) in THF (50 mL) at -78 °C. After stirring at -78 °C for 4 h, the reaction mixture was stirred at rt for another 12 h. The mixture was filtered and concentrated under reduced pressure. The crude product was purified by flash chromatography on silica gel (5-10%, ethyl acetate:hexanes) to yield the product **S1** mixture (12.8 g, 99% yield at 90% purity)**,** based on the proton NMR, it contains ~10% byproduct, as orange oil:

$R_f$ = 0.34 (1:9, ethyl acetate:hexanes).

**$^1$H NMR** (500 MHz, CDCl3) δ = 7.80 (s, 1 H), 6.60 (s, 1 H), 4.62 (t, *J* = 4.5 Hz, 1 H), 3.85 (s, 3 H), 3.25-3.18 (m, 1 H), 2.84-2.78 (m, 1 H), 2.48-2.35 (m, 2 H), 2.14 (s, 3 H).

**$^{13}$C NMR** (125 MHz, CDCl3) δ = 189.6, 162.6, 143.6, 130.6, 126.3, 122.5, 108.8, 55.6, 50.8, 32.2, 26.3, 15.8.

**IR** (Diamond-ATR, neat) $\tilde{\nu}_{max}$ ($cm^{-1}$): 2917, 1674, 1595, 1495, 1341, 1253, 1119, 1046, 918, 891, 843, 736, 668.

**HRMS** (*m/z*): calculated for $C_{12}H_{14}BrO_2$ $[M+H]^+$ 269.0172, found 269.0174.

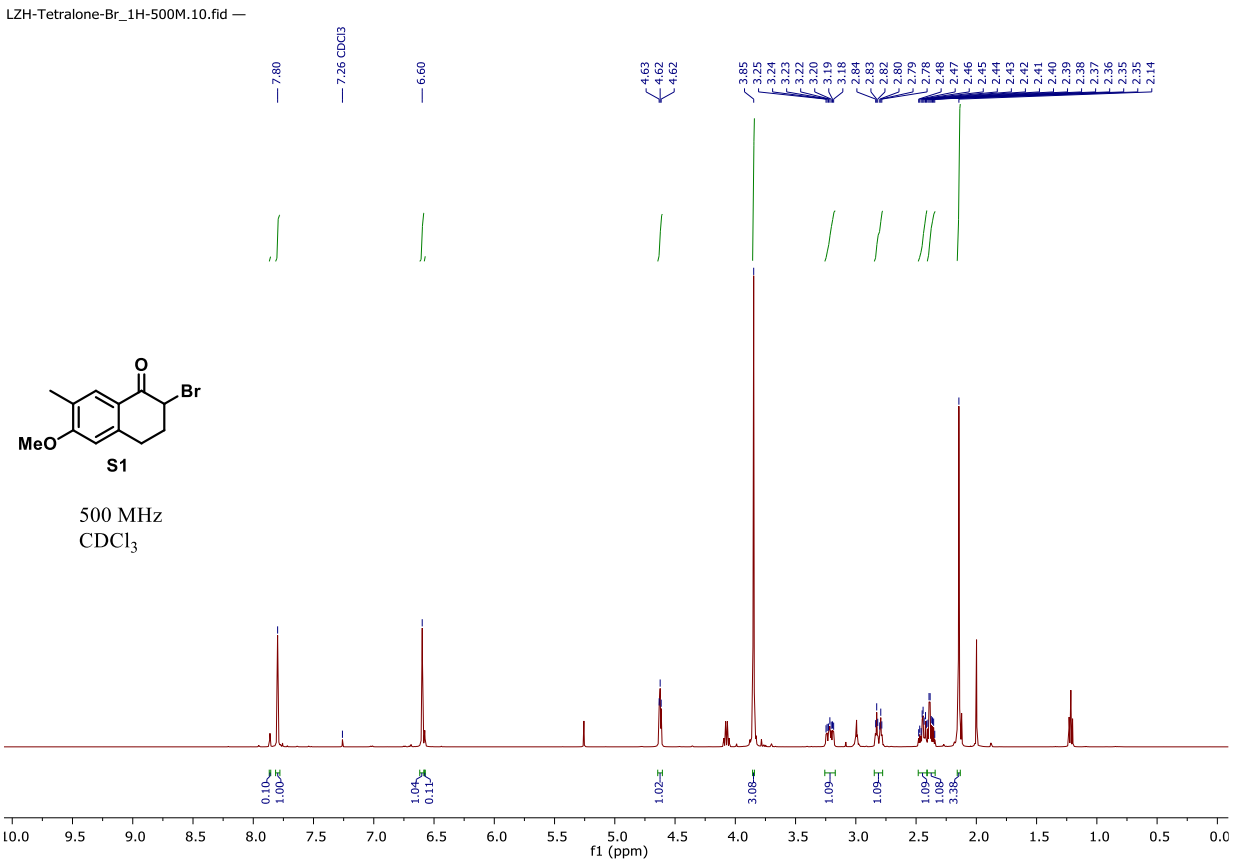


**Figure 13.** $^{1}$H NMR of compound **S1**.

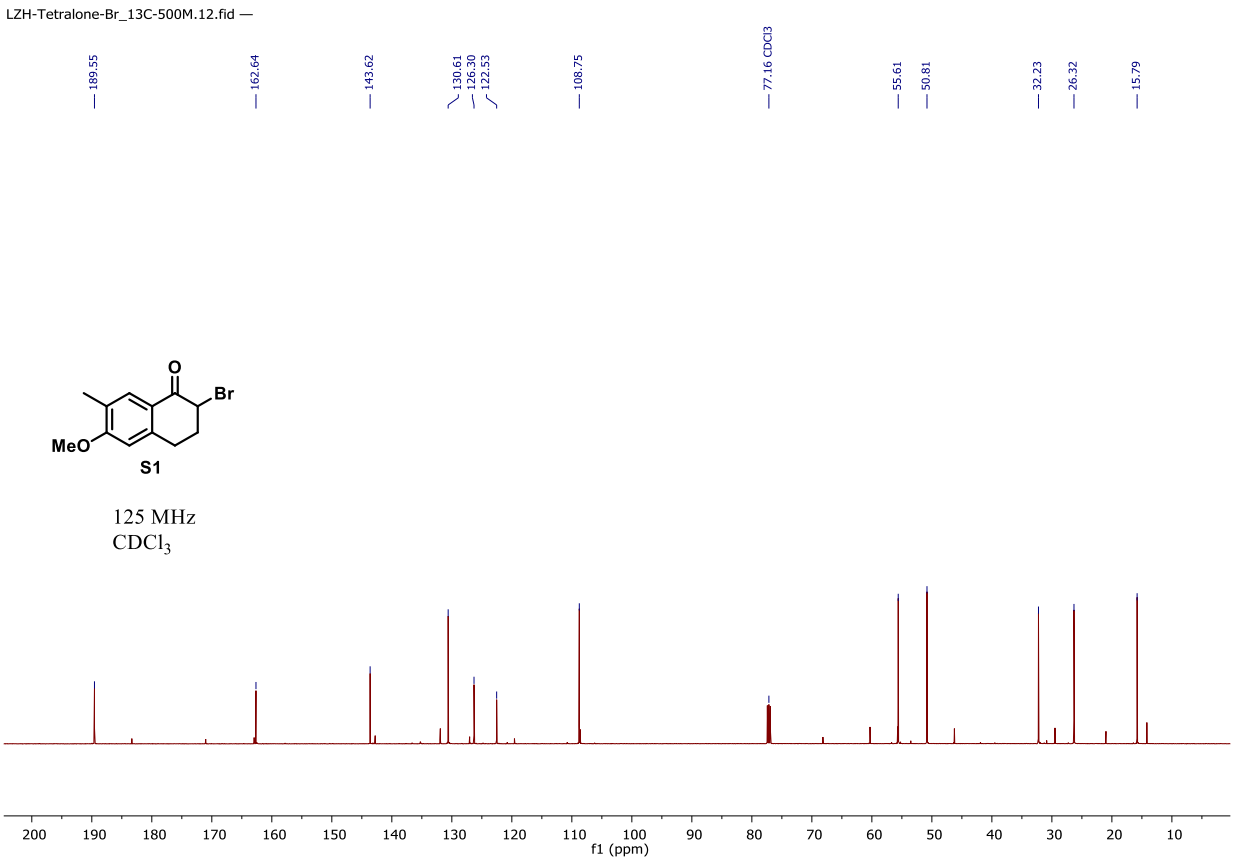


**Figure 14.** $^{13}C$ NMR of compound **S1**.

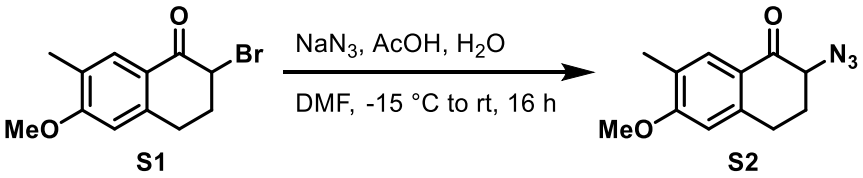


**Compound S2:** To a solution of **S1** (11.7 g, 43.5 mmol) in DMF (220 mL) was added AcOH (6.28 mL, 108 mmol) and a solution of $NaN_3$ (5.65 g, 87.0 mmol) in $H_2O$ (15 mL) at -15 °C. After stirring at from -15 °C to rt for 16 h, the reaction was quenched by the addition of $H_2O$. The mixture was filtered and concentrated under reduced pressure. The crude product was purified by flash chromatography on silica gel (5-10%, ethyl acetate:hexanes) to yield the product **S2** (8.54 g, 85%) as pale purple solid:

$R_f$ = 0.45 (1:3, ethyl acetate:hexanes).

**Melting point** (°C) = 94-96.

**$^1$H NMR** (500 MHz, CDCl3) δ = 7.76 (s, 1 H), 6.57 (s, 1 H), 4.11 (dd, $J_1$ = 5 Hz, $J_2$ = 10 Hz 1 H), 3.85 (s, 3 H), 2.96 (dd, $J_1$ = 5 Hz, $J_2$ = 10 Hz, 2 H), 2.31-2.26 (m, 1 H), 2.15 (s, 3 H), 2.06-1.98 (m, 1 H).

**$^{13}$C NMR** (125 MHz, CDCl3) δ = 192.6, 162.6, 144.0, 129.9, 126.2, 123.7, 108.7, 64.0, 55.6, 29.5, 27.7, 15.8.

**IR** (Diamond-ATR, neat) $\tilde{\nu}_{max}$ ($cm^{-1}$): 2936, 2839, 2100, 1665, 1603, 1500, 1245, 1126, 1053, 988, 898, 845, 767.

**HRMS** (*m/z*): calculated for $C_{12}H_{14}N_3O_2$ $[M+H]^+$ 232.1081, found 232.1080.

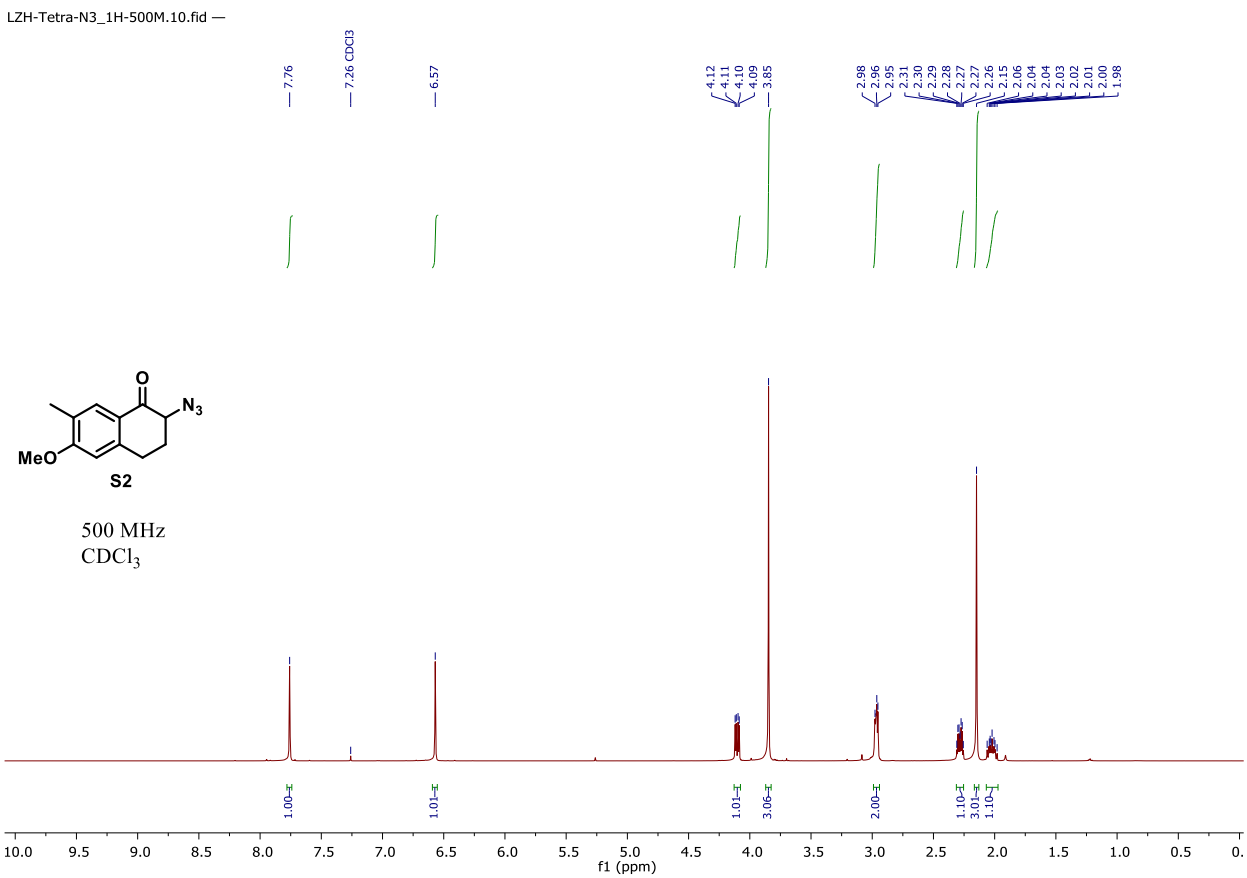


**Figure 15.** $^{1}$H NMR of compound **S2**.

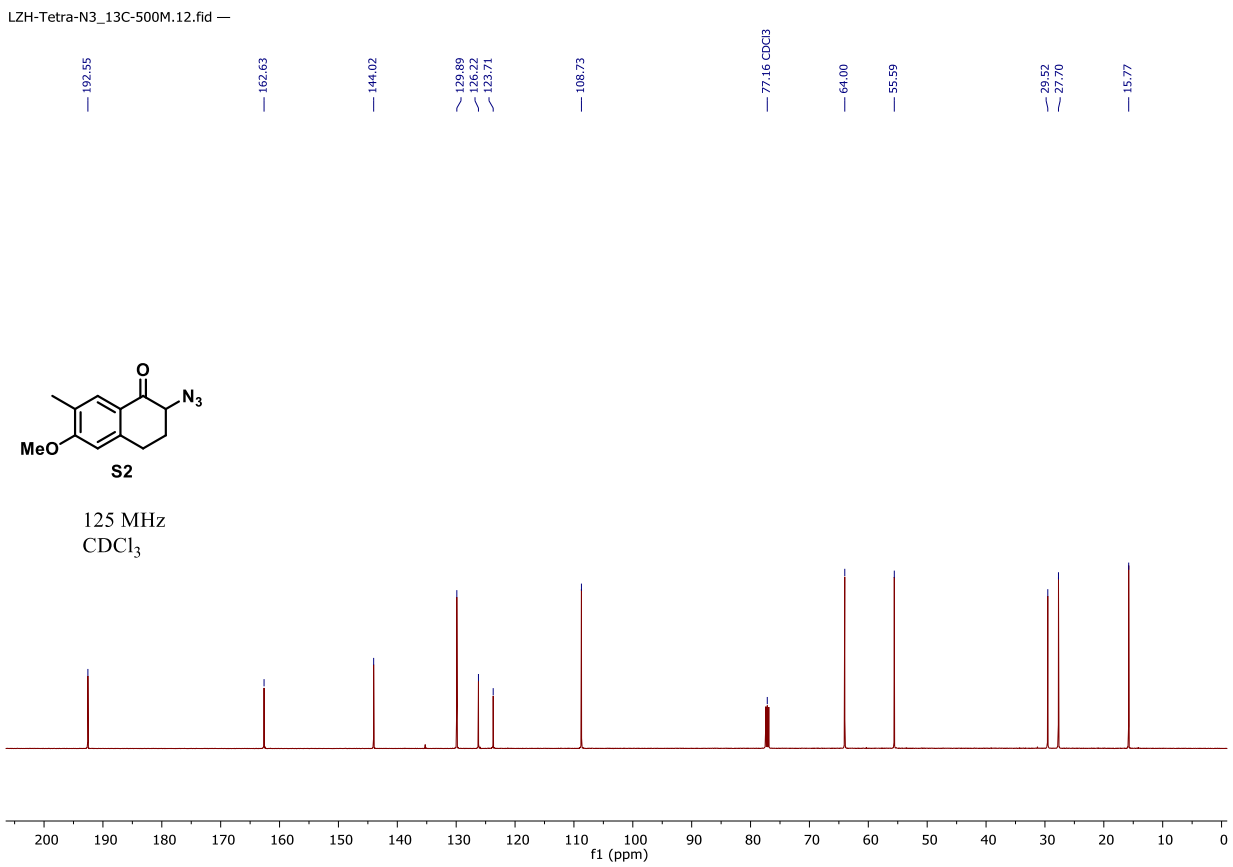


**Figure 16.** $^{13}C$ NMR of compound **S2**.

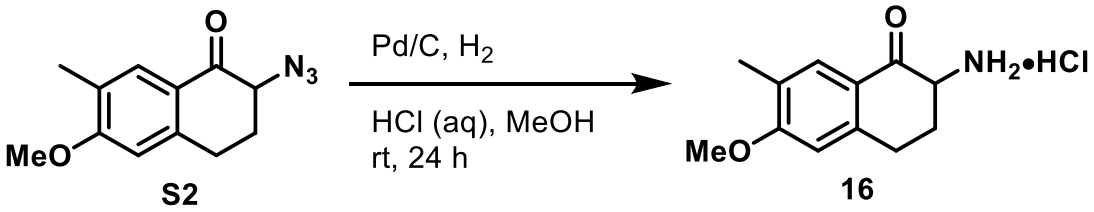


**Compound 16:** To a solution of **S2** (8.54 g, 36.9 mmol) in MeOH (190 mL), 10% Pd/C (3.93 g, 3.69 mmol) was carefully added in one portion under argon atmosphere. After stirring 24 h at room temperature under $H_2$ (1 atm), reaction was monitored by TLC for full consumption of **S2**. The mixture was filtered through Celite® and concentrated to yield the product **16** (7.14 g, 80%) as off-white solid without further purification:

**$^1$H NMR** (500 MHz, DMSO-$d_6$) δ = 8.83 (br, 1 H), 7.69 (s, 1 H), 6.91 (s, 1 H), 4.24 (d, $J$ = 10.0 Hz, 1 H), 3.87 (s, 3 H), 3.14 (t, $J$ = 10.0 Hz, 1 H), 2.99 (d, $J$ = 15.0 Hz, 1 H), 2.52 (br, 1 H), 2.14 (s, 3 H), 2.12 (br, 1 H).

**$^{13}$C NMR** (125 MHz, DMSO-$d_6$) δ = 191.5, 162.4, 145.1, 128.7, 125.2, 123.0, 109.8, 56.0, 54.2, 27.6, 27.2, 15.6.

**IR** (Diamond-ATR, neat) $\tilde{\nu}_{max}$ ($cm^{-1}$): 3430, 3213, 2811, 1669, 1600, 1498, 1272, 1253.

**HRMS** (*m/z*): calculated for $C_{12}H_{16}NO_2$ $[M+H]^+$ 206.1176, found 206.1176.

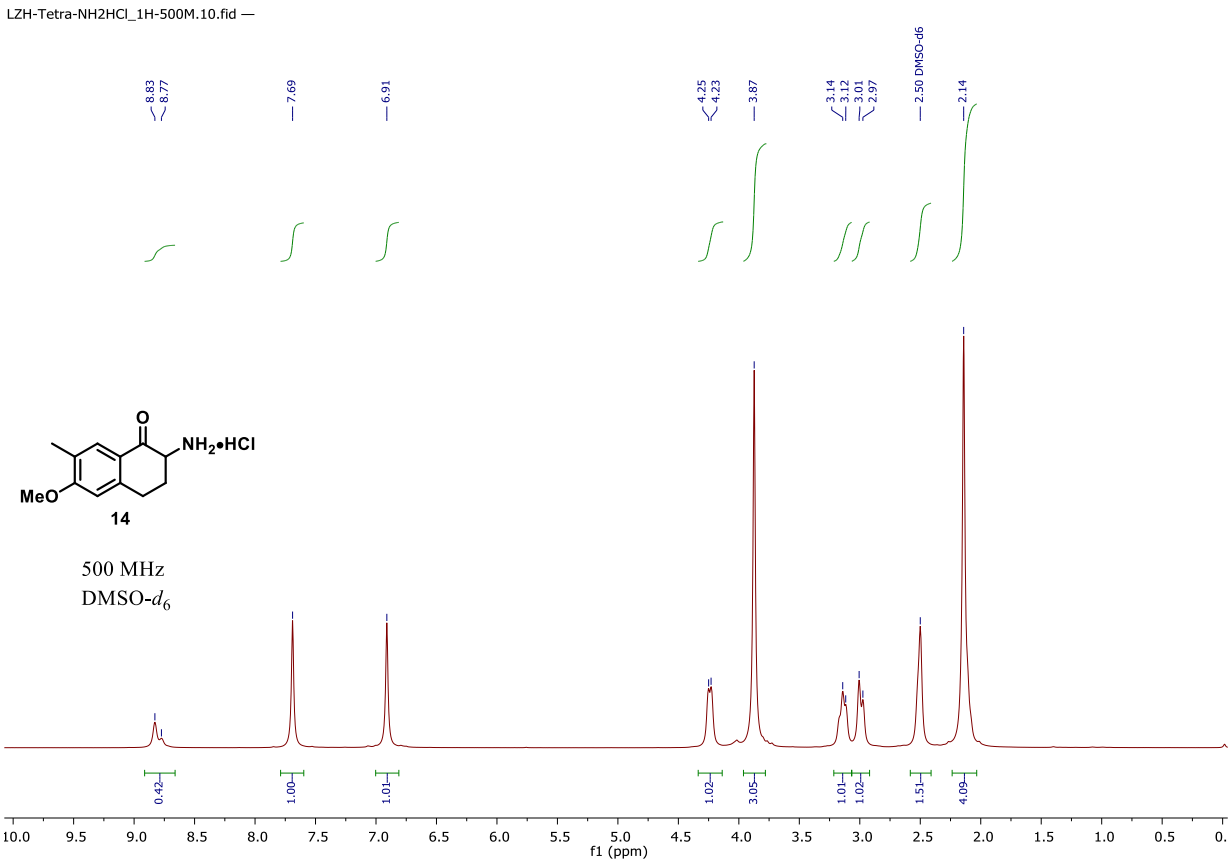


**Figure 17.** $^{1}$H NMR of compound **14**.

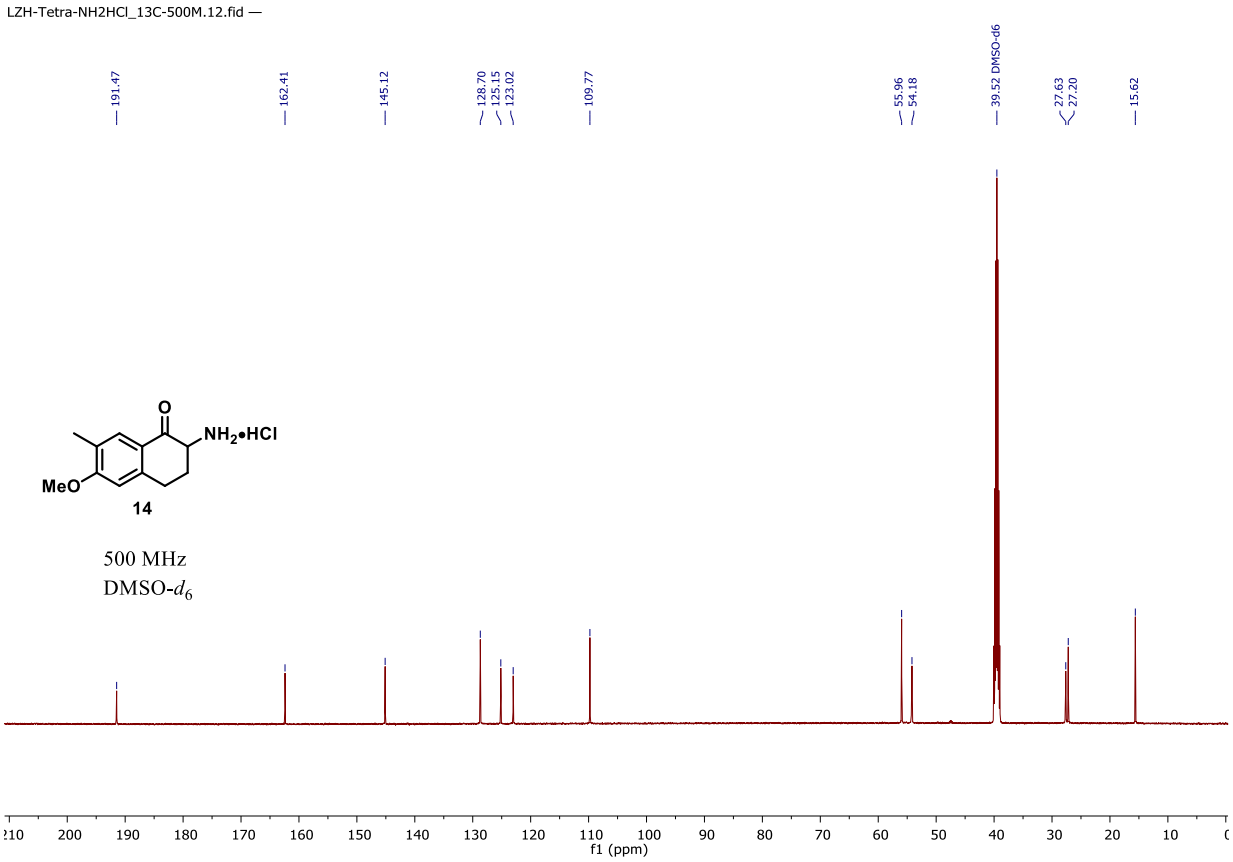


**Figure 18.** $^{13}$C NMR of compound **14**.

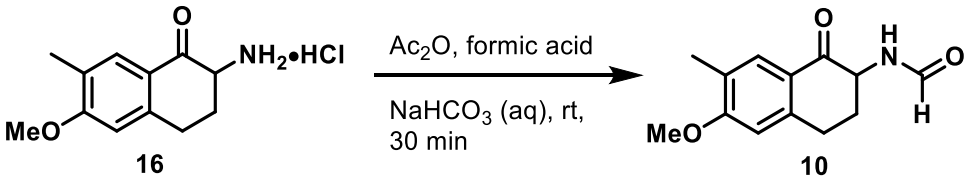


**Compound 10:** To a flame-dried round bottom flask was added $Ac_2O$ (41.4 mL, 438 mmol) and formic acid (18.2 mL, 482 mmol). The reaction was stirred at 60 °C for 2 h, at which point the mixture was cooled to room temperature and **16** (3.00 g, 14.6 mmol) was added in one portion. To the stirring solution under ambient atmosphere was added $NaHCO_3$ solution (1.5 M in water, 877 mmol) slowly over 15 min (The reaction will effervesce violently if the $NaHCO_3$ solution added too quickly). After the addition of $NaHCO_3$ solution was complete, the reaction mixture was transferred to a separatory funnel and extracted with ethyl acetate for (3x). The organic layers were combined, washed with saturated $NaHCO_3$ (aq) and brine, dried over $Na_2SO_4$, filtered and concentrated under reduced pressure. The crude product was purified by flash chromatography on silica gel (50-75%, ethyl acetate:hexanes) to yield the product **10** (2.56 g, 75%) as white solid:

$R_f$ = 0.15 (1:1, ethyl acetate:hexanes).

**Melting point** (°C) = 150-153.

**$^1$H NMR** (500 MHz, CDCl3) δ = 8.32 (s, 1 H), 7.79 (s, 1 H), 6.84 (br, 1 H), 6.61 (s, 1 H), 4.63-4.58 (m, 1 H), 3.88 (s, 3 H), 3.26-3.19 (m, 1 H), 2.97-2.92 (m, 1 H), 2.86-2.82 (m, 1 H), 2.19 (s, 3 H), 1.93-1.85 (m, 1 H).

**$^{13}$C NMR** (150 MHz, CDCl3) δ = 194.1, 162.7, 161.4, 144.4, 129.8, 126.1, 124.0, 109.0, 55.7, 55.3, 30.7, 28.5, 15.9.

**IR** (Diamond-ATR, neat) $\tilde{\nu}_{max}$ ($cm^{-1}$): 3272, 1673, 1633, 1610, 1255, 1135, 1085, 900, 850, 679.

**HRMS** (*m/z*): calculated for $C_{13}H_{16}N_3O_3$ $[M+H]^+$ 234.1125, found 234.1120.

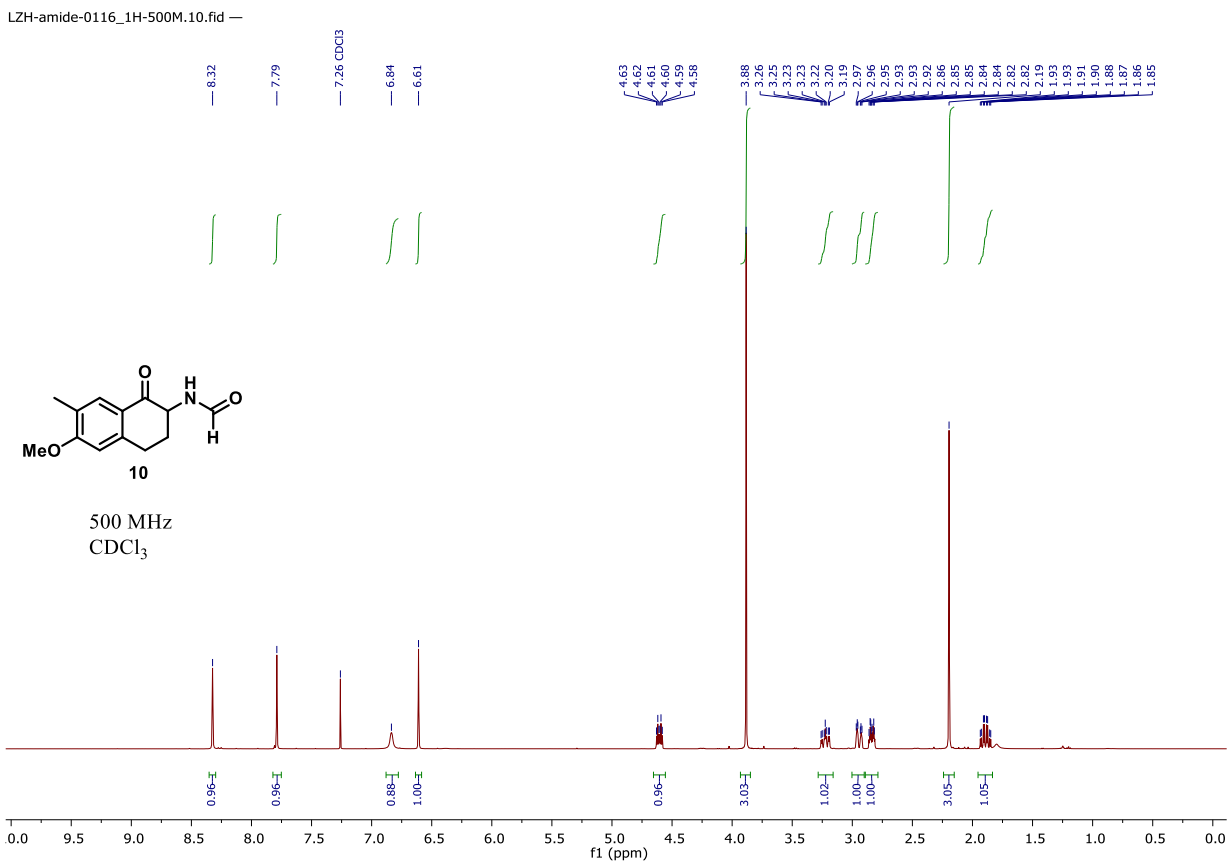


**Figure 19.** $^{1}$H NMR of compound **10**.

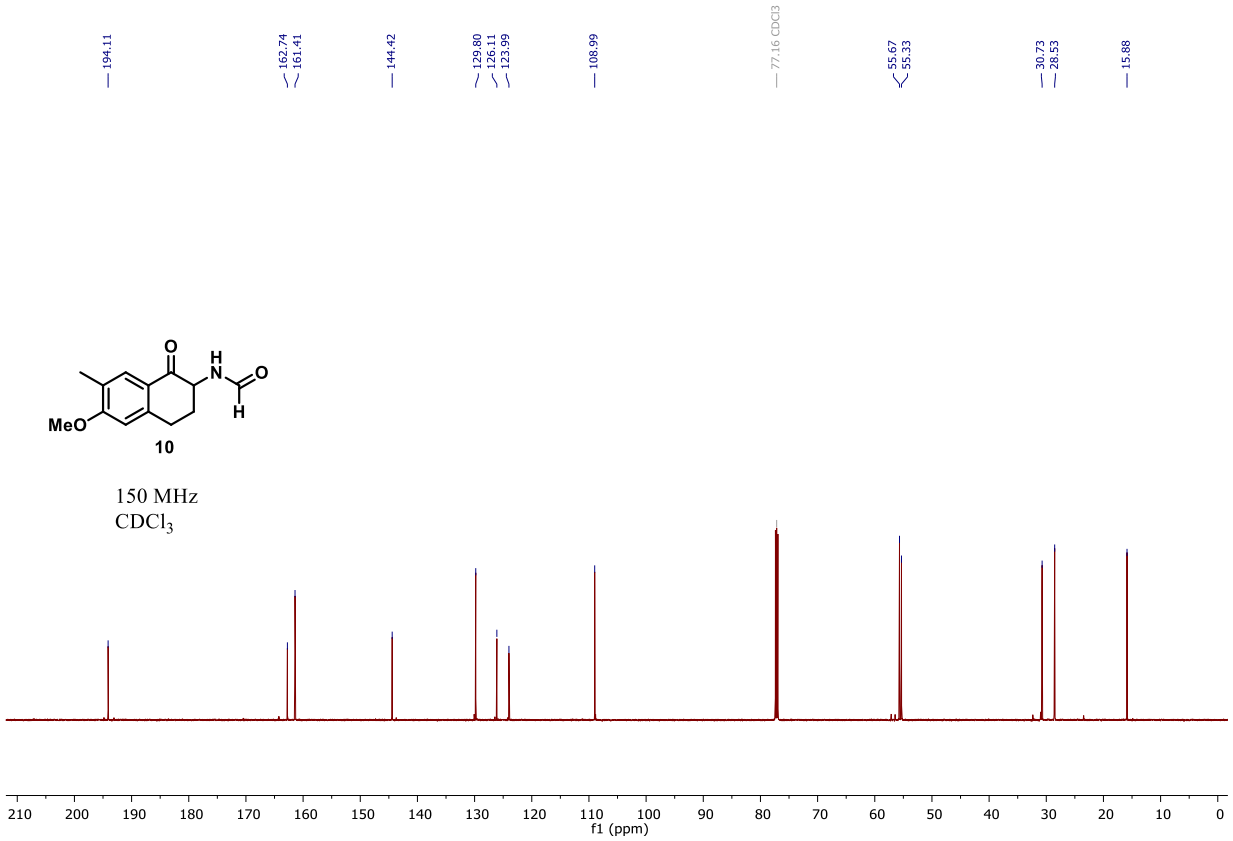


**Figure 20.** $^{13}C$ NMR of compound **10**.

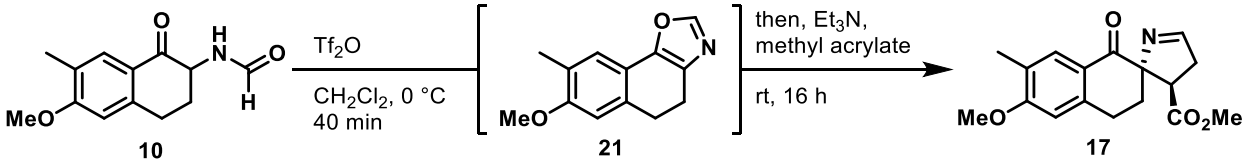


**Compound 17:** To a flame-dried round bottom flask was added formamide **10** (0.25 g, 1.07 mmol) in anhydrous $CH_2Cl_2$ (2 mL). The reaction was cooled to 0 °C and then $Tf_2O$ (0.198 mL, 1.18 mmol) was added in one portion. After stirring at 0 °C for 40 min, $Et_3N$ (0.030 mL, 0.214 mmol) and methyl acrylate (0.194 mL, 2.14 mmol) were added in sequence, the mixture was stirred at rt for 16 h. The reaction was monitored by TLC for full conversion of **10** and quenched by saturated $NaHCO_3$ (aq). The reaction mixture was transferred to a separatory funnel and extracted with $CH_2Cl_2$ three times. The organic layers were combined, washed with saturated $NaHCO_3$ (aq) and brine, dried over $Na_2SO_4$, filtered and concentrated under reduced pressure. The crude product was purified by flash chromatography on silica gel (40-60%, ethyl acetate:hexanes) to yield the product **17** (0.213 g, 65%) as brown oil:

$R_f$ = 0.21 (1:1, ethyl acetate:hexanes).

**$^1$H NMR** (600 MHz, CDCl3) δ = 7.74 (s, 1 H), 7.68 (s, 1 H), 6.64 (s, 1 H), 3.88 (s, 3 H), 3.58 (s, 3 H), 3.56-3.50 (m, 1 H), 3.41 (dd, *J* = 18.0 Hz, 1 H), 2.98-2.92 (m, 2 H), 2.88 (t, *J* = 9.6 Hz, 1 H), 2.82-2.77 (m, 1 H), 2.22-2.18 (m, 1 H), 2.17 (s, 3 H).

**$^{13}$C NMR** (150 MHz, CDCl3) δ = 194.0, 172.5, 168.2, 162.7, 145.1, 130.4, 126.0, 124.4, 108.9, 85.1, 55.7, 52.0, 50.8, 41.2, 36.9, 27.2, 16.0.

**IR** (Diamond-ATR, neat) $\tilde{\nu}_{max}$ ($cm^{-1}$): 2926, 2843, 1734, 1669, 1600, 1258, 1203, 1096.

**HRMS** (*m/z*): calculated for $C_{17}H_{20}NO_4$ $[M+H]^+$ 302.1387, found 302.1384.

Note 1: Compound **21** was formed after $Tf_2O$ added and reacted with alkene to yield the [3+2] product **17**. However, **21** is air sensitive:

$R_f$ = 0.55 (1:1, ethyl acetate:hexanes).

**LCMS** (*m/z*): calculated for $C_{17}H_{19}NO_4$ $[M+H]^+$ 216.1, found 216.

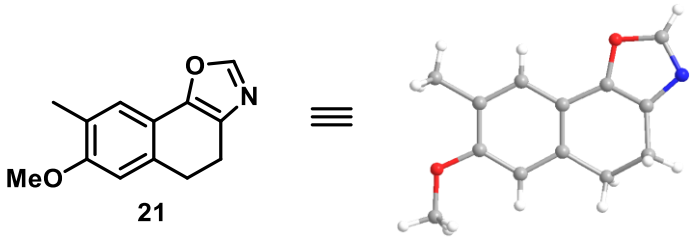


21

**X-ray sample preparation: 21** was prepared as saturated solution in $CH_2Cl_2$ in a 5 mL scintillation vial. This vial was put into a 20 mL scintillation vial which contains hexanes as same height level as $CH_2Cl_2$. After the $CH_2Cl_2$ evaporated completely, crystals formed inside of 5 mL vial. The crystals were a colorless plate-like specimen of $C_{13}H_{13}NO_2$, approximate dimensions 0.044 mm x 0.142 mm x 0.183 mm, was used for the X-ray crystallographic analysis. The X-ray intensity data were measured on a Bruker D8 VENTURE system equipped with a Incoatec IμS 3.0 microfocus sealed tube (Cu Kα, λ = 1.54178 Å) and a multilayer mirror monochromator.

The total exposure time was 4.66 hours. The frames were integrated with the Bruker SAINT software package using a narrow-frame algorithm. The integration of the data using an orthorhombic unit cell yielded a total of 50833 reflections to a maximum θ angle

of 80.06° (0.78 Å resolution), of which 2240 were independent (average redundancy 22.693, completeness = 99.9%, $R_{int}$ = 2.66%, $R_{sig}$ = 0.98%) and 2171 (96.92%) were greater than $2\sigma(F^2)$. The final cell constants of a = 7.4687(2) Å, b = 13.4477(3) Å, c = 20.3877(5) Å, volume = 2047.68(9) $Å^3$, are based upon the refinement of the XYZ-centroids of 488 reflections above 20 σ(I) with 14.26° < 2θ < 100.1°. Data were corrected for absorption effects using the Multi-Scan method (SADABS). The ratio of minimum to maximum apparent transmission was 0.931. The calculated minimum and maximum transmission coefficients (based on crystal size) are 0.8730 and 0.9670.

The structure was solved and refined using the Bruker SHELXTL Software Package, using the space group *P*bca, with Z = 8 for the formula unit, $C_{13}H_{13}NO_2$. The final anisotropic full-matrix least-squares refinement on $F^2$ with 147 variables converged at R1 = 3.35%, for the observed data and wR2 = 8.83% for all data. The goodness-of-fit was 1.049. The largest peak in the final difference electron density synthesis was 0.365 $e^-/Å^3$ and the largest hole was -0.208 $e^-/Å^3$ with an RMS deviation of 0.041 $e^-/Å^3$. On the basis of the final model, the calculated density was 1.396 $g/cm^3$ and F(000), 912 $e^-$.

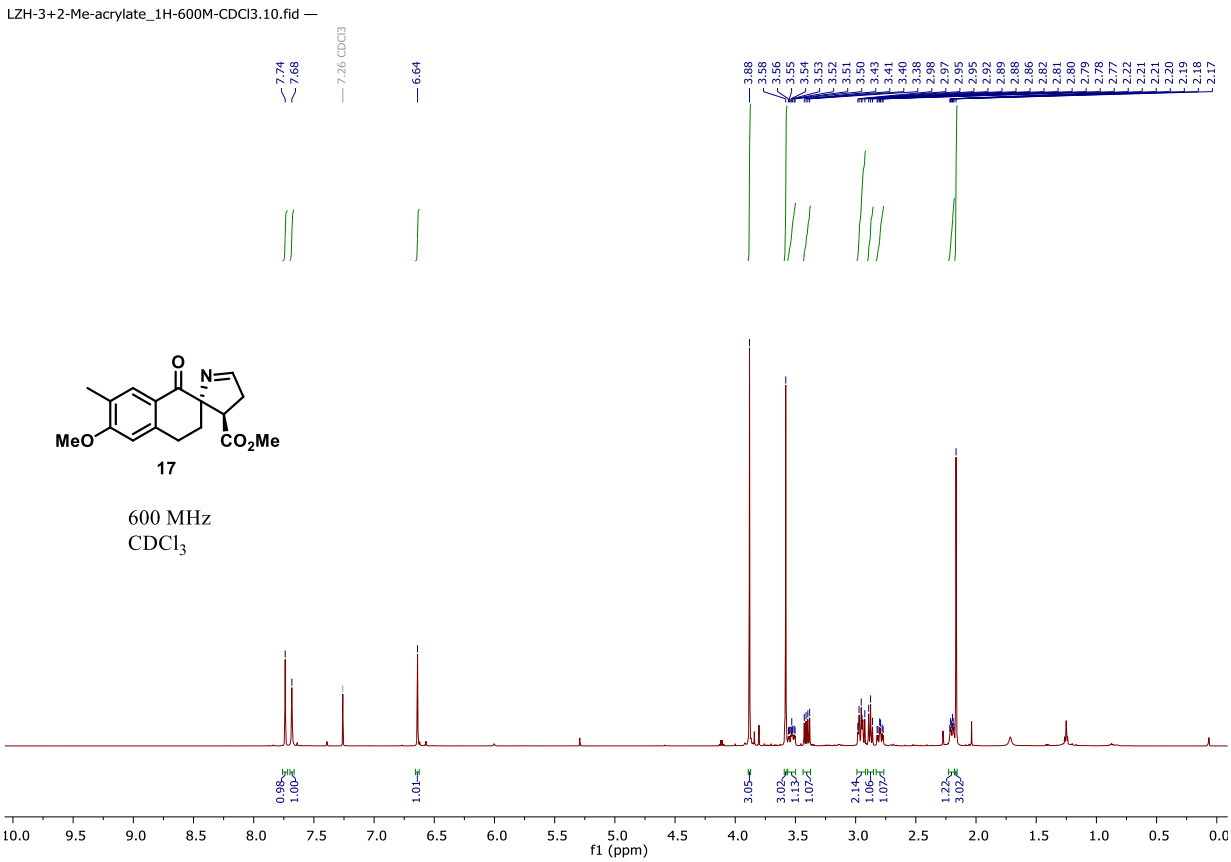


**Figure 21.** $^{1}$H NMR of compound **17**.

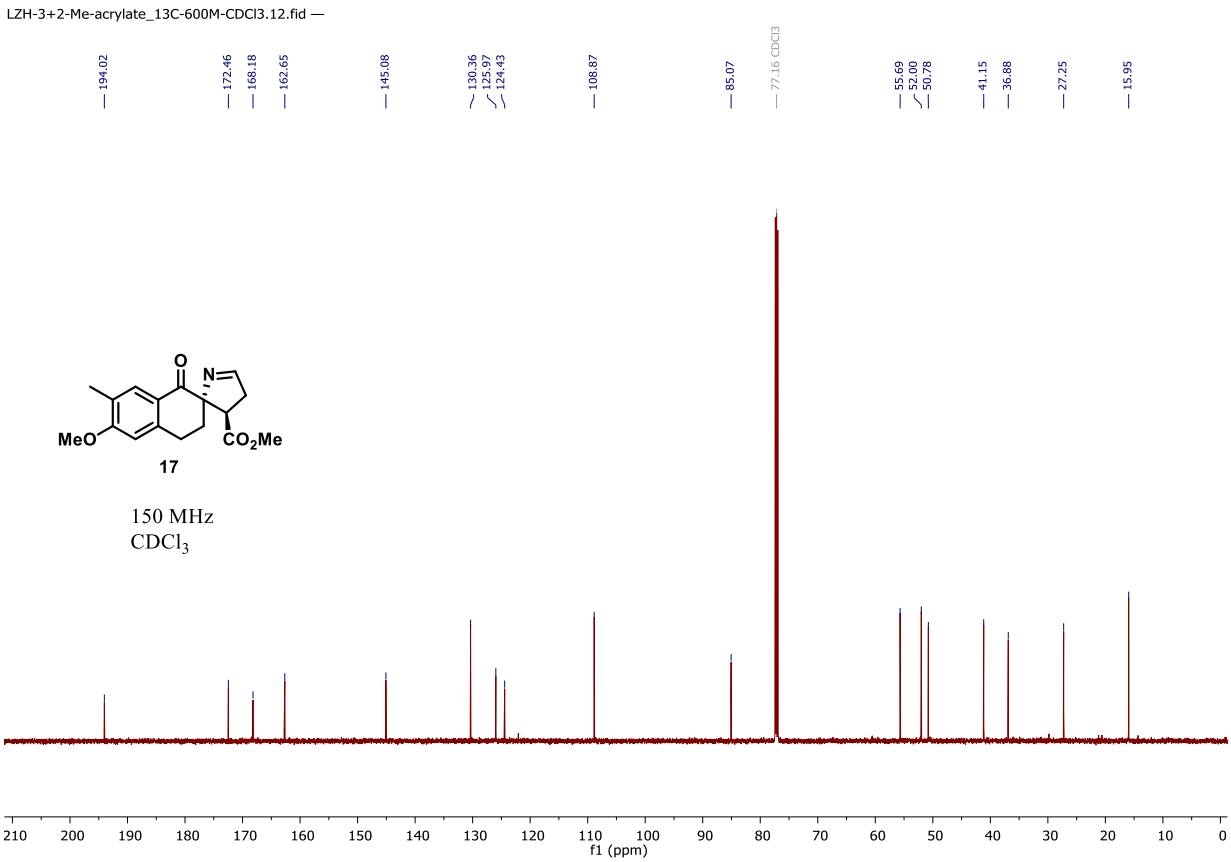


**Figure 22.** $^{13}C$ NMR of compound **17**.

**Table 1.** Sample and crystal data for **21**.

| | | |
|---|---|---|
| **Identification code** | rs106 | |
| **Chemical formula** | $C_{13}H_{13}NO_2$ | |
| **Formula weight** | 215.24 g/mol | |
| **Temperature** | 100(2) K | |
| **Wavelength** | 1.54178 Å | |
| **Crystal size** | 0.044 x 0.142 x 0.183 mm | |
| **Crystal habit** | colorless plate | |
| **Crystal system** | orthorhombic | |
| **Space group** | *P*bca | |
| **Unit cell dimensions** | a = 7.4687(2) Å | α = 90° |
| | b = 13.4477(3) Å | β = 90° |
| | c = 20.3877(5) Å | γ = 90° |
| **Volume** | 2047.68(9) $Å^3$ | |
| **Z** | 8 | |
| **Density (calculated)** | 1.396 $g/cm^3$ | |
| **Absorption coefficient** | 0.765 $mm^{-1}$ | |
| **F(000)** | 912 | |

**Table 2.** Data collection and structure refinement for **21**.

| | |
|---|---|
| **Diffractometer** | Bruker D8 VENTURE |
| **Radiation source** | Incoatec IμS 3.0 microfocus sealed tube (Cu Kα, λ = 1.54178 Å) |
| **Theta range for data collection** | 4.34 to 80.06° |
| **Index ranges** | -9<=h<=9, -17<=k<=15, -25<=l<=25 |
| **Reflections collected** | 50833 |
| **Independent reflections** | 2240 [R(int) = 0.0266] |
| **Coverage of independent reflections** | 99.9% |
| **Absorption correction** | Multi-Scan |
| **Max. and min. transmission** | 0.9670 and 0.8730 |
| **Structure solution technique** | direct methods |
| **Structure solution program** | XT, VERSION 2014/5 (Sheldrick, 2015) |
| **Refinement method** | Full-matrix least-squares on $F^2$ |
| **Refinement program** | SHELXL, (Sheldrick, 2015) |
| **Function minimized** | $\Sigma\, w(F_o^2 - F_c^2)^2$ |
| **Data / restraints / parameters** | 2240 / 0 / 147 |

**Table 2** (continued)

| | | |
|---|---|---|
| **Goodness-of-fit on $F^2$** | 1.049 | |
| **$\Delta/\sigma_{max}$** | 0.001 | |
| | 2171 | |
| **Final R indices** | data; | R1 = 0.0335, wR2 = 0.0874 |
| | I>2σ(I) | |
| | all data | R1 = 0.0344, wR2 = 0.0883 |
| **Weighting scheme** | $w=1/[\sigma^2(F_o^2)+(0.0404P)^2+1.1178P]$ | |
| | where $P=(F_o^2+2F_c^2)/3$ | |
| **Largest diff. peak and hole** | 0.365 and -0.208 $eÅ^{-3}$ | |
| **R.M.S. deviation from mean** | 0.041 $eÅ^{-3}$ | |

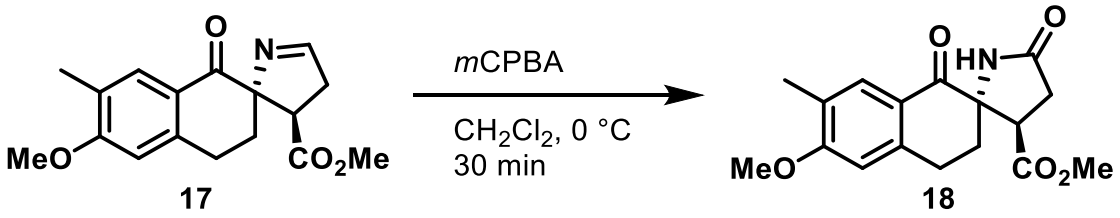


**Compound 18:** A solution of **17** (0.213 g, 0.71 mmol) in $CH_2Cl_2$ (3.5 mL) was cooled to 0 °C. *m*CPBA (0.321 g, 1.41 mmol) in $CH_2Cl_2$ (3.5 mL) was added dropwise. After the reaction stirred for 30 min, the mixture was quenched by 10% $Na_2S_2O_3$ (aq), transferred to a separatory funnel and extracted with $CH_2Cl_2$ three times. The organic layers were combined, washed with saturated $NaHCO_3$ (aq) and brine, dried over $Na_2SO_4$, filtered and concentrated under reduced pressure. The crude product was purified by flash chromatography on silica gel (8-18%, ethyl acetate:hexanes) to yield the product **18** (0.202 g, 90%) as white solid:

$R_f$ = 0.31 (1:3, ethyl acetate:hexanes).

**Melting point** (°C) = 130-133.

**$^1$H NMR** (600 MHz, CDCl3) δ = 7.76 (s, 1 H), 6.66 (s, 1 H), 4.60 (s, 1 H), 3.90 (s, 3 H), 3.60-3.56 (m, 4 H), 2.94-2.86 (m, 2 H), 2.82-2.76 (m, 2 H), 2.57 (t, *J* = 10.2 Hz, 1 H), 2.33 (d, *J* = 13.8 Hz, 1 H), 2.18 (s, 3 H).

**$^{13}$C NMR** (150 MHz, CDCl3) δ = 192.6, 172.5, 163.0, 145.3, 130.4, 126.2, 124.8, 109.0, 80.4, 77.1, 55.8, 52.1, 46.6, 33.2, 32.3, 27.0, 16.0.

**IR** (Diamond-ATR, neat) $\tilde{\nu}_{max}$ ($cm^{-1}$): 2926, 2949, 2852, 1725, 1660, 1600, 1498, 1443, 1355, 1263, 1221, 1101, 848, 753.

**HRMS** (*m/z*): calculated for $C_{17}H_{20}NO_5$ $[M+H]^+$ 318.1336, found 318.1331.

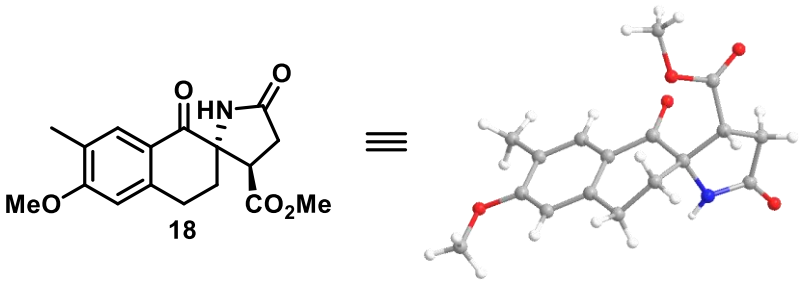


**X-ray sample preparation:** Compound **18** was prepared as saturated solution in $CH_2Cl_2$ in a 5 mL scintillation vial. This vial was put into a 20 mL scintillation vial which contains hexanes as same height level as $CH_2Cl_2$. After the $CH_2Cl_2$ evaporated completely, crystals formed inside of 5 mL vial. The crystals were a colorless plate-like specimen of $C_{18}H_{21}Cl_2NO_5$, approximate dimensions 0.068 mm x 0.309 mm x 0.379 mm, was used for the X-ray crystallographic analysis. The X-ray intensity data were measured on a Bruker D8 VENTURE system equipped with a Incoatec IμS 3.0 microfocus sealed tube (Cu Kα, λ = 1.54178 Å) and a multilayer mirror monochromator.

The total exposure time was 5.98 hours. The frames were integrated with the Bruker SAINT software package using a narrow-frame algorithm. The integration of the data using a monoclinic unit cell yielded a total of 42316 reflections to a maximum θ angle of 77.77° (0.79 Å resolution), of which 3936 were independent (average redundancy 10.751, completeness = 99.5%, $R_{int}$ = 4.40%, $R_{sig}$ = 2.37%) and 3789 (96.27%) were greater than $2\sigma(F^2)$. The final cell constants of a = 15.1907(7) Å, b = 12.9321(6) Å, c = 9.4653(4) Å, β = 91.384(2)°, volume = 1858.89(14) $Å^3$, are based upon the refinement of the XYZ-centroids of 9444 reflections above 20 σ(I) with 5.819° < 2θ < 154.5°. Data were corrected for absorption effects using

the Multi-Scan method (SADABS). The ratio of minimum to maximum apparent transmission was 0.673. The calculated minimum and maximum transmission coefficients (based on crystal size) are 0.3590 and 0.8020.

The structure was solved and refined using the Bruker SHELXTL Software Package, using the space group P 1 21/c 1, with Z = 4 for the formula unit, $C_{18}H_{21}Cl_2NO_5$. The final anisotropic full-matrix least-squares refinement on $F^2$ with 241 variables converged at R1 = 6.30%, for the observed data and wR2 = 15.14% for all data. The goodness-of-fit was 1.242. The largest peak in the final difference electron density synthesis was 0.459 $e^-/Å^3$ and the largest hole was -0.627 $e^-/Å^3$ with an RMS deviation of 0.081 $e^-/Å^3$. On the basis of the final model, the calculated density was 1.437 $g/cm^3$ and F(000), 840 $e^-$.

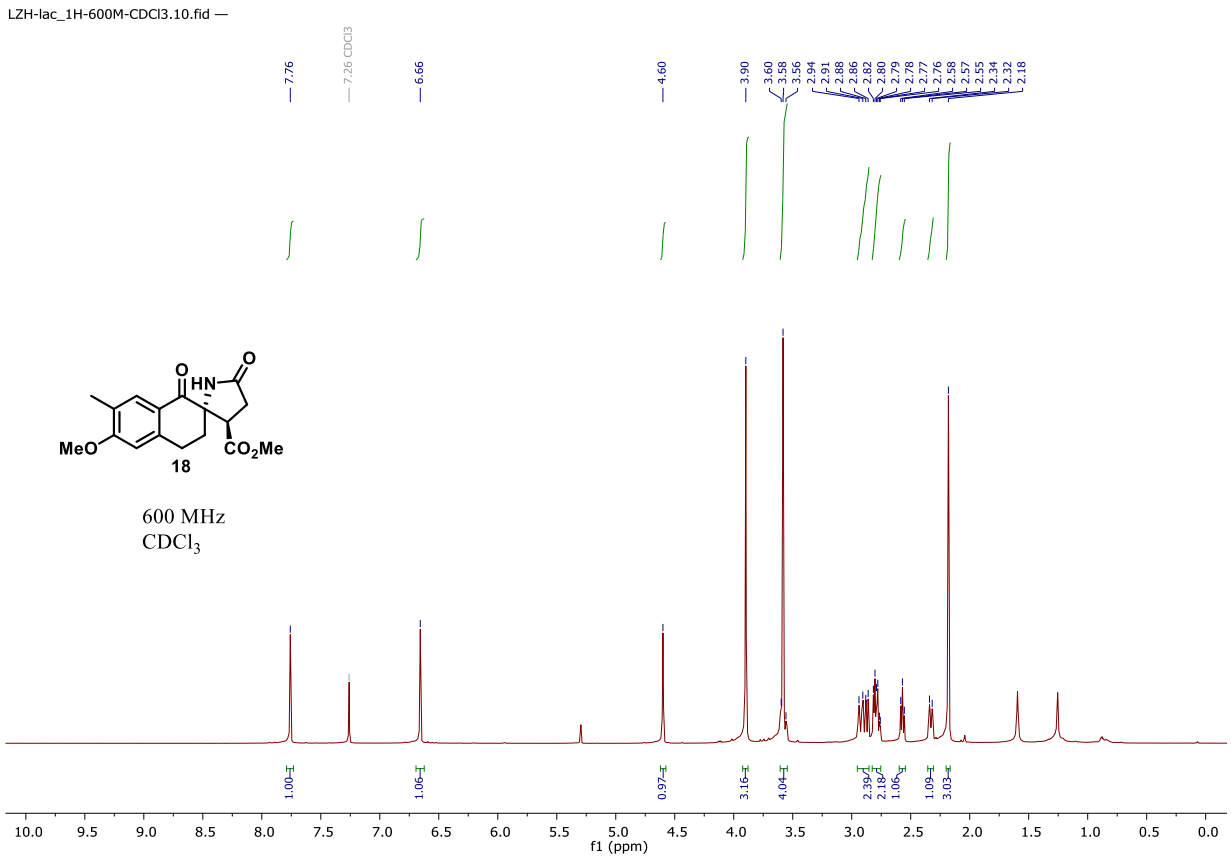


**Figure 23.** $^{1}$H NMR of compound **18**.

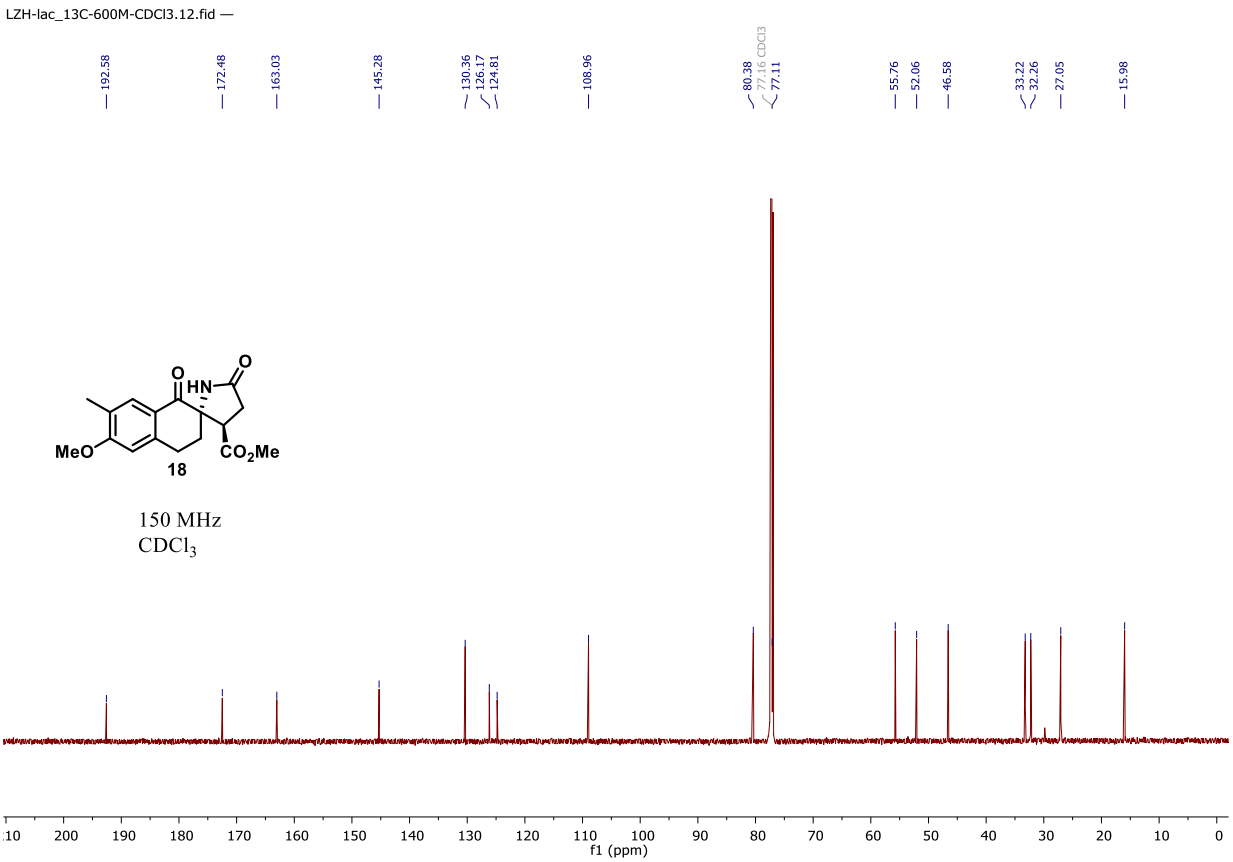


**Figure 24.** $^{13}C$ NMR of compound **18**.

**Table 3.** Sample and crystal data for **18**.

| | |
|---|---|
| **Identification code** | rds977 |
| **Chemical formula** | $C_{18}H_{21}Cl_2NO_5$ |
| **Formula weight** | 402.26 g/mol |
| **Temperature** | 100(2) K |
| **Wavelength** | 1.54178 Å |
| **Crystal size** | 0.068 x 0.309 x 0.379 mm |
| **Crystal habit** | colorless plate |
| **Crystal system** | monoclinic |
| **Space group** | P 1 21/c 1 |
| **Unit cell dimensions** | a = 15.1907(7) Å α = 90° |
| | b = 12.9321(6) Å β = 91.384(2)° |
| | c = 9.4653(4) Å γ = 90° |
| **Volume** | 1858.89(14) $Å^3$ |
| **Z** | 4 |
| **Density (calculated)** | 1.437 $g/cm^3$ |
| **Absorption coefficient** | 3.401 $mm^{-1}$ |
| **F(000)** | 840 |

**Table 4.** Data collection and structure refinement for **18**.

| | |
|---|---|
| **Diffractometer** | Bruker D8 VENTURE |
| **Radiation source** | Incoatec IμS 3.0 microfocus sealed tube (Cu Kα, λ = 1.54178 Å) |
| **Theta range for data collection** | 2.91 to 77.77° |
| **Index ranges** | -19<=h<=19, -13<=k<=16, -11<=l<=11 |
| **Reflections collected** | 42316 |
| **Independent reflections** | 3936 [R(int) = 0.0440] |
| **Coverage of independent reflections** | 99.5% |
| **Absorption correction** | Multi-Scan |
| **Max. and min. transmission** | 0.8020 and 0.3590 |
| **Structure solution technique** | direct methods |
| **Structure solution program** | SHELXT 2014/5 (Sheldrick, 2014) |
| **Refinement method** | Full-matrix least-squares on $F^2$ |
| **Refinement program** | SHELXL-2018/3 (Sheldrick, 2018) |
| **Function minimized** | $\Sigma\, w(F_o^2 - F_c^2)^2$ |

**Table 4** (continued)

| | |
|---|---|
| **Data / restraints / parameters** | 3936 / 0 / 241 |
| **Goodness-of-fit on $F^2$** | 1.242 |
| **Final R indices** | 3789 data; $I>2\sigma(I)$ R1 = 0.0630, wR2 = 0.1507 |
| | all data R1 = 0.0645, wR2 = 0.1514 |
| **Weighting scheme** | $w=1/[\sigma^2(F_o^2)+(0.0157P)^2+5.9994P]$ where $P=(F_o^2+2F_c^2)/3$ |
| **Largest diff. peak and hole** | 0.459 and -0.627 eÅ$^{-3}$ |
| **R.M.S. deviation from mean** | 0.081 eÅ$^{-3}$ |

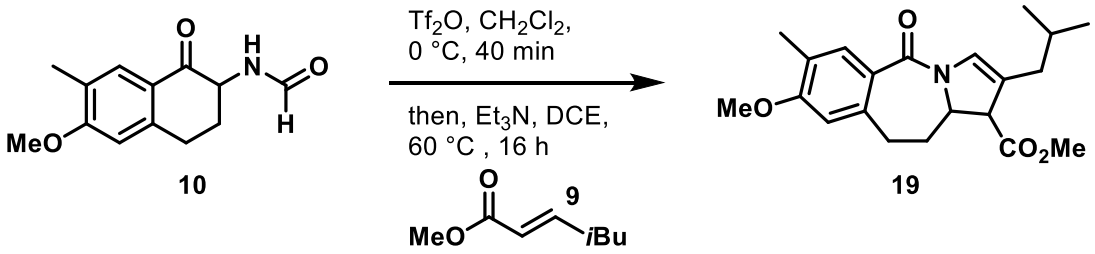


**Compound 19:** To a flame-dried round bottom flask was added formamide **10** (0.10 g, 0.43 mmol) in anhydrous $CH_2Cl_2$ (2 mL). The reaction was cooled to 0 °C and then $Tf_2O$ (0.079 mL, 0.47 mmol) was added in one portion. After stirring at 0 °C for 40 min, the reaction was monitored by TLC for full consumption of **10** and concentrated under reduced pressure. Then the crude intermediate was dissolved in DCE (0.8 mL), $Et_3N$ (0.012 mL, 0.085 mmol) and methyl, 5-methyl-2-hexenoate **9** (0.14 mL, 0.85 mmol) were added in sequence, the mixture was stirred at 60 °C for 16 h. The reaction was quenched by saturated $NaHCO_3$ (aq) and transferred to a separatory funnel, extracted with $CH_2Cl_2$ three times. The organic layers were combined, washed with saturated $NaHCO_3$(aq) and brine, dried over $Na_2SO_4$, filtered and concentrated under reduced pressure. The crude product was purified by flash chromatography on silica gel (15-25%, ethyl acetate:hexanes) to yield the product **19** (0.075 g, 49%) as brown green solid:

$R_f$ = 0.28 (1:3, ethyl acetate:hexanes).

**$^1$H NMR** (600 MHz, CDCl3) δ = 7.73 (s, 1 H), 7.56 (s, 1 H), 6.63 (s, 1 H), 3.87 (s, 3 H), 3.73 (q, *J* = 8.4 Hz 1 H), 3.55 (s, 3 H), 3.53-3.48 (m, 1 H), 2.98-2.94 (m, 1 H), 2.80-2.75 (m, 1 H), 2.45 (d, *J* = 9.0 Hz 1 H), 2.24-2.20 (m, 1 H), 2.16 (s, 3 H), 1.77 (p, *J* = 7.2 Hz 1 H), 1.48-1.45 (m, 2 H), 0.99 (d, *J* = 7.2 Hz, 6 H).

**$^{13}$C NMR** (150 MHz, CDCl3) δ = 193.8, 172.4, 172.0, 162.6, 145.0, 130.4, 125.9, 124.4, 108.8, 85.5, 58.3, 55.7, 51.9, 51.8, 42.7, 37.5, 27.1, 26.7, 23.0, 22.7, 15.9.

**IR** (Diamond-ATR, neat) $\tilde{\nu}_{max}$ ($cm^{-1}$): 2947, 2868, 1734, 1662, 1598, 1498, 1256, 1180, 1099, 994, 931, 775, 679.

**HRMS** (*m/z*): calculated for $C_{21}H_{28}NO_4$ $[M+H]^+$ 358.2013, found 358.2013.

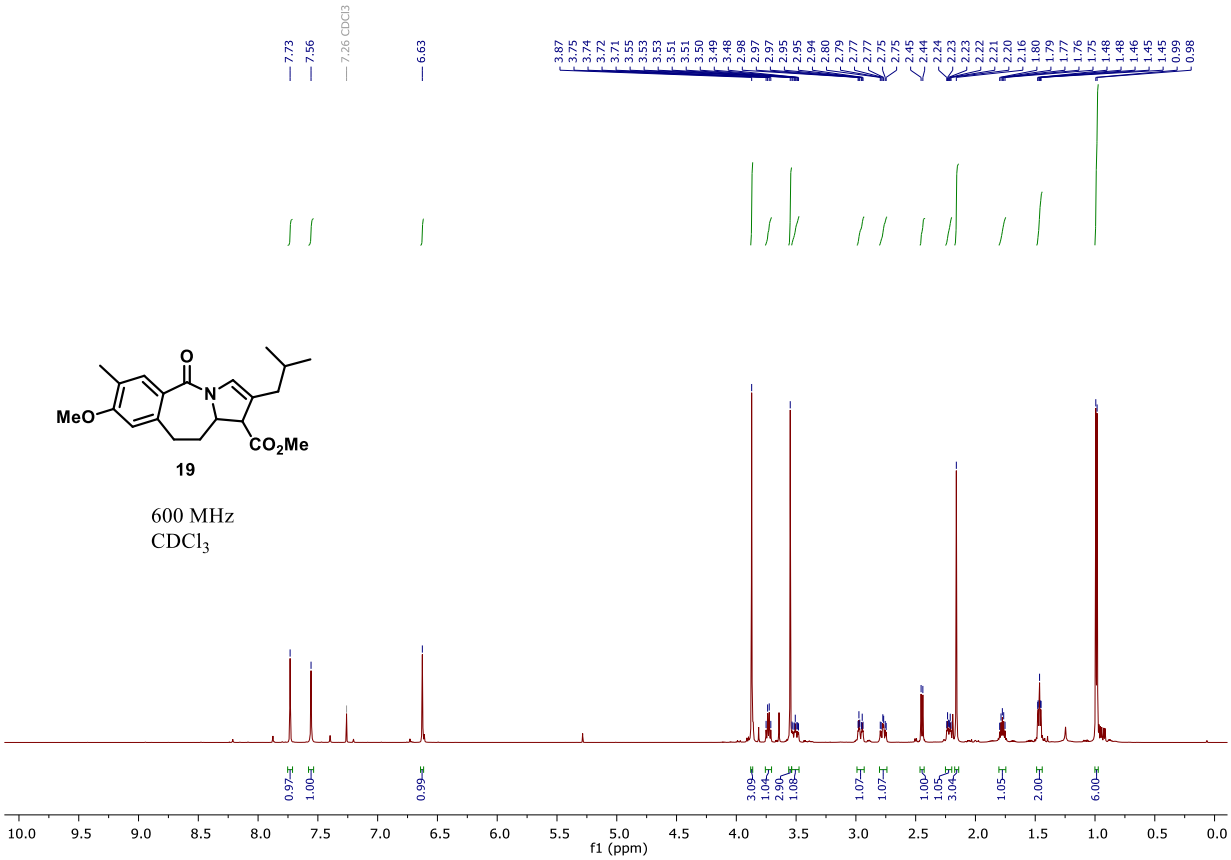


**Figure 25.** $^{1}$H NMR of compound **19**.

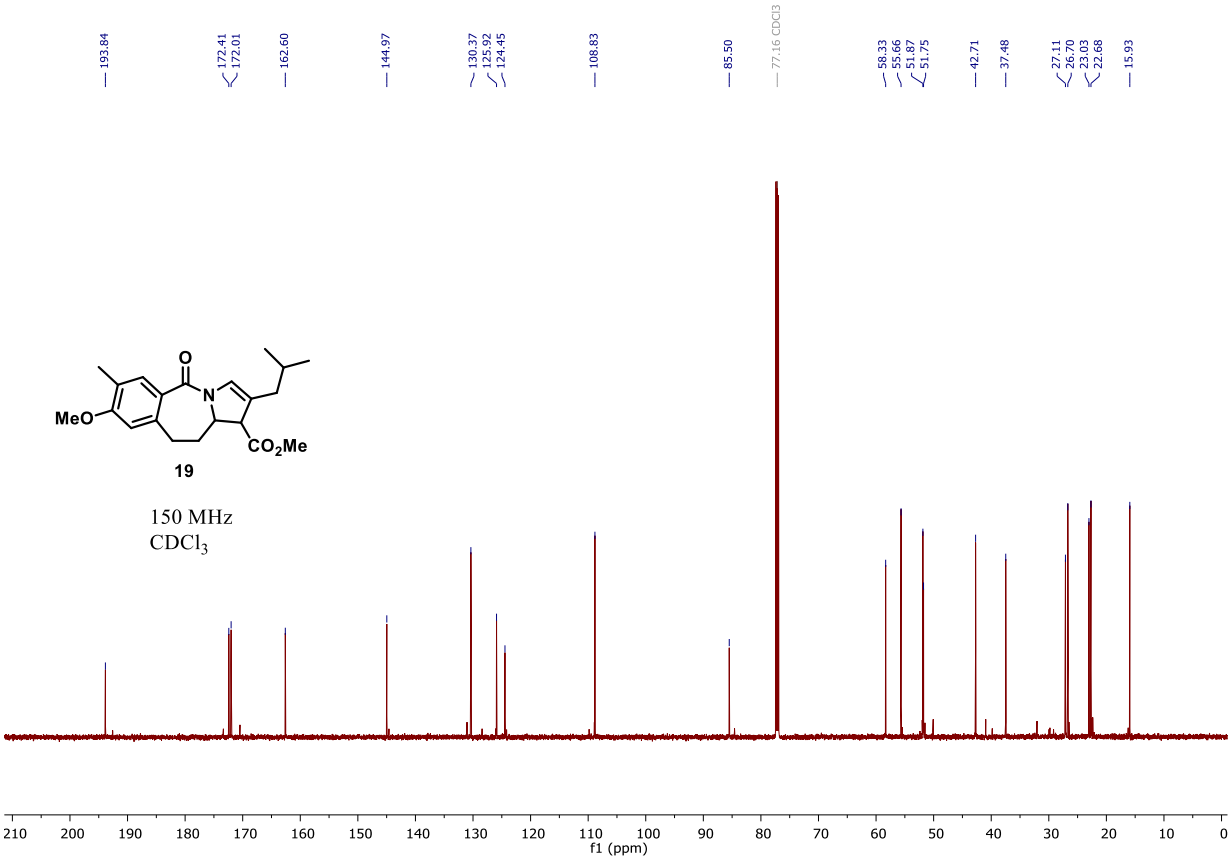


**Figure 26.** $^{13}C$ NMR of compound **19**.

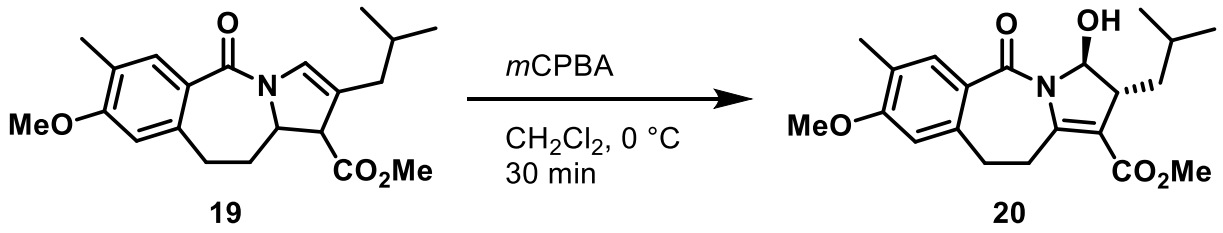


**Compound 20:** A solution of **19** (0.050 g, 0.14 mmol) in $CH_2Cl_2$ (0.5 mL) was cooled to 0 °C. 70% *m*CPBA (0.064 g, 0.28 mmol) in $CH_2Cl_2$ (1 mL) was added dropwise. After the reaction stirred for 30 min, the mixture was quenched by 10% $Na_2S_2O_3$ (aq), transferred to a separatory funnel and extracted with $CH_2Cl_2$ for (3x). The organic layers were combined, washed with saturated $NaHCO_3$ (aq) and brine, dried over $Na_2SO_4$, filtered and concentrated under reduced pressure. The crude product was purified by flash chromatography on silica gel (4-8%, ethyl acetate:hexanes) to yield the product **20** (0.030 g, 57%) as colorless crystal:

$R_f$ = 0.32 (1:9, ethyl acetate:hexanes).

**Melting point** (°C) = 171-175.

**$^1$H NMR** (500 MHz, CDCl3) δ = 7.75 (s, 1 H), 6.64 (s, 1 H), 4.56 (s, 1 H), 3.89 (s, 3 H), 3.54 (s, 3 H), 3.54-3.50 (m, 1 H), 3.23-3.19 (m, 1 H), 2.95-2.90 (m, 1 H), 2.77-2.71 (m, 1 H), 2.38-2.34 (m, 1 H), 2.18 (s, 3 H), 2.16 (t, *J* = 9.5 Hz 1 H), 1.87-1.78 (m, 1 H), 1.73-1.67 (m, 1 H), 1.57-1.51 (m, 1 H), 1.05 (d, *J* = 6.5 Hz, 3 H), 1.00 (d, *J* = 6.5 Hz, 3 H).

**$^{13}$C NMR** (125 MHz, CDCl3) δ = 192.6, 172.4, 163.0, 145.2, 130.3, 126.2, 124.7, 108.9, 82.8, 77.8, 55.8, 52.8, 51.9, 42.3, 39.1, 33.6, 27.1, 26.9, 23.9, 22.2, 16.0.

**IR** (Diamond-ATR, neat) $\tilde{\nu}_{max}$ ($cm^{-1}$): 2924, 2853, 1741, 1598, 1500, 1448, 1352, 1239, 1094, 1028, 907, 843, 765.

**HRMS** (*m/z*): calculated for $C_{21}H_{28}NO_5$ $[M+H]^+$ 374.1962, found 374.1963.

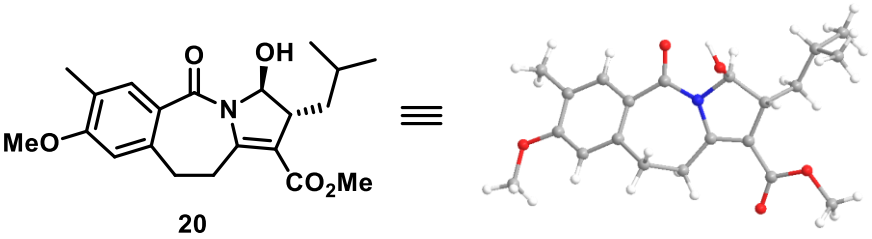


20

**X-ray sample preparation:** Compound **20** was prepared as saturated solution in $CH_2Cl_2$ in a 5 mL scintillation vial. This vial was put into a 20 mL scintillation vial which contains hexanes as same height level as $CH_2Cl_2$. After the $CH_2Cl_2$ evaporated completely, crystals formed inside of 5 mL vial. The crystals were colorless plate-like specimen of $C_{21}H_{27}NO_5$, approximate dimensions 0.058 mm x 0.102 mm x 0.172 mm, was used for the X-ray crystallographic analysis. The X-ray intensity data were measured on a Bruker D8 VENTURE system equipped with a Incoatec IμS 3.0 microfocus sealed tube (Cu Kα, λ = 1.54178 Å) and a multilayer mirror monochromator.

The total exposure time was 10.11 hours. The frames were integrated with the Bruker SAINT software package using a narrow-frame algorithm. The integration of the data using a monoclinic unit cell yielded a total of 45007 reflections to a maximum θ angle of 74.55° (0.80 Å resolution), of which 3978 were independent (average redundancy 11.314, completeness = 99.8%, $R_{int}$ = 2.79%, $R_{sig}$ = 1.52%) and 3791 (95.30%) were greater than $2\sigma(F^2)$. The final cell constants of a = 10.9384(6) Å, b = 8.8234(5) Å, c = 20.2948(7) Å, β = 95.254(3)°, volume = 1950.50(17) $Å^3$, are based upon the refinement of the XYZ-centroids of 398 reflections above 20 σ(I) with 8.460° < 2θ < 97.70°. Data were corrected for absorption effects using

the Multi-Scan method (SADABS). The ratio of minimum to maximum apparent transmission was 0.948. The calculated minimum and maximum transmission coefficients (based on crystal size) are 0.7149 and 0.7538.

The structure was solved and refined using the Bruker SHELXTL Software Package, using the space group P 1 21/c 1, with Z = 4 for the formula unit, $C_{21}H_{27}NO_5$. The final anisotropic full-matrix least-squares refinement on $F^2$ with 252 variables converged at R1 = 4.01%, for the observed data and wR2 = 10.19% for all data. The goodness-of-fit was 1.037. The largest peak in the final difference electron density synthesis was 0.475 $e^-/Å^3$ and the largest hole was -0.239 $e^-/Å^3$ with an RMS deviation of 0.041 $e^-/Å^3$. On the basis of the final model, the calculated density was 1.272 $g/cm^3$ and F(000), 800 $e^-$.

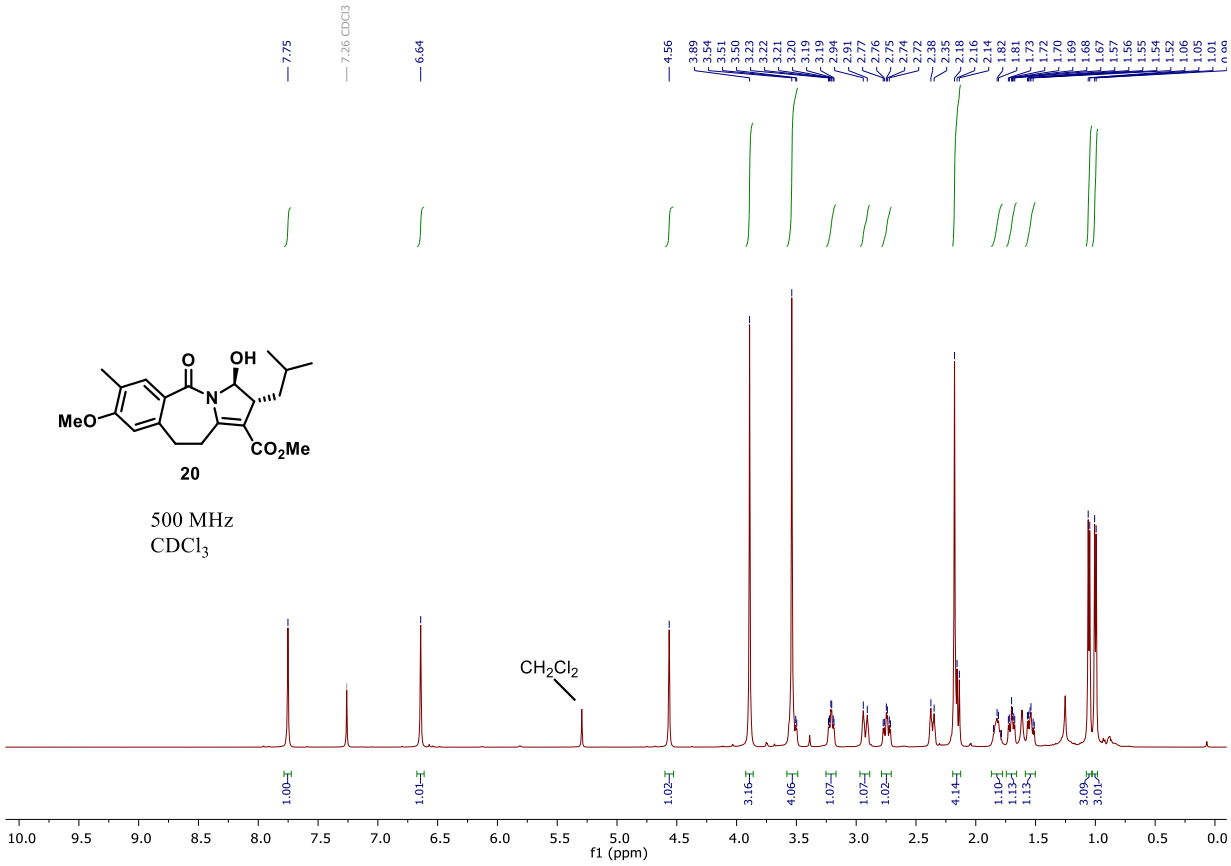


**Figure 27.** $^{1}$H NMR of compound **20**.

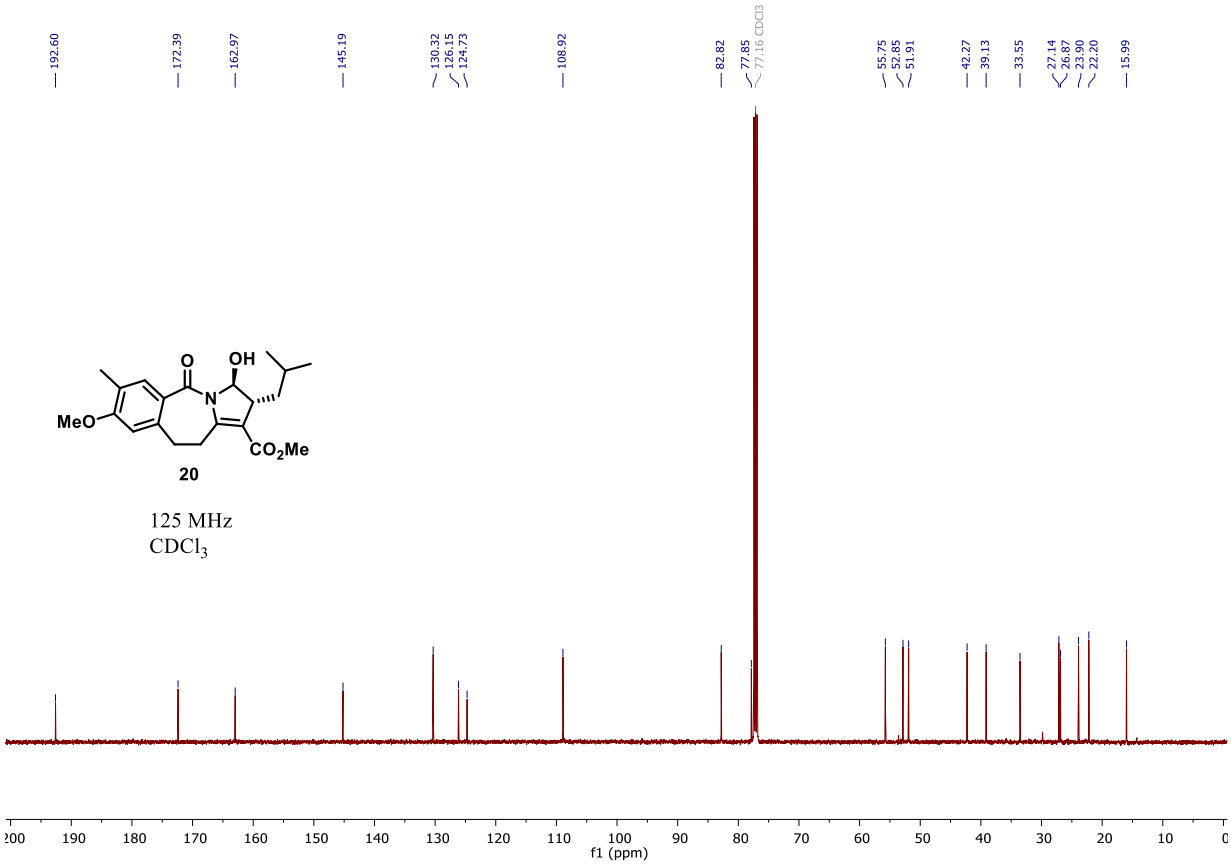


**Figure 28.** $^{13}C$ NMR of compound **20**.

**Table 5.** Sample and crystal data for **20**.

| | |
|---|---|
| **Identification code** | rs032 |
| **Chemical formula** | $C_{21}H_{27}NO_5$ |
| **Formula weight** | 373.43 g/mol |
| **Temperature** | 108(2) K |
| **Wavelength** | 1.54178 Å |
| **Crystal size** | 0.058 x 0.102 x 0.172 mm |
| **Crystal habit** | colorless plate |
| **Crystal system** | monoclinic |
| **Space group** | $P2_1/c$ |
| **Unit cell dimensions** | a = 10.9384(6) Å α = 90° |
| | b = 8.8234(5) Å β = 95.254(3)° |
| | c = 20.2948(7) Å γ = 90° |
| **Volume** | 1950.50(17) $Å^3$ |
| **Z** | 4 |
| **Density (calculated)** | 1.272 $g/cm^3$ |
| **Absorption coefficient** | 0.738 $mm^{-1}$ |
| **F(000)** | 800 |

**Table 6.** Data collection and structure refinement for **20**.

| | |
|---|---|
| **Diffractometer** | Bruker D8 VENTURE |
| **Radiation source** | Incoatec IμS 3.0 microfocus sealed tube (Cu Kα, λ = 1.54178 Å) |
| **Theta range for data collection** | 4.38 to 74.55° |
| **Index ranges** | -13<=h<=13, -11<=k<=11, -25<=l<=25 |
| **Reflections collected** | 45007 |
| **Independent reflections** | 3978 [R(int) = 0.0279] |
| **Coverage of independent reflections** | 99.8% |
| **Absorption correction** | Multi-Scan |
| **Max. and min. transmission** | 0.7538 and 0.7149 |
| **Structure solution technique** | direct methods |
| **Structure solution program** | XT, VERSION 2014/5 (Sheldrick, 2015) |
| **Refinement method** | Full-matrix least-squares on $F^2$ |
| **Refinement program** | SHELXL-2018/3 (Sheldrick, 2015) |
| **Function minimized** | $\Sigma\, w(F_o^2 - F_c^2)^2$ |
| **Data / restraints / parameters** | 3978 / 0 / 252 |
| **Goodness-of-fit on $F^2$** | 1.037 |
| **$\Delta/\sigma_{max}$** | 0.001 |

**Table 6** (continued)

| | |
|---|---|
| | 3791 |
| **Final R indices** | data; R1 = 0.0401, wR2 = 0.1006 |
| | I>2σ(I) |
| | all data R1 = 0.0416, wR2 = 0.1019 |
| **Weighting scheme** | $w=1/[\sigma^2(F_o^2)+(0.0465P)^2+1.0962P]$ where $P=(F_o^2+2F_c^2)/3$ |
| **Largest diff. peak and hole** | 0.475 and -0.239 eÅ$^{-3}$ |
| **R.M.S. deviation from mean** | 0.041 eÅ$^{-3}$ |

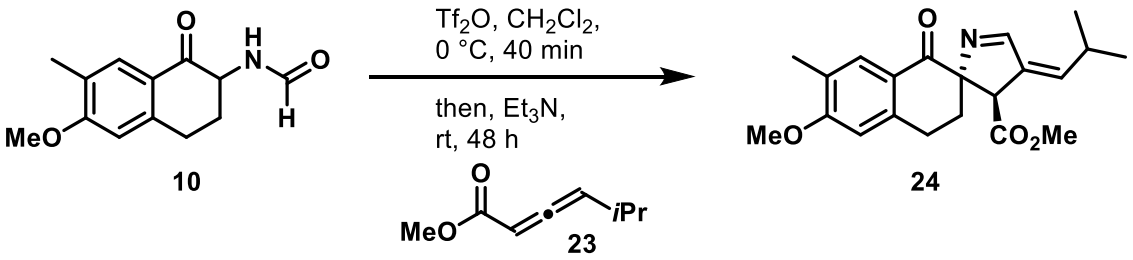


**Compound 24:** To a flame-dried round bottom flask was added formamide **10** (1.00 g, 3.43 mmol) in anhydrous $CH_2Cl_2$ (6 mL). The reaction was cooled to 0 °C and then $Tf_2O$ (0.634 mL, 3.77 mmol) was added in one portion. After stirring at 0 °C for 40 min, the reaction was monitored by TLC for full consumption of **10** and concentrated the mixture to 4 M in $CH_2Cl_2$. Then, $Et_3N$ (0.048 mL, 0.343 mmol) and a half portion of allene **23** (0.537 mL, 3.43 mmol) were added in sequence, the mixture was stirred at rt for 24 h. The other half portion of allene **23** (0.537 mL, 3.43 mmol) was added and the reaction was stirred for another 24 h. The reaction was quenched by saturated $NaHCO_3$ (aq) and transferred to a separatory funnel and extracted with $CH_2Cl_2$ three times. The organic layers were combined, washed with saturated $NaHCO_3$ (aq) and brine, dried over $Na_2SO_4$, filtered and concentrated under reduced pressure. The crude product was purified by flash chromatography on silica gel (25-50%, ethyl acetate:hexanes) to yield the product **24** (0.95 g, 62%) as brown solid:

$R_f$ = 0.31 (1:1, ethyl acetate:hexanes).

**$^1$H NMR** (600 MHz, CDCl3) δ = 7.75 (s, 1 H), 7.71 (s, 1 H), 6.60 (s, 1 H), 5.91 (dd, $J_1$ = 2.4 Hz, $J_2$ = 10.2 Hz, 1 H), 3.86 (s, 3 H), 3.58 (d, $J$ = 2.4 Hz, 1 H), 3.43 (s, 3 H), 3.23-3.18 (m, 1 H), 3.13-3.08 (m, 1 H), 2.45-2.41 (m, 1 H), 2.32-2.25 (m, 2 H), 2.15 (s, 3 H), 1.03 (d, $J$ = 6.6 Hz, 3 H), 0.98 (d, $J$ = 6.6 Hz, 3 H).

**$^{13}$C NMR** (150 MHz, CDCl3) δ = 192.9, 170.9, 166.5, 162.3, 144.1, 141.6, 138.4, 130.3, 125.9, 124.7, 108.6, 86.0, 55.6, 52.1, 52.0, 37.2, 30.3, 26.4, 22.2, 21.6, 15.9.

**IR** (Diamond-ATR, neat) $\tilde{\nu}_{max}$ ($cm^{-1}$): 2949, 2861, 1743, 1674, 1600, 1267, 1244, 1165, 1075, 1030, 901, 848, 782.

**HRMS** (*m/z*): calculated for $C_{21}H_{26}NO_4$ $[M+H]^+$ 356.1856, found 356.1852.

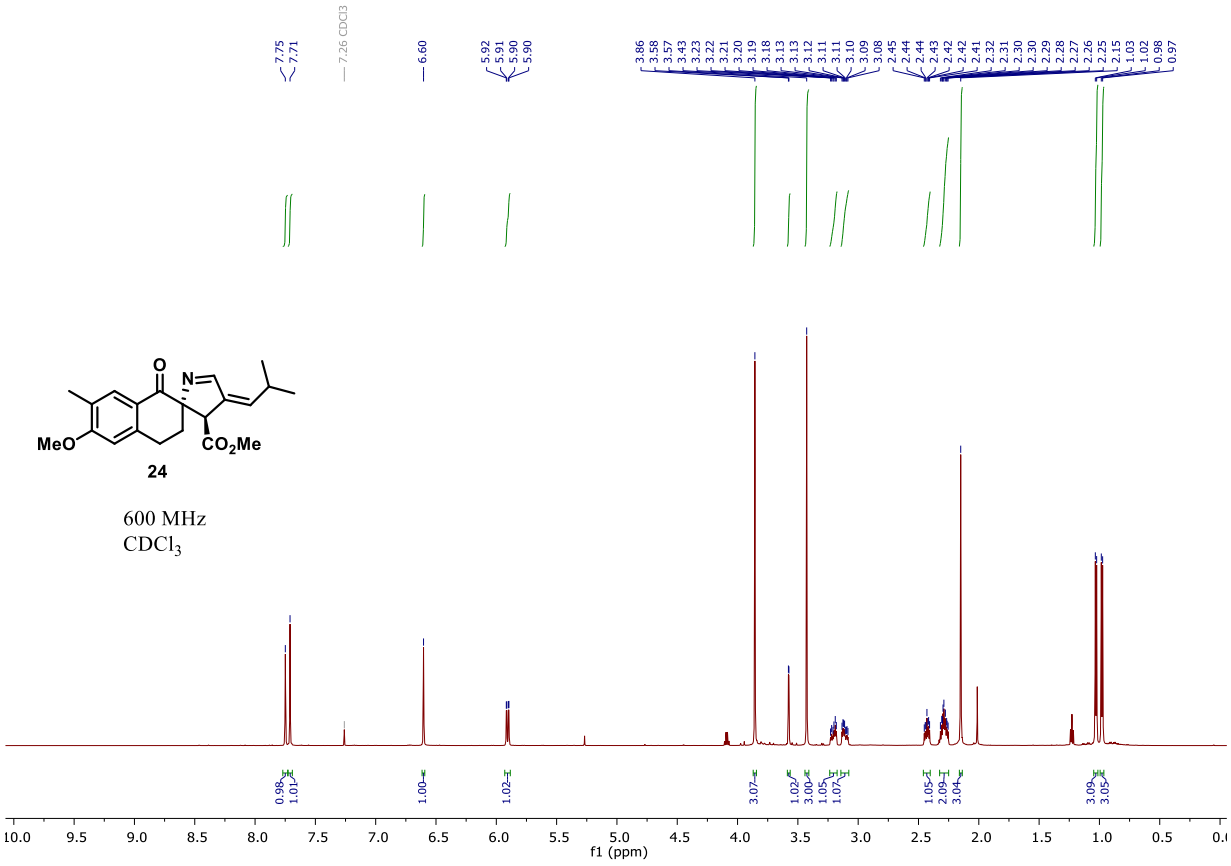


**Figure 29.** $^{1}$H NMR of compound **24**.

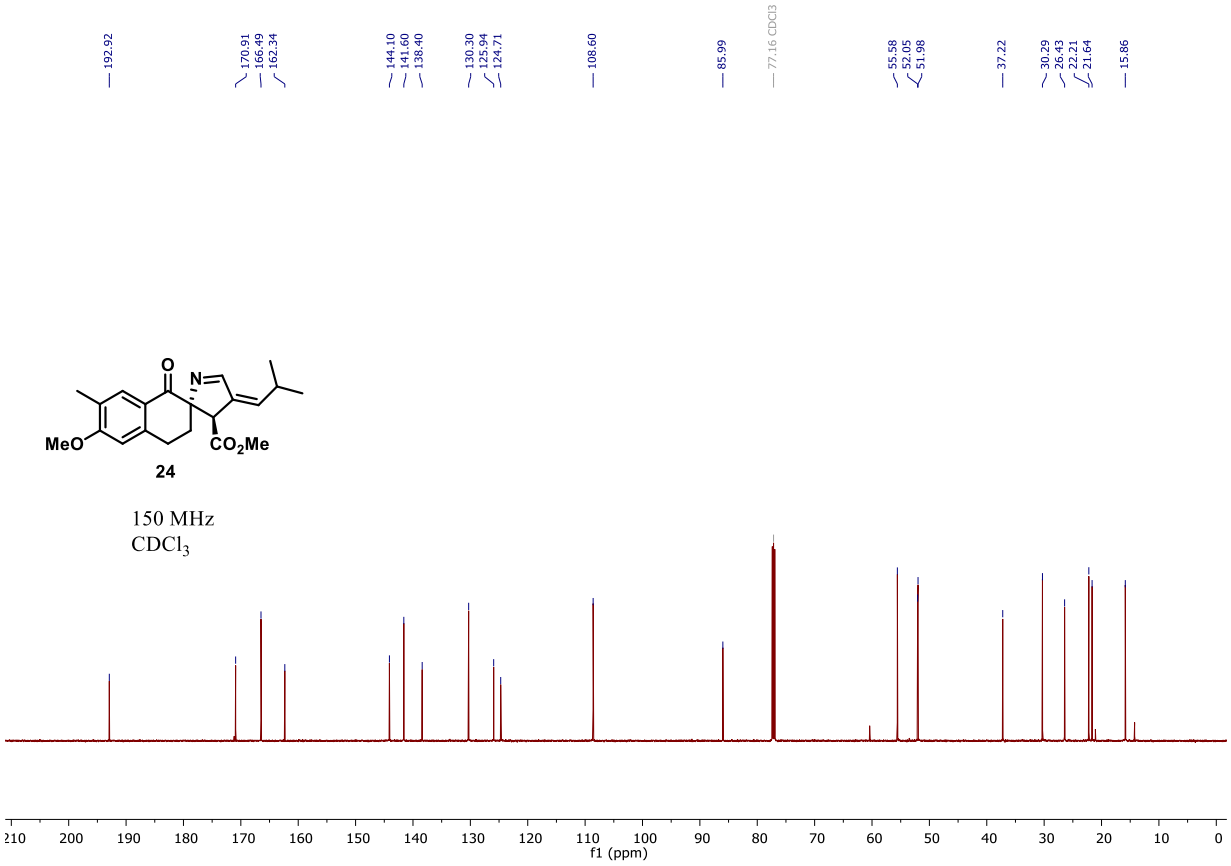


**Figure 30.** $^{13}C$ NMR of compound **24**.

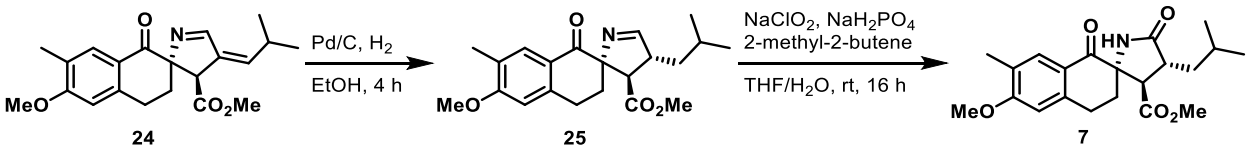


**Compound 7:** 10% Pd/C (0.095 g, 10 wt%) was added to a round bottom flask under argon atmosphere and a solution of **24** (0.950 g, 2.67 mmol) in EtOH (25 mL) was added in one portion. The mixture was stirred under $H_2$ (1 atm). After stirring for about 4 h, the reaction was monitored by TLC for full consumption of **24** and filtered with Celite, concentrated under reduced pressure to yield the crude imine **25**, which will be used for next step without further purification. The crude **25** was dissolved in THF (10 mL), $NaClO_2$ (1.51 g, 13.4 mmol) and 2-methyl-2-butene solution (13.4 mL, 2 M) in THF were added in sequence. An aqueous solution (3.3 M) of $NaH_2PO_4$ (1.60 g, 13.4 mmol) was added dropwise to the stirred mixture over 5 min. Then, the reaction was stirred for 16 h, quenched with 10% $Na_2S_2O_3$ (aq) and extracted with ethyl acetate (2x). The organic layers were combined, washed with brine, dried over $Na_2SO_4$, filtered and concentrated under reduced pressure. The crude product was purified by flash chromatography on silica gel (20-40%, ethyl acetate:hexanes) to yield the product **7** (0.628 g, 63%) as pale yellow solid:

***R*f** of **25** = 0.56 (1:1, ethyl acetate:hexanes), ***R*f** of **7** = 0.25 (1:1, ethyl acetate:hexanes).

**Melting point** (°C) = 212-215.

**$^1$H NMR** (700 MHz, CDCl3) δ = 7.73 (s, 1 H), 6.94 (br, 1 H), 6.58 (s, 1 H), 3.88 (s, 3 H), 3.40 (s, 3 H), 3.20-3.14 (m, 2 H), 3.08-3.04 (m, 1 H), 2.81 (d, *J* = 10.5 Hz, 1 H), 2.63-2.60

(m, 1 H), 2.29-2.26 (m, 1 H), 2.16 (s, 3 H), 1.75-1.67 (m, 2 H), 1.29 (p, $J$ = 6.3 Hz, 1 H), 0.87 (dd, $J_1$ = 6.0 Hz, $J_2$ = 16.1 Hz, 6 H).

**$^{13}$C NMR** (175 MHz, CDCl3) δ = 193.9, 178.6, 171.6, 162.7, 143.5, 130.5, 126.5, 123.9, 108.7, 64.5, 56.5, 55.7, 52.1, 42.4, 41.1, 36.4, 26.0, 25.6, 23.0, 22.2, 16.0.

**IR** (Diamond-ATR, neat) $\tilde{\nu}_{max}$ ($cm^{-1}$): 3172, 3062, 2947, 2863, 1734, 1605, 1494, 1346, 1263, 1107, 1028, 914, 780, 668.

**HRMS** (*m/z*): calculated for $C_{21}H_{28}NO_5$ $[M+H]^+$ 374.1962, found 374.1958.

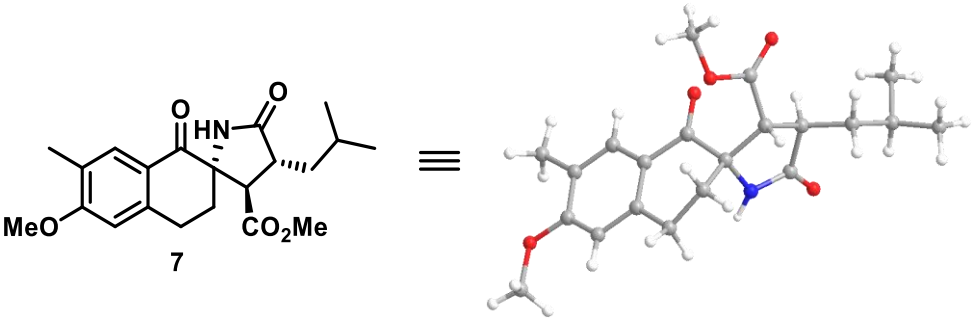


7

**X-ray sample preparation:** Compound **7** was prepared as saturated solution in $CH_2Cl_2$ in a 5 mL scintillation vial. This vial was put into a 20 mL scintillation vial which contains hexanes as same height level as $CH_2Cl_2$. After the $CH_2Cl_2$ evaporated completely, crystals formed inside of 5 mL vial. The crystals were a colorless needle-like specimen of $C_{21}H_{27}NO_5$, approximate dimensions 0.037 mm x 0.060mm x 0.194 mm, was used for the X-ray crystallographic analysis. The X-ray intensity data were measured on a Bruker D8 VENTURE κ-geometry diffractometer system equipped with a Incoatec IμS 3.0 microfocus sealed tube (Cu Kα, λ = 1.54178 Å) and a multilayer mirror monochromator.

The total exposure time was 5.37 h. The frames were integrated with the Bruker SAINT software package using a narrow-frame algorithm. The integration of the data using a monoclinic unit cell yielded a total of 88942 reflections to a maximum θ angle of 74.80° (0.80Å resolution), of which 7939 were independent (average redundancy 11.203, completeness = 99.6%, $R_{int}$ = 7.05%, $R_{sig}$ = 2.51%) and 6389 (80.48%) were greater than $2\sigma(F^2)$. The final cell constants of a = 11.0457(4) Å, b = 13.6258(5) Å, c = 26.0315(9) Å, β = 97.137(2)°, volume = 3887.6(2) $Å^3$, are based upon the refinement of the XYZ-centroids of 9843 reflections above 20 σ(I) with 6.844° < 2θ < 159.4°. Data were corrected

for absorption effects using the Multi-Scan method (SADABS). The ratio of minimum to maximum apparent transmission was 0.894.

The structure was solved and refined using the Bruker SHELXTL Software Package, using the space group $P2_1/c$, with Z = 8 for the formula unit, $C_{21}H_{27}NO_5$. The final anisotropic full-matrix least-squares refinement on $F^2$ with 503 variables converged at R1 = 3.64%, for the observed data and wR2 = 9.54% for all data. The goodness-of-fit was 1.027. The largest peak in the final difference electron density synthesis was 0.267 $e^-/Å^3$ and the largest hole was -0.218 $e^-/Å^3$ with an RMS deviation of 0.044 $e^-/Å^3$. On the basis of the final model, the calculated density was 1.276 $g/cm^3$ and F(000), 1600 $e^-$.

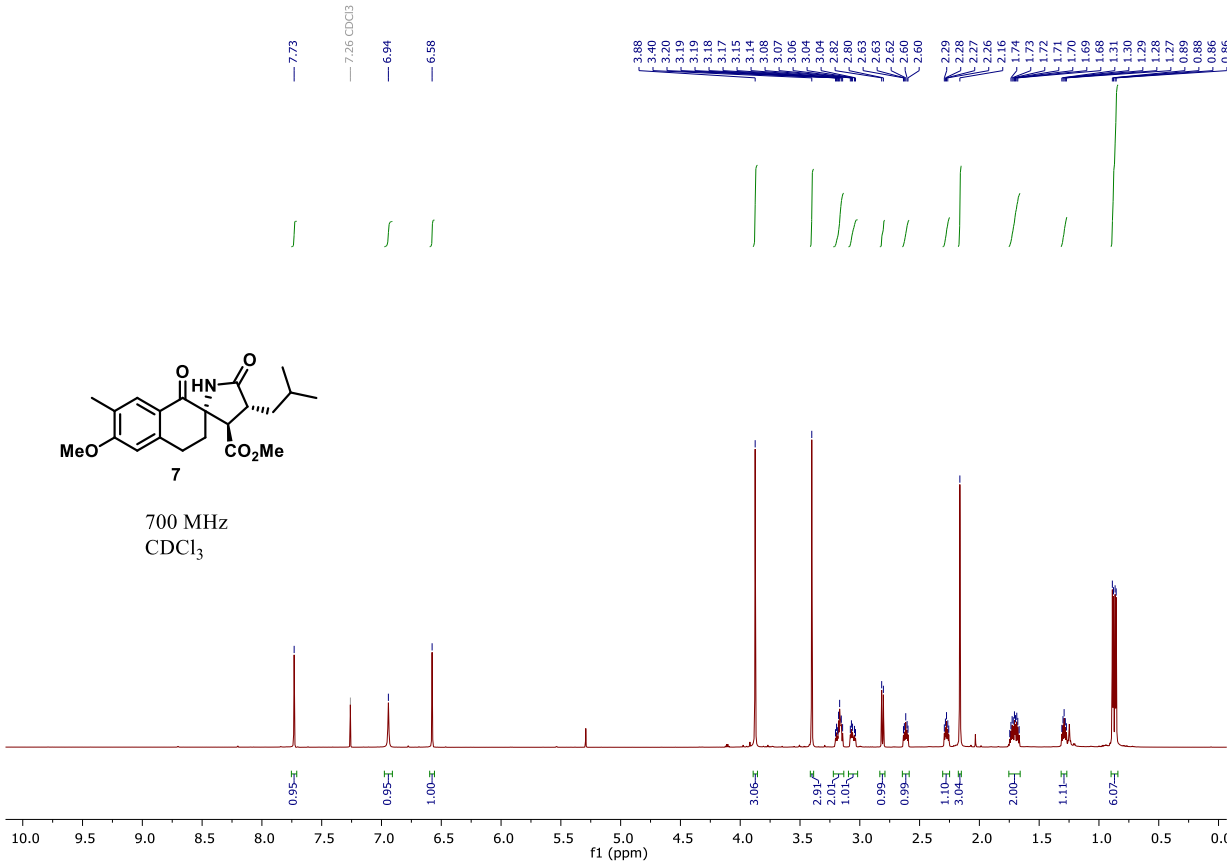


**Figure 31.** $^{1}$H NMR of compound **7**.

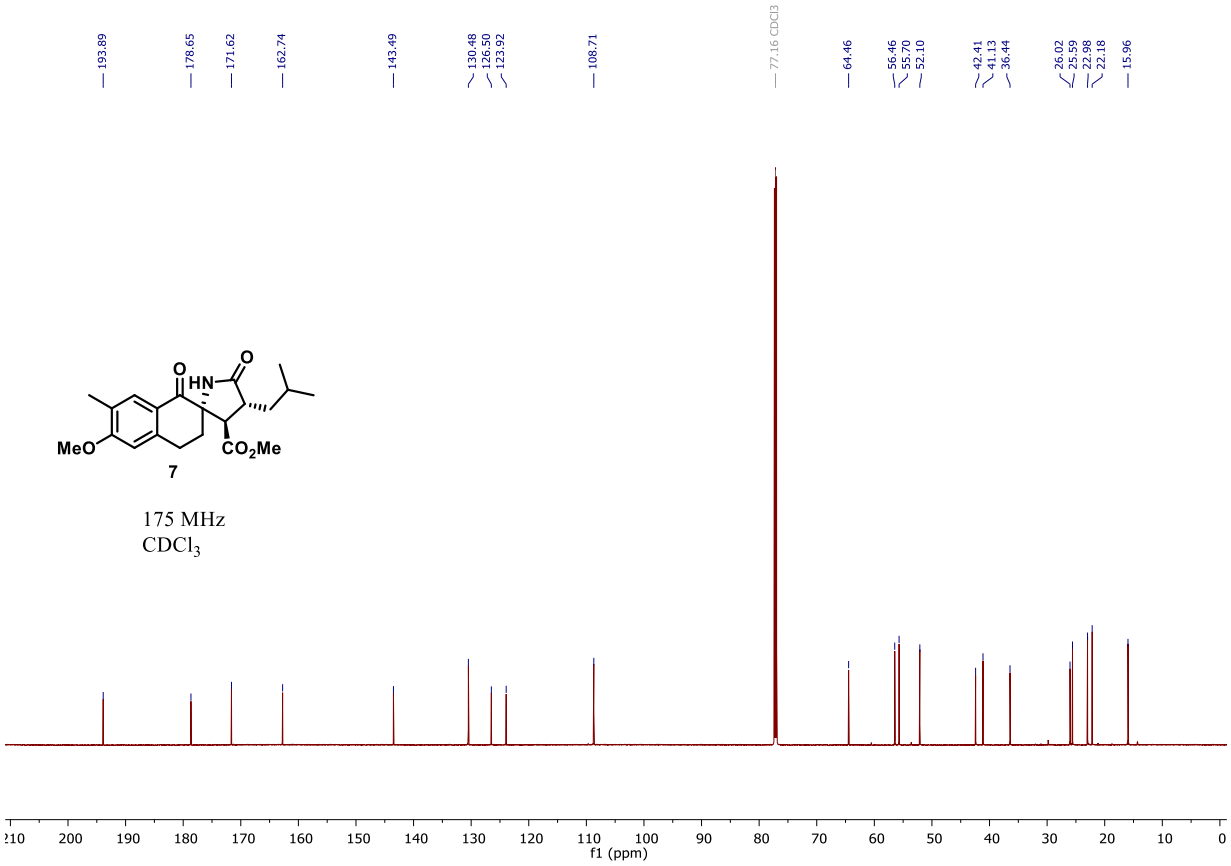


**Figure 32.** $^{13}C$ NMR of compound **7**.

**Table 7.** Sample and crystal data for **7**.

| | |
|---|---|
| **Identification code** | rs092 |
| **Chemical formula** | $C_{21}H_{27}NO_5$ |
| **Formula weight** | 373.43 g/mol |
| **Temperature** | 100(2) K |
| **Wavelength** | 1.54178 Å |
| **Crystal size** | 0.037 x 0.060 x 0.194 mm |
| **Crystal habit** | colorless needle |
| **Crystal system** | Monoclinic |
| **Space group** | $P2_1/c$ |
| **Unit cell dimensions** | a = 11.0457(4) Å α = 90° |
| | b = 13.6258(5) Å β = 97.137(2)° |
| | c = 26.0315(9) Å γ = 90° |
| **Volume** | 3887.6(2) $Å^3$ |
| **Z** | 8 |
| **Density (calculated)** | 1.276 $g/cm^3$ |
| **Absorption coefficient** | 0.741 $mm^{-1}$ |
| **F(000)** | 1600 |

**Table 8.** Data collection and structure refinement for **7**.

| | |
|---|---|
| **Diffractometer** | Bruker D8 VENTURE κ-geometry diffractometer |
| **Radiation source** | Incoatec IμS 3.0 microfocus sealed tube (Cu Kα, λ = 1.54178 Å) |
| **Theta range for data collection** | 3.42 to 74.80° |
| **Index ranges** | -13<=h<=13, -16<=k<=16, -32<=l<=32 |
| **Reflections collected** | 88942 |
| **Independent reflections** | 7939 [R(int) = 0.0705] |
| **Coverage of independent reflections** | 99.6% |
| **Absorption correction** | Multi-Scan |
| **Structure solution technique** | direct methods |
| **Structure solution program** | XT, VERSION 2014/5 (Sheldrick, 2015) |
| **Refinement method** | Full-matrix least-squares on $F^2$ |
| **Refinement program** | SHELXL-2018/3 (Sheldrick, 2015) |
| **Function minimized** | $\Sigma\, w(F_o^2 - F_c^2)^2$ |
| **Data / restraints / parameters** | 7939 / 0 / 503 |
| **Goodness-of-fit on $F^2$** | 1.027 |
| **$\Delta/\sigma_{max}$** | 0.001 |

**Table 8** (continued)

| | |
|---|---|
| | 6389 |
| **Final R indices** | data; R1 = 0.0364, wR2 = 0.0881 |
| | I>2σ(I) |
| | all data R1 = 0.0492, wR2 = 0.0954 |
| **Weighting scheme** | $w=1/[\sigma^2(F_o^2)+(0.0447P)^2+1.3700P]$ where $P=(F_o^2+2F_c^2)/3$ |
| **Largest diff. peak and hole** | 0.267 and -0.218 eÅ$^{-3}$ |
| **R.M.S. deviation from mean** | 0.044 eÅ$^{-3}$ |

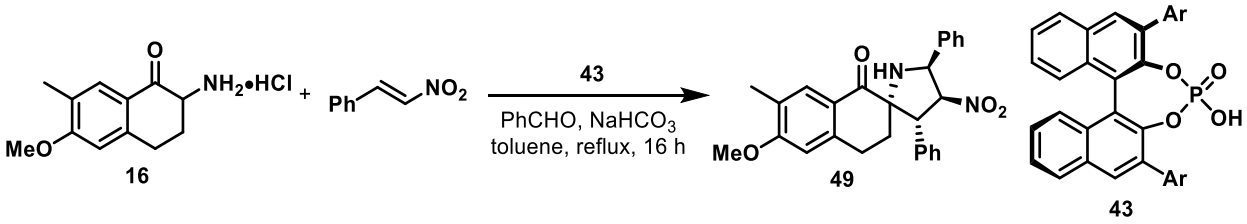


**Compound 49:** The substrate **16** (0.060 g, 0.25 mmol) was added $NaHCO_3$ (0.023 g, 0.27 mmol) and benzaldehyde (0.029 g, 0.27 mmol) in THF (2 mL) at room temperature. After stirred for 0.5 h, the catalyst **43** (0.019 g, 0.025 mmol) and *trans*-*β*-nitrostyrene (0.056 g, 0.37 mmol) were added. The reaction mixture was stirred under reflux for 16 h. The mixture was filtered and concentrated under reduced pressure. The crude product was purified by flash chromatography on silica gel (5-10%, ethyl acetate:hexanes) to yield the product **49** (0.024 g, 22%).

$R_f$ = 0.43 (1:3, ethyl acetate:hexanes).

**$^1$H NMR** (500 MHz, CDCl3) δ = 7.87 (s, 1 H), 7.75 (s, 1 H), 7.28 (d, *J* = 7.5 Hz, 2 H), 7.21 (t, *J* = 7.5 Hz, 2 H), 7.17-7.12 (m, 6 H), 6.53 (s, 1 H), 6.52 (s, 1 H), 6.17 (d, *J* = 8.5 Hz, 1 H), 4.22 (d, *J* = 10.5 Hz, 1 H), 4.02 (t, *J* = 9.0 Hz, 1 H), 3.80 (s, 3 H), 3.24 (m, 1 H), 2.83 (t, *J* = 6.0 Hz, 2 H), 2.51 (t, *J* = 6.5 Hz, 2 H), 2.23 (m, 1 H), 2.14 (s, 3 H), 2.03 (m, 2 H).

**LCMS** (*m/z*): calculated for $C_{27}H_{26}N_2O_4$ $[M+H]^+$ 443, found 443.

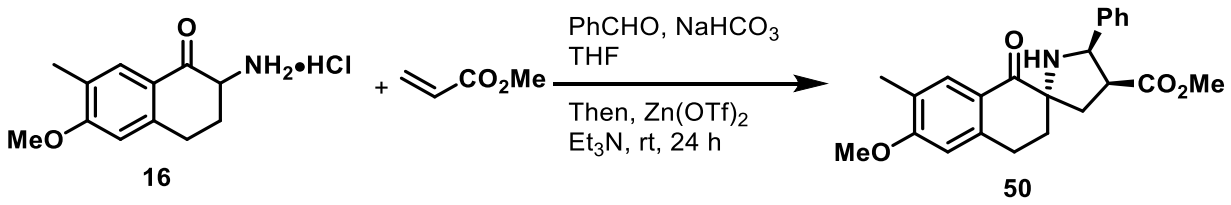


**Compound 50:** $Zn(OTf)_2$ (0.018 g, 0.050 mmol) was placed in a dried flask and connected to a vacuum while heated. After cooling to room temperature, the ligand 2,2'-isopropylidenebis[(4*S*)-4-*tert*-butyl-2-oxazoline] (0.017g, 0.060 mmol) was added and the mixture was stirred for 1 h. The flask was refilled with dry THF (1 mL) and then stirred for another 1 h. The substrate **16** (0.12 g, 0.50 mmol) was added $NaHCO_3$ (0.044 g, 0.52 mmol) and benzaldehyde (0.058 g, 0.55 mmol) in THF (1 mL) at room temperature. After stirred for 0.5 h, $Et_3N$ (0.005 g, 0.050 mmol), the mixture of catalyst and methyl acrylate (0.047 g, 0.55 mmol) were added at room temperature. The reaction mixture was stirred for 24 h and then filtered, concentrated to give the crude mixture. The crude product was purified by flash chromatography on silica gel (15-25%, ethyl acetate:hexanes) to yield the product **50** (0.065 g, 35%) as pale yellow oil.

$R_f$ = 0.23 (1:1, ethyl acetate:hexanes).

**$^1$H NMR** (500 MHz, CDCl3) δ = 7.90 (s, 1 H), 7.40 (d, *J* = 7.5 Hz, 2 H), 7.32 (t, *J* = 7.5 Hz, 2 H), 7.25 (t, *J* = 7.5 Hz, 1 H), 6.60 (s, 1 H), 4.69 (d, *J* = 8.5 Hz, 1 H), 3.88 (s, 3 H), 3.51 (dd, $J_1$ = 8.0 Hz, $J_2$ = 8.0 Hz, 1 H), 3.19 (s, 3 H), 3.13-3.04 (m, 1 H), 2.98 (d, *J* = 13.0 Hz, 1 H), 2.51-2.38 (m, 1 H), 2.33 (dd, $J_1$ = 7.5 Hz, $J_2$ = 5.5 Hz, 1 H), 2.24 (t, *J* = 9.0 Hz, 2 H), 2.21 (s, 3 H).

**$^{13}$C NMR** (175 MHz, CDCl3) δ = 197.0, 172.7, 162.4, 143.5, 139.6, 130.5, 128.6, 128.2, 127.6, 127.1, 127.1, 126.0, 124.1, 108.8, 68.3, 64.8, 55.6, 51.2, 51.1, 35.1, 34.9, 26.8, 15.9.

**LCMS** (*m/z*): calculated for $C_{23}H_{25}NO_4$ $[M+H]^+$ 380, found 380.

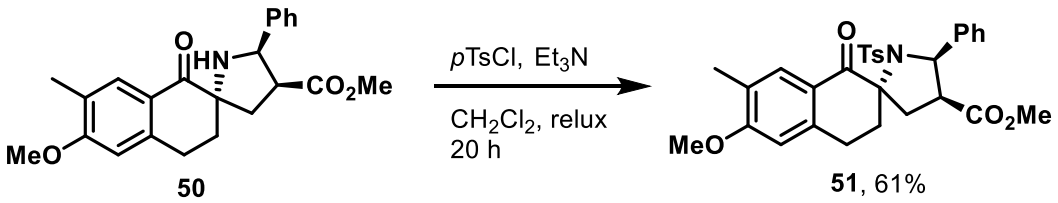


**Compound 51:** The substrate **50** (0.0035 g, 0.092 mmol) and *p*TsCl (0.021 g, 0.11 mmol) was dissolved in $CH_2Cl_2$ (2 mL). $Et_3N$ (0.010 g, 0.10 mol) was added, and the mixture was refluxed for 20 h. The mixture was concentrated and was purified by flash chromatography on silica gel (8-15%, ethyl acetate:hexanes) to yield the product **51** (0.030 g, 61%) as white solid.

***R*f** = 0.55 (1:1, ethyl acetate:hexanes).

**$^1$H NMR** (500 MHz, CDCl3) δ = 7.96 (s, 1 H), 7.38 (d, *J* = 8.5 Hz, 2 H), 7.18 (d, *J* = 7.5 Hz, 2 H), 6.92-6.85 (m, 3 H), 6.78 (d, *J* = 8.0 Hz, 2 H), 6.54 (s, 1 H), 5.21 (d, *J* = 9.5 Hz, 1 H), 3.83 (s, 3 H), 3.73-3.67 (m, 1 H), 3.41-3.34 (m, 1 H), 3.13 (s, 3 H), 3.04-2.93 (m, 2 H), 2.42 (t, *J* = 13.0 Hz, 1 H), 2.34 (dd, $J_1$ = 6.0 Hz, $J_2$ = 6.5 Hz, 2 H), 2.17 (s, 3 H), 2.14 (s, 3 H).

**LCMS** (*m/z*): calculated for $C_{30}H_{31}NO_6S$ $[M+H]^+$ 534, found 534.

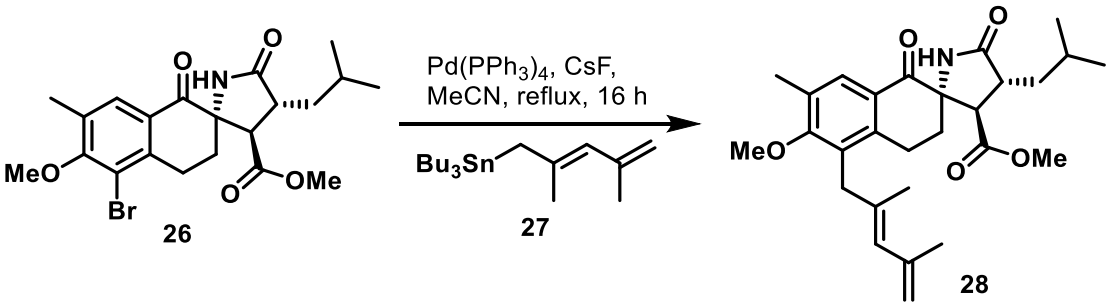


**Compound 28:** To a mixture of **26** (0.10 mg, 0.22 mmol) and diene **27** (0.51 mg, 0.78 mmol) in freshly distilled MeCN (2.5 mL) was added dried CsF (0.074 g, 0.48 mmol) and $Pd(PPh_3)_4$ (0.026 g, 0.022 mmol) under nitrogen at room temperature. Then the mixture was heated to reflux for 16 h. After the resulting mixture was cooled to room temperature The solvent was evaporated in vacuo and the residue was purified by flash column chromatography on silica gel (15-30%, ethyl acetate:hexanes) to yield the product 28 (0.052 g, 50%) as white solid:

$R_f$ = 0.22 (3:5, ethyl acetate:hexanes).

**$^1$H NMR** (500 MHz, CDCl3) δ = 7.75 (s, 1 H), 7.28 (s, 1 H), 5.26 (s, 1 H), 4.91 (s, 1 H), 4.70 (s, 1 H), 3.69 (s, 3 H), 3.39 (s, 2 H), 3.36 (s, 3 H), 3.12-3.01 (m, 2 H), 2.96-2.88 (m, 1 H), 2.81 (d, *J* = 10.0 Hz 1 H), 2.55-2.50 (m, 1 H), 2.28 (s, 3 H), 2.26-2.21 (m, 1 H), 1.87 (s, 3 H), 1.75 (s, 3 H), 1.72-1.65 (m, 2 H), 1.29-1.22 (m, 1 H), 0.85 (dd, $J_1$ = 5.0 Hz, $J_2$ = 10.0 Hz, 6 H).

**LCMS** (*m/z*): calculated for $C_{28}H_{37}NO_5$ $[M+H]^+$ 468, found 468.

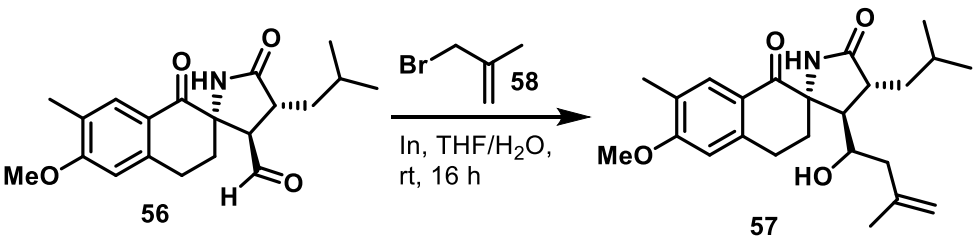


**Compound 57:** To a flame dried flask Indium metal (0.031 g, 0.27 mmol) and 1:1 THF/H2O (2 mL) was taken, followed by the addition of aldehyde **56** (0.062 g, 0.18 mmol) and allyl bromide **58** (0.037 g, 0.27 mmol). Resultant suspension was stirred at room temperature for 16 h. Then, the reaction mixture quenched by saturated $NH_4Cl$ solution. The aqueous layer was extracted with ethyl acetate and dried, concentrated under reduced pressure. Purification by column chromatography over silica gel (25-50%, ethyl acetate:hexanes) to yield the product **57** (0.052 g, 50%) as pale yellow oil:

$R_f$ = 0.24 (1:1, ethyl acetate:hexanes).

**$^1$H NMR** (500 MHz, CDCl3) δ = 7.84 (s, 1 H), 6.71 (s, 1 H), 6.58 (s, 1 H), 4.73 (s, 1 H), 4.54 (s, 1 H), 3.89 (s, 3 H), 3.64 (t, *J* = 7.0 Hz, 1 H), 3.15-3.08 (m, 1 H), 3.00-2.95 (m, 1 H), 3.00-2.95 (m, 1 H), 2.83-2.79 (m, 2 H), 2.33 (d, *J* = 3.0 Hz 1 H), 2.24 (t, *J* = 5.0 Hz, 1 H), 2.19 (s, 3 H), 2.15 (d, *J* = 5.0 Hz 2 H), 1.96-1.90 (m, 1 H), 1.76-1.71 (m, 1 H), 1.44 (s, 3 H), 1.42-1.36 (m, 1 H), 0.95 (dd, $J_1$ = 5.0 Hz, $J_2$ = 12.0 Hz, 6 H).

**LCMS** (*m/z*): calculated for $C_{24}H_{33}NO_4$ $[M+H]^+$ 400, found 400.

## REFERENCES


1) R.L. Bunch, J.M. McGuire, *U.S. Patent* 2,653,899, September 29, **1953**.

2) C. Ve´zina, A. Kudelski, S.N. Sehgal, *J. Antibiot. 28*, **1975**, 721.

3) F. Arcamone, G. Cassinelli, G. Fantini, A. Grein, P. Orezzi, C. Pol, C. Spalla, *Biotechnol. Bioeng. 11*, **1969**, 1101.

4) P. Sensi, P. Margalith, M.T. Timbal, Farmaco *Ed. Sci. 14*, **1959**, 146.

5) H.G. Floss, T.-W. Yu, *Chem. Rev. 105*, **2005**, 621.

6) V. Prelog, W. Oppolzer*, Helv. Chim. Acta 56*, **1973**, 2279.

7) Iwona E. Wrona, Vangelis Agouridas, James S. Panek, *C. R. Chimie*, *11*, **2008**, 1483-1522.

8) W. Wehrli, M. Staehelin, *Bacteriol. Rev. 35*, **1971,** 290.

9) M. Balerna, W. Keller-Schierlein, C. Martius, *H. Wolf H. Zahner, Arch. Mikrobiol. 65*, **1969**, 303.

10) Wilson, M. C.; Nam, S.-J.; Gulder, T. A. M.; Kauffman, C. A.; Jensen, P. R.; Fenical, W.; Moore, B. S., *J. Am. Chem. Soc.* **2011**, *133* (6), 1971–1977.

11) Le, T. C.; Yang, I.; Yoon, Y. J.; Nam, S.-J.; Fenical, W., *Org. Lett.* **2016**, *18* (9), 2256–2259.

12) Floss, H. G.; Yu, T.-W., *Chem. Rev.* **2005**, *105* (2), 621–632.

13) Fukuyo, Y.; Hunt, C. R.; Horikoshi, N., *Cancer Lett* **2010**, *290* (1), 24–35.

14) Valdes-Pena, M. A.; Massaro, N. P.; Lin, Y.-C.; Pierce, J. G., *Accounts Chem. Res*. **2021**, *54* (8), 1866–1877.

15) Hager, A.; Kuttruff, C. A.; Herrero-Gomez, E.; Trauner, D., *Tetrahedron Letters* **2014**, *55*, 59-62.

16) Breugst, M.; Reissig, H., *Angew. Chem., Int. Ed.* **2020**, *59 (30)*, 12293−12307.

17) Narayan, R.; Potowski, M.; Jia, Z.-J.; Antonchick, A. P.; Waldmann, H., *Acc. Chem. Res.* **2014**, *47 (4)*, 1296−1310.

18) Kaur, T.; Wadhwa, P.; Bagchi, S.; Sharma, A., *Chem Commun* **2016**, *52* (43), 6958–6976.

19) Kurata, H., Kusumi, K., Otsuki, K., Suzuki, R., Kurono, M., Komiya, T., Hagiya, H., Mizuno, H., Shioya, H., Ono, T., Takada, Y., Maeda, T., Matsunaga, N., Kondo, T., Tominaga, S., Nunoya, K., Kiyoshi, H., Komeno, M., Nakade, S., Habashita, H., *J. Med. Chem.* **2017**, *60*, 9508-9530.

20) Huisgen, R., *Angew. Chem., Int. Ed. Engl.* **1963**, *2*, 565−598.

21) Huisgen, R., *Angew. Chem.,Int. Ed. Engl.* **1963,** *2*, 633−645.

22) Gothelf, K. V.; Jørgensen, K. A., *Chem. Rev.* **1998**, *98*, 863−910.

23) Kanemasa, S., *Synlett.* **2002**, 1371−1387.

24) Kanemasa, S., *Heterocycles*, **2010**, *82*, 87−200.

25) Pellissier, H., *Tetrahedron* **2007**, *63*, 3235−3285.

26) Comprehensive Asymmetric Catalysis, Vol. 1–3, Suppl. 1–2 (Eds.: E. N. Jacobsen, A. Pfaltz, H. Yamamoto), Springer, Heidelberg, **2004**.

27) C. NLjera, J. M. Sansano, Curr., *Org. Chem.* **2003**, *7*, 1105–1150.

28) S. Kanemasa, *Synlett*, **2002**, 1371–1387.

29) Nájera, C., Sansano, J., *Org. Chem.* **2003**, *7*, 1105−1150.

30) Nájera, C.; Sansano, J. M., *Angew. Chem., Int. Ed.* **2005**, *44*, 6272−6276.

31) Coldham,I., Hufton, R., *Chem. Rev.* **2005**, *105*, 2765−2810.

32) Pandey, G., Banerjee, P., Gadre, S. R., *Chem. Rev.* **2006**, *106*, 4484−4517.

33) Adrio, J., Carretero, J. C., *Chem. Commun.* **2011**, *47*, 6784−6794.

34) Grigg, R., Montgomery, J., Somasunderam, A., *Tetrahedron,* **1992**, *48*, 10431−10442.

35) Gothelf, A. S., Gothelf, K. V., Hazell, R. G., Jørgensen, K. A., *Angew. Chem. Int. Ed.,* **2002**, *41*, 4236−4238.

36) Chen, X.-H., Zhang, W.-Q., Gong, L.-Z., *J. Am. Chem. Soc.* **2008**, *130*, 5652−5653.

37) He, L., Chen, X. H., Wang, D. N., Luo, S. W., Zhang, W. Q., Yu, J., Ren, L., Gong, L. Z., *J. Am. Chem. Soc.,* **2011**, *133*, 13504−13518.

38) Cheng, M. N., Wang, H., Gong, L. Z., *Org. Lett.,* **2011**, *13*, 2418− 2421.

39) Yu, J., Shi, F., Gong, L. Z. *Acc. Chem. Res.,* **2011**, *44*, 1156−1171.

40) Grigg, R., Gunaratne, H. Q. N. J. *Chem. Soc. Chem. Commun.,* **1982**, 384−386.

41) Grigg, R.; Gunaratne, H. Q. N.; Sridharan, V. *Tetrahedron,* **1987**, *43*, 5887−5898.

42) Vicario, J. L., Reboredo, S., Badía, D., Carrillo, L., *Angew. Chem. Int. Ed.* **2007**, *46*, 5168−5170.

43) Reboredo, S., Reyes, E., Vicario, J. L., Badía, D., Carrillo, L., De Cózar, A., Cossío, F. P., *Chem. Eur. J.* **2012**, *18*, 7179−7188.

44) Reboredo, S., Vicario, J. L., Carrillo, L., Reyes, E., Uria, U., *Synthesis* **2013**, 2669−2678.

45) Shiqi W., Guodong Z., Shiqiang W., Baomin W*., Org. Biomol. Chem.*, **2018,** *16*, 807–815.

46) Mohamed, M.; Yamada, K.; Tomioka, K., *Tetrahedron Lett.* **2009**, *50*, 3436−3438.

47) Terwilliger, D. W., Trauner, D., *J. Am. Chem. Soc.* **2018**, *140*, 2748-2751.

48) Lv, L., Shen, B., Li, Z., *Angew. Chem. Int. Ed.* **2014**, *53*, 4164-4167.

49) Chen, Q., Schweitzer, D., Kane, J., Davisson, V. J., Helquist, P., *J. Org. Chem.* **2011**, *76*, 5157-5169.

50) Chatterjee, A. K., Choi, T., Sanders, D. P., Grubbs, R. H., *J. Am. Chem. Soc.* **2003**, *125*, 11360-11370.

51) Funk, T. W., Efskind, J., Grubbs, R. H., *Org. Lett.,* **2005***, 7, 2,* 187-190.

52) Scholl, M., Ding, S., Lee, C. W., Grubbs, R. H., *Org. Lett.,* **1999***, 1, 6,* 953-956.

53) Modica, E., Bombieri, G., Colombo, D., Marchini, N., Ronchetti, F., Scala, A., Toma, L., *Eur. J. Org. Chem.* **2003**, 2964-2971.

54) Tanwar, L., Borgel, J., Ritter, T., *J. Am. Chem. Soc.* **2019**, *141*, 17983-17988.

55) Moriyama, K., Takemura, M., Togo, H., *Org. Lett.,* **2012***, 14, 9,* 2414-2417.

56) Catino, A. J., Nichols, J. M., Choi, H., Gottipamula, S., Doyle, M. P., *Org. Lett.,* **2005***, 7, 23, 5167-5170*.

57) Tripathi, C. B., Mukherjee, S., *Angew. Chem. Int. Ed.* **2013**, *52*, 8450-8453.